HIDDEN IN PLAIN SIGHT:

MORPHOLOGICAL AND GENETIC DIVERSITY

OF BLOOD PROTOZOA FROM

NORTH AMERICAN AMPHIBIANS

By

RYAN PATRICK SHANNON

Bachelor of Science in Microbiology
Oklahoma State University
Stillwater, Oklahoma
2013

Master of Science in Zoology
Oklahoma State University
Stillwater, Oklahoma
2016

Submitted to the Faculty of the
Graduate College of the
Oklahoma State University
in partial fulfillment of
the requirements for
the Degree of
DOCTOR OF PHILOSOPHY
December, 2022

HIDDEN IN PLAIN SIGHT:

MORPHOLOGICAL AND GENETIC DIVERSITY

OF BLOOD PROTOZOA FROM

NORTH AMERICAN AMPHIBIANS

Dissertation Approved:

Dr Matthew Bolek

Dissertation Adviser

Dr. Daniel Moen

Dr. Polly Campbell

Dr. Bruce Noden

ACKNOWLEDGEMENTS

I would like to thank my advisor Dr. Matthew Bolek for his guidance and patience throughout my academic career. His enthusiasm and support have made working in his lab both enjoyable and rewarding. I am also grateful for Dr. Bolek's expertise in numerous parasite systems and his interest in understudied organisms like the amphibian blood protozoa.

I also thank my committee members, Drs. Daniel Moen, Polly Campbell, and Bruce Noden, for their guidance and advice during this project and on this dissertation. Additionally, I thank Daniel Moen, Chris McAllister, Ethan Royal, and TJ Fayton, who provided additional samples from across the US that increased the scope of this study.

I would also like to acknowledge my family, especially my parents Chris and Terry Shannon and brothers Eric and Kevin Shannon for their continued support and contributions to my education. Lastly, I would like to thank my spouse Ashley Love for her assistance in the field, in the laboratory, and overall support and companionship throughout this project.

This work is dedicated to the memory of my grandfather Alfred Frampton III, my grandmother Ellen Shannon, and my uncle John Shannon, who each had a passion and appreciation for science and nature. From a young age, their influences encouraged my pursuit of a career in science.

Name: RYAN PATRICK SHANNON

Date of Degree: DECEMBER, 2022

Title of Study: HIDDEN IN PLAIN SIGHT: MORPHOLOGICAL AND GENETIC DIVERSITY OF BLOOD PROTOZOA FROM NORTH AMERICAN AMPHIBIANS

Major Field: INTEGRATIVE BIOLOGY

Abstract: Blood parasites represent an incredibly diverse subset of parasites that infect all major groups of vertebrates and are transmitted by numerous blood feeding invertebrates. However, quantifying blood parasite diversity is difficult due to the challenges presented by a lack of morphological characters and genetic markers suitable for species delineation. This dissertation investigates the diversity of two genera of blood parasites that infect amphibians and reptiles. *Trypanosoma* spp. of amphibians present numerous morphological characters for species differentiation, however the possibility for species to take multiple forms has historically inhibited the use of morphology in trypanosome species delineation. *Hepatozoon* spp. have the opposite problem, where genetically divergent species across wide host ranges can all have very similar gamont morphology in the bloodstream of their hosts, and morphology is not a useful character to identify species. The studies presented here address the challenges to identify *Trypanosoma* spp. and *Hepatozoon* spp. of amphibians and reptiles and develop methods to link morphological and genetic data to better investigate blood parasite diversity.

TABLE OF CONTENTS

Chapter Page

I. INTRODUCTION 1

II. A METHOD FOR ISOLATING AND SEQUENCING TRYPANOSOME CELLS TO INVESTIGATE SPECIES ASSOCIATIONS IN MULTIPLE MORPHOTYPE INFECTIONS 5

Introduction 6
Materials and Methods 8
Sample Material and Morphotype Identification 8
Trypanosome Isolation 9
Extraction of Isolated Trypanosoma DNA 11
Amplification of Isolated Trypanosome DNA 13
Comparing Success of Extraction and Amplification Methods 15
Results 16
Discussion 17

III. INSIGHTS INTO AMPHIBIAN TRYPANOSOME DIVERSITY WITH THE ADDITION OF SEQUENCES MATCHED TO ISOLATE CELL MORPHOLOGY 28

Introduction 29
Materials and Methods 35
Collection of Specimens 35
Blood Processing and Examination 36
Trypanosome Isolation and Sequencing 38
Extraction and Amplification of Isolated Trypansome DNA 39
Phylogenetic Analyses 41
Results 45
Trypanosome Morphotype Prevalence 45
Descriptions of Trypanosome Morphology and Motility 47
Trypanosomes of Ranids 47
Trypanosomes of Hylids 50
Trypanosome Morphology and Principal Component Analysis 52
Phylogenetic Analyses of Trypanosome Morphotypes 53

Chapter Page

Discussion 56
Morphological Diversity and Coinfection of Amphibian Trypanosomes 56
Inferences from Phylogeny with the Addition of Trypanosome Sequences Linked to Morphology 58
Trypanosoma rotatorium in North America and Europe 59
Trypanosoma ranarum in North America and Europe 61
Phylogenetic Conservation of Amphibian Trypanosome Morphology 63
Potential problems with Sequencing Trypanosome Cultures 65
Conclusions 67

IV. DESCRIPTION OF TRYPANOSOME SPECIES INFECTING RANID HOSTS IN THE CENTRAL UNITED STATES 86

Introduction 87
Materials and Methods 89
Sample Material and Morphotype Identification 89
Trypanosome Isolation and Sequencing 90
Results 90
Species Descriptions 90
Trypanosoma desseri n. sp. 90
Taxonomic Summary 91
Remarks 92
Trypanosoma curvus n. sp. 97
Taxonomic Summary 97
Remarks 98
Trypanosoma louisdiamondi n. sp. 101
Taxonomic Summary 101
Remarks 102
Trypanosoma cf. *ranarum*. 105
Taxonomic Summary 105
Remarks 106
Discussion 110

V. MORPHOLOGICAL AND MOLECULAR CHARACTERIZATION OF *HEPATOZOON* SPECIES INFECTING FROGS AND SNAKES ACROSS THE CENTRAL AND EASTERN UNITED STATES 113

Introduction 114
Hepatozoon spp. Infecting Amphibians 116
Hepatozoon spp. Infecting Snakes 118

Chapter Page

Materials and Methods....120
Collection of Specimens....120
Blood Processing and Examination....121
DNA Extraction....122
PCR Amplification and Sequencing....122
Phylogenetic Analyses....123
Results....125
Parasite Prevalence and Morphology in Anurans....125
Parasite Prevalence and Morphology in Snakes....126
Phylogenetic Analyses of Anuran *Hepatozoon* Genotypes....126
Phylogenetic Inferences on *Hepatozoon* spp. in Snakes....128
Discussion....129
Morphological and Phylogenetic Relationships of *Hepatozoon* spp. Infecting Anurans....129
Morphological and Phylogenetic Relationships of *Hepatozoon* spp. Infecting Snakes....132

VI. CONCLUSIONS....149

REFERENCES....152

APPENDICES....167

LIST OF TABLES

Table Page

1. Sequencing success of the 18s rRNA and gGAPDH genes from isolated trypanosome cells 26

2. Sequencing success of the 18s rRNA and gGAPDH genes from isolated trypanosome cells 27

3. Species, Life stage, and numbers of amphibians collected and examined for trypanosomes 69

4. Ranid hosts infected with trypanosomes, their collection locations, and prevalence of trypanosome morphotypes 70

5. Hylid hosts infected with trypanosomes, their collection locations, and prevalence of trypanosome morphotypes 71

6. Dimensions of the six trypanosome morphotypes infecting ranids. 78

7. Dimensions of the six trypanosome morphotypes infecting hylids. 79

8. Dimensions of the four trypanosome species 112

9. Prevalence of *Hepatozoon* spp. infecting amphibians and reptiles in Arkansas, New Hampshire, Oklahoma, and Wisconsin.....136

10. PCR primers used for amplification and sequencing of the 18s rRNA, ITS-1, and CO3 genes from frogs and snakes 140

11. Measurements of *Hepatozoon* gamonts infecting red blood cells of frogs and snakes, arranged by host.....141

Table Page

12. Measurements of *Hepatozoon* gamonts infecting red blood cells of frogs arranged by the effect on the host cell nucleus 141

13. Measurements of *Hepatozoon* gamonts from frogs and snakes arranged by genotype 142

14. Effect on the host erythrocyte nucleus and genotype sequenced from samples of infected frogs 143

LIST OF FIGURES

Figure Page

1. Photomicrograph of the R1 and R2 morphotypes coinfecting a single *Rana sphenocephala*.....20

2. Photomicrographs of the six trypanosome morphotypes isolated 21

3. Blood collection and preparation to view and isolate trypanosomes.....23

4. Photomicrographs of live trypanosome showing before and after isolation for DNA amplification 24

5. Schematic for the five different nested primer combinations used for PCR amplification 25

6. Key landmarks used to measure trypanosome morphology 72

7. Photomicrographs of trypanosome morphotypes infecting ranid frogs.....74

8. Photomicrographs of trypanosome morphotypes infecting hylid frogs.....75

9. Plots comparing trypanosome morphotypes infecting ranid frogs 76

10. Plots comparing trypanosome morphotypes infecting hylid frogs 77

11. Maximum Likelihood phylogeny of the partial 18s rRNA gene 81

12. Maximum Likelihood phylogeny of the partial gGAPDH gene.....83

13. Maximum Likelihood phylogeny of the partial 18s rRNA gene using only sequences for which there is good morphological data 85

14. *Trypanosoma desseri* n. sp. on stained blood smears showing the variation in cell length and width.....96

Figure Page

15. *Trypanosoma curvus* n. sp. on stained blood smears showing the variation in cell width 100

16. *Trypanosoma lousidiamondi* n. sp. on stained blood smears.....104

17. *Trypanosoma* cf. *ranarum* on stained blood smears showing the variation in cell length and width.....109

18. Photomicrographs of *Hepatozoon* spp. cells from frogs and snakes 137

19. Photomicrographs of *Hepatozoon* spp. infecting green frogs *Rana clamitans* showing the variation in the effects on the host erythrocyte nuclei 138

20. Photomicrographs showing variation and possible progression of cytoplasm clearing in snake erythrocytes infected with *Hepatozoon* cf. *sipedon*.....139

21. Maximum Likelihood phylogeny of the partial cytochrome oxidase subunit III nucleotide gene sequences 144

22. Maximum Likelihood phylogeny of the internal transcribed spacer region 1.....145

23. Maximum Likelihood phylogeny of the partial 18s rRNA gene 146

24. The Bartazoon clade from the 18s rRNA phylogeny (Fig. 23).....148

.

CHAPTER I

INTRODUCTION

Parasitism is a type of symbiotic association between two organisms. The most common definition of parasitism is a symbiotic relationship between two organisms where the parasite lives in or on a host at the expense of the host (Roberts et al., 2013). Some parasites are highly pathogenic to their hosts and cause mechanical damage to host tissues and stimulate inflammatory and/or immune responses (Roberts et al., 2013). Other parasites are more subtle and simply divert resources away from the host. This can happen in various degrees including many cases where the harm caused by parasite is debatable (Combes, 2001). In any case, parasites are metabolically dependent on their hosts and have remarkable adaptations to obtain host resources and survive host immunological defenses (Roberts et al., 2013).

It has been estimated that more than 50% of all plant and animal species are parasitic at some point in their life cycle (Price, 1980). Additionally, it has been estimated that nearly all plants and animals serve as hosts for parasites (Esch and Fernandez, 1993). Therefore, parasitism is a very common ecological relationship that is represented in most species. To the parasite, the host represents a resource and habitat where the parasite can grow and reproduce (Combes, 2001). Parasite reproductive stages must then find their way to a new host, either by exiting the host into the external environment, or by

ingestion by a predator or vector (Roberts et al., 2013). Therefore, unlike most free-living organisms, a defining feature of parasite diversity are the adaptations particular parasite species have evolved to increase the chance of contact with a suitable host in order to propagate the next generation and complete their life cycle. The spatial and temporal difficulties parasites face to successfully transfer from one host to another must be overcome by enormous reproductive outputs and/or by exploiting complex ecological associations between successive hosts (Tinsley, 1990).

Combes (2001) identified the processes that limit a given parasites' range of suitable hosts into two general categories defined as filters. The encounter filter includes ecological barriers to parasite transmission. Ecological barriers can result through a biodiversity parameter, where the geographic ranges of the parasite and host must overlap for successful transmission, and a behavioral parameter, where the spatial and temporal activities of the parasite and host must coincide for parasite transmission to occur. Once a parasite is in contact with a potential host, the compatibility filter further excludes some hosts through physiological or immunological barriers. Physiological barriers can result through a resource parameter, where the host must be able to support the requirements of a parasite's infection spatially or metabolically, and a defense parameter, where the parasite must be able to evade host defenses such as immune responses or other mechanisms (Combes, 2001).

Despite these barriers, parasites are immensely successful organisms and, as mentioned above, they are estimated to have colonized almost all animal and plant species (Esch and Fernandez, 1993). However, given the estimated vastness of their

diversity, it is extremely difficult to quantify parasite diversity due to a lack of morphological characters and genetic markers suitable for species delineation.

This dissertation investigates the diversity of two genera of amphibian blood parasites, *Trypanosoma* and *Hepatozoon*, both of which are cryptic and challenging to identify. Trypanosomes of amphibians present numerous morphological characters for species differentiation, however the possibility for species to take multiple forms has historically inhibited the use of morphology in trypanosome species delineation. In contrast, *Hepatozoon* spp. have the opposite problem, where genetically divergent species across wide host ranges can all have very similar gamont morphology in the bloodstream of their hosts, and morphology is not a useful character to identify species. It is fairly common to observe up to five morphologies of trypanosomes and *Hepatozoon* spp. infecting the blood of a single frog. However, the challenges posed to identify these parasites keeps their diversity hidden in plain sight.

The following chapters address these problems and propose a way forward to generating data useful for blood parasite identification. Chapter II details novel methods to address the challenge of mixed trypanosome infections and characterize trypanosomes morphologically and genetically. Chapter III uses the sequence data linked to trypanosome morphology generated in Chapter II to investigate amphibian trypanosome morphological diversity in a phylogenetic context. Chapter IV reports the description of three new trypanosome species and one redescription of a trypanosome species previously misidentified in North American anurans based on the data generated in Chapters II and III. Finally, Chapter V investigates characters for species differentiation

of three *Hepatozoon* species in North America, two that infect frogs, *Hepatozoon catesbianae* and *Hepatozoon clamatae*, and one, *Hepatozoon sipedon*, that infects snakes.

CHAPTER II

A METHOD FOR ISOLATING AND SEQUENCING TRYPANOSOME CELLS TO INVESTIGATE SPECIES ASSOCIATIONS IN MULTIPLE MORPHOTYPE INFECTIONS

ABSTRACT: Amphibians are commonly infected by multiple trypanosome morphologies and these mixed infections make linking sequence data to bloodstream trypanosome morphology extremely challenging. This chapter presents a method to isolate individual trypanosome cells from frog blood for nested PCR for the 18s rRNA and gGAPDH genes. Single trypanosome cells were isolated by dilution and three DNA extraction methods and five nested PCR primer regimes were utilized to optimize amplification from very low starting concentrations. The success rates of extraction methods ranged from 29% to 50% with the use of a Direct PCR kit having the highest success rate. Even though the sequence success rate varied in the different combinations of extraction methods and primer regimes, multiple individuals of all 6 trypanosome morphotypes were sequenced for both genes in a novel way that links sequence data to cell morphology by observing isolated cells before PCR amplification with a microscope. The methods presented here offer a promising solution to overcome the difficulties of

multiple morphotype infections and the data generated here has interesting consequences for the current amphibian trypanosome phylogeny, which is explored in Chapter III.

INTRODUCTION

Amphibians are commonly infected by multiple trypanosome morphologies and these mixed infections make it challenging to evaluate amphibian trypanosome diversity (Diamond, 1965; Bardsley and Harmsen, 1973; Werner and Walewski, 1976; Desser, 2001; Attias et al., 2016; Spodareva et al., 2018). For example, studies often find that 85-100% of frogs infected by trypanosomes are infected with two to five different trypanosome morphotypes (Diamond, 1965; Werner and Walewski, 1976; Jones and Woo, 1986; Attias et al., 2016; Spodareva et al., 2018; Fig. 1). When observing these mixed trypanosome infections on amphibian blood smears, it is not clear whether the forms present in the bloodstream represent different species (genetic lineages) or a single pleomorphic species (one genetic lineage that takes more than one morphological form in the bloodstream). However, many authors have considered trypanosome morphotypes found infecting the same frogs to be a single species and this has led to the assumption that most amphibian trypanosomes are pleomorphic (Fantham et al., 1942; Nigrelli, 1945; Diamond, 1965; Werner and Walewski, 1976, Desser, 2001). This assumption has been based on life cycle and culturing studies performed on a limited number of trypanosome species more than 40 years ago and only recently has this assumption been tested with genetic methods. However, there is currently no genetic evidence that multiple morphotypes infecting the same frog individual represent a single pleomorphic

trypanosome species (Fantham et al., 1942; Nigrelli, 1945; Diamond, 1965; Bardsley and Harmsen, 1973; Werner and Walewski, 1976; Spodareva et al., 2018).

With the advancement of molecular technology and increases in affordability for gene sequencing, determining pleomorphic trypanosome species using genetic techniques is now possible. However, mixed morphotype infections provide challenges in acquiring and interpreting sequence data. One common problem is that amplifying and sequencing trypanosome genes from blood samples with multiple morphotypes can yield messy chromatograms, indicating there are multiple genotypes present in the sample. A second problem is that if one of the multiple morphotypes is more numerous in the blood of their amphibian host, PCR can favor that genotype and result in clean chromatograms which look like a single genotype is present, hiding the true diversity of these infections (Shannon, unpublished observation).

To overcome these difficulties and obtain sequence data from individual trypanosome morphotypes, specific methods are needed. Spodareva et al. (2018) used cloning to separate and sequence gene copies amplified from multiple morphotype infections. This method provides clean sequences from each cloned bacterial colony, yet the origin of the sequence is usually unknown. Sequences must be assigned to morphotypes indirectly by repeating the cloning process on different frogs with different combinations of morphotypes. Additionally, PCR errors are exposed in this process, resulting in each clone sequence having 1-2 bases different at random positions. The assembly of cloned sequences into consensus sequences is then required to represent the taxa in phylogenetic comparisons (Brown, 2020).

In this chapter, I detail an improved method to link trypanosome morphology to sequence data by directly sequencing single cells with a known morphology. In the following sections I present the trials performed in the development of this method and evaluate the success rates of the different extraction methods and PCR regimes utilized. These methods can be used to provide definitive links between amphibian trypanosome gene sequences and the original trypanosome morphology in the bloodstream. With this novel technique, we can begin to uncover the true hidden diversity of amphibian trypanosomes and discover any true pleomorphic trypanosome species.

MATERIALS AND METHODS

Sample Material and Morphotype Identification

Infected blood samples were obtained from five frog species: *Rana blairi*, *Rana catesbeiana*, *Rana clamitans*, *Rana sphenocephala*, and *Hyla cinerea*. Frogs were collected from Oklahoma, Arkansas, and Wisconsin, USA, as described in Chapter III. Briefly, blood was collected in capillary tubes and blood smears on glass slides were created. Additionally, capillary tubes were centrifuged to concentrate trypanosomes at the buffy coat layer (Woo, 1969; see below). Concentrated trypanosomes from centrifuged capillary tubes were deposited into phosphate buffered saline for examination of live trypanosomes (Woo, 1969; see below). Blood smears and live blood plasma preparations were examined for parasites and blood samples only containing mixed trypanosome infections were used in these experiments (Fig. 1). Blood samples from individual frogs contained two to five trypanosome morphotypes, and in total six different trypanosome

morphotypes were isolated for DNA extraction and amplification (Fig. 2). These morphotypes were identified based on morphological characteristics by examining thin blood smears stained with the JorVet Dip Quick Stain Kit (Jorgensen Labs, CO) with a compound microscope. Identifications were based on comparisons to the primary literature; however trypanosome taxonomy is in a state of flux (Desser, 2001). Therefore, the morphotypes in this study were numbered with designations of the frog host family they infected, except for two forms that conform to previously described species and were given the cf. designation. The current taxonomical problems and decisions regarding naming are covered in Chapter III and IV. Morphotypes R1, R2, R3, *T.* cf. *ranarum*, and *T.* cf. *chattoni* originated from ranid hosts including *R. blairi*, *R. catesbeiana*, *R. clamitans*, *R. sphenocephala*, and morphotype H3 was from the hylid *H. cinerea*. These morphotypes range in morphological characteristics and include broad cells without free flagella (R1 and R2), broad cells with free flagella (R3 and *T.* cf. *ranarum*), large spherical cells (*T.* cf. *chattoni*), and long slender cells (H3, Fig. 2). In blood plasma preparations, live trypanosome general size, shape, and swimming behavior was compared to morphology observed on slides to identify morphotypes (Supplementary Videos 1 - 4). Specific identification characteristics of the morphotypes in this study are given in Chapters III and IV.

Trypanosome Isolation

Trypanosomes were isolated from amphibian blood by dilution of plasma obtained by the hematocrit centrifugation technique of Woo (1969; Fig. 3). Capillary

tubes with fresh, naturally infected frog blood were sealed with Cha-Seal compound (Kimble, NJ) and centrifuged for 1 minute at 4,000g with an Allegra X-22 centrifuge (Beckman Coulter, CA). This concentrates trypanosomes and white blood cells in the buffy coat layer in between packed red blood cells and clear blood plasma. The capillary tubes were the scored with a glass scratcher just below the buffy coat layer, allowing the tube to be snapped right at that spot and providing easy access to concentrated trypanosomes (Fig. 3B). The buffy coat and plasma were then dispensed into a tube with 50 µL phosphate buffered saline (PBS) using a pipette bulb attached to the snapped capillary tube (Fig. 3C). This stock solution of trypanosomes in buffer was kept in a refrigerator for trypanosome isolation for about a week.

Small samples (5 µL) of trypanosomes in buffer were then pipetted into a 20 µL drop of buffer on a glass microscope slide and examined with a microscope to find trypanosomes to isolate (Fig. 3D). The motion of trypanosomes swimming in these live preparations makes them fairly easy to spot against the background of nonmotile frog blood cells. Specific morphologies of trypanosomes were recognized by comparing live trypanosomes and their size to trypanosomes observed on prepared stained blood smears. In addition, specific trypanosome morphotypes had characteristic movement based on their morphological characteristics, including the length of the undulating membrane and presence or absence of a free flagellum (Supplementary Videos 1 - 4), which allowed for accurate identification of live trypanosome morphotypes in the blood plasma/buffer mixture.

When a specific trypanosome morphotype was recognized for isolation, a 2 µL aliquot was pipetted from the approximate area of the drop where the trypanosome was

observed and deposited into a new 20 µL drop of buffer (Fig. 3D). The new drop was then observed to see if transferring the trypanosome was successful. Most of the time multiple trypanosomes were transferred, but by repeating this process of pipetting 2 µL samples with a trypanosome into new drops of buffer, one can make drops of buffer containing only a single trypanosome cell (Fig. 4). These cells were then collected in 2 µL samples and transferred into 200 µL PCR tubes for DNA extraction, and/or PCR, and gene sequencing (see below). Additionally, 2 µL samples not containing trypanosomes were collected as negative controls to ensure trypanosome DNA is not distributed throughout the stock buffer solution.

The ease of this dilution process depended on the intensity/parasitemia of the sample. Isolating single cells was much easier from blood samples with relatively low trypanosome numbers (e.g. 10 to 20 trypanosomes per capillary tube) compared to samples containing thousands of trypanosomes per capillary tube. In samples with low parasitemia, trypanosomes of a target morphology were often swimming alone and could be easily isolated and observed in a subsequent drop. In samples with high parasitemia, a few trypanosomes were often pipetted together and require repeated dilutions to get down to a single cell.

Extraction of Isolated Trypanosome DNA

The isolated trypanosome samples from the above dilutions have very low DNA concentrations and require modifications to typical DNA extraction protocols to successfully obtain DNA for PCR amplification (Hamilton et al., 2015). The problem is

typical DNA extraction kits result in elutions of 50-200 µL in which the initial 2 µL trypanosome samples would be too dilute for reliable PCR amplification (Hamilton et al., 2015). To successfully extract DNA from these samples, three modified methods of DNA extraction were employed.

The first method attempted was to perform DNA extractions by following the instructions provided in the DNeasy Blood and Tissue Kit (Qiagen, CA), but with the modification of using only $1/10^{th}$ the reagents to maximize DNA concentration from the isolated trypanosome cell. Additionally, an elution volume of 20 µL instead of the recommend 200 µL was used. Nested PCR with the Hotstartaq Master Mix Kit (Qiagen, CA) was then performed as detailed below for either the 18s rRNA or gGAPDH genes.

To improve on the success rate of the first method, a second method was performed which attempted to minimize DNA losses by forgoing DNA extraction. DNA extraction is not always necessary for PCR amplifications from small (1 – 2 µL) blood samples, as in addition to not having very much DNA present, small samples also contain low levels of PCR inhibitors (Mercier et al., 1990). The second method used a modified PCR protocol with three hot-cold cycles before the normal denaturation-annealing-extension cycles to lyse cells in the sample and free the DNA for amplification (Mercier et al., 1990). This PCR used the Hotstartaq Master Mix Kit (Qiagen, CA) and the protocol was as follows: Three cycles of 94°C for 3 minutes, 55°C for 3 minutes, then denaturation for 30s at 95°C, annealing for 30s at the appropriate temperature for the primer pair listed below, extension for 60s at 72°C, repeated for 30-40 cycles before a final extension period of 420s at 72°C.

The third method used the Platinum Direct PCR Universal Master Mix Kit (Thermofisher) for a combined extraction and amplification protocol. DNA was obtained by lysing single cell isolates using lysis buffer and proteinase K, but without a column or beads to elute DNA. Additionally, I used the following modifications to the normal kit protocol. A stock lysis buffer containing 19.4 µL of lysis buffer and 0.6 µL proteinase K was prepared and 1-2 µL of this stock buffer was added to the 1-2 µL sample containing a single trypanosome for a total volume of 3 µL. This sample was incubated at room temperature for one minute, followed by one minute at 98°C on a thermal cycler. The sample was then returned to room temperature and PCR reagents were added and nested PCR was performed.

Amplification of Isolated Trypanosome DNA

For all three of the above methods, amplification of the 18s rRNA and gGAPDH genes were performed with nested PCR. Five different Nested PCR primer regimens (A, B, C, D, E) were implemented to sequence both genes from isolated trypanosome cells (Fig. 5). These regimens consisted of combinations of reactions with external and internal primers for both the 18s and gGAPDH genes (Fig. 5). Regimen A targeted the 18s rRNA gene and regimen B targeted gGAPDH gene. Regimens C, D, and E were used with the goal of sequencing both genes from the DNA of the single isolated trypanosome cell using multiplex PCR (Fig. 5). However, balancing amplification of the two genes, which have different starting copy numbers, proved difficult. Regime C tended to favor amplification of only the gGAPDH gene, which were the initial external primers (Fig. 5).

Regime D was attempted in which amplification of both genes was first performed in the reaction. This unfortunately only amplified the 18s rRNA gene. Therefore, regime E was devised which delayed the addition of 18s rRNA primers six cycles to allow the gGAPDH gene, which has two copies in the trypanosome genome (Hamilton et al., 2004), to catch up to the concentration of the 18s rRNA gene of about 100 copies (Stothard, 2000).

For 18s, the external reaction was performed with external primers Tryp_18s_EF (5'-GATAACTTGGCGAAACGCC-3') and Tryp_18s_ER (5'-GCAATACTCGGTCCCAAGTG-3') with an annealing temperature of 58°C. For the internal reaction, 1 µL of the first PCR was used as the template for the second reaction, and internal primers Tryp_18s_IF (5'-AACCCATCCAATATCGAGTAAC-3') and Tryp_18s_IR (5'-GTTGCCCAAAATCTCACC-3') were used with an annealing temperature of 55°C. The internal and external primer sets were designed from an alignment of available frog trypanosome 18s rRNA sequences (Martin et al., 2002).

For gGAPDH, the external reaction used the external primers Tryp_gGAPDH_EF (5'-GACATGAACACSGACGC-3') and Tryp_gGAPDH_ER (5'-GATGGAGCTRCGGTTGTC-3') with an annealing temperature of 55°C. The internal reaction was performed with 1 µL of the first reaction as template, and the internal primers Tryp_gGAPDH_IF (5'- CGCGTACCAGATGAAGTACG-3') and Tryp_gGAPDH_IR (5'- CGGTTGTCRTTGATGAAGTC-3') with an annealing temperature of 55°C. These primers were designed using an alignment of available frog trypanosome gGAPDH sequences (Hamilton et al., 2004).

Depending on the method, PCR was either performed with Hotstartaq Master Mix Kit (Qiagen, CA) or the Platinum Direct PCR Universal Master Mix Kit (Thermofisher) as follows unless specified previously: initial activation for 300s at 95°C, denaturation for 30s at 95°C, annealing for 30s at the appropriate temperature for the primer pair listed above, extension for 60s at 72°C, repeated for 30-40 cycles before a final extension period of 420s at 72°C. The products of the internal PCRs were checked with gel electrophoresis for single bands of the appropriate size, 1200 base pairs for 18s rRNA and 800 for gGAPDH. If PCR was successful, the product was cleaned up with the Wizard® SV gel and PCR cleanup kit (Promega, WI), and submitted for Sanger sequencing at the Oklahoma State University Core Facility. The 18s rRNA gene fragments were sequenced bidirectionally with primers Tryp_18s_IF, Tryp_18s_IR, as well as 827F and 662R from Maslov et al. (1996). The gGAPDH gene fragments were sequenced bidirectionally with primers Tryp_gGAPDH_IF and Tryp_gGAPDH_IR.

Comparing Success of Extraction and Amplification Methods

The number of cells isolated and successfully sequenced in each trial was tabulated and organized by the extraction and amplification methods (Table 1) as well as by morphotype (Table 2). A successful sequencing attempt was determined as one where the isolation, amplification, and sequencing led to high quality chromatograms that produced a sequence matching the expected morphology of the original isolated cell. The expected sequence for trypanosome morphotypes was not initially known but sequencing multiple cells of a given morphology established the sequence(s) defining that

morphotype. Comparisons of success between extraction and amplification methods as well as between morphotypes were performed with chi-square tests (Freund et al., 2010).

RESULTS

In total, 79 of 241 (33%) single trypanosome cell isolates were successfully amplified and sequenced. Trials for the 18s rRNA gene (50/122 41%) were more successful than gGAPDH (29/119 24%, Table 1). When comparing extraction methods, the Direct PCR kit method was the most successful (14/28 = 50%) and the No Extraction, Initial Hot/Cold PCR cycles method was the least successful (42/151 = 29%, $\chi^2 = 13.016$, $p = 0.0015$, Table 1). Across all methods and both genes, six morphotypes were successfully sequenced and success did not statistically differ between morphotypes ($\chi^2 = 4.0495$, $p = 0.5423$, Fig. 2). However, for 18s, the R2 morphotype had the highest success rate (9/16 = 56%) and the R3 morphotype had the lowest success rate (3/14 = 21%, Table 2). For gGAPDH, the H3 morphotype was the most successful (4/7 = 57%) and the *T.* cf. *ranarum* was the least successful (4/23 = 17%, Table 2).

Of the trials, the three nested PCR regimes (C, D, E) designed to multiplex and amplify both the 18s rRNA and gGAPDH from the same isolated cells were markedly less successful than those aiming for a single gene (A, B, $\chi^2 = 36.01$, $p = 1.97E-09$). Multiplexing worked for the 18s rRNA gene 18/84 (23%) times, and worked for gGAPDH 21/89 (22%) times, where nested PCR for a single gene worked more often, 31/38 (82%) times for 18s and 12/30 (40%) times for gGAPDH.

Included in the definition of a success as reported above was that the sequence obtained for a cell matched a sequence expected for a cell's morphology. There were four times (4/241 = 1.7%) when a cell was successfully sequenced but the sequence matched an unexpected morphology. This happened once for 18s, when a R3 morphotype came out as an R2 morphotype, and three times for gGAPDH, all three were expected to be R1 morphotypes but came out as *T. chattoni*, the R2 morphotype, and the R3 morphotype. These four sequences were counted as failures in Table 1 and were not used for further analyses in Chapter III.

DISCUSSION

The goal of the study was to develop a method to obtain sequences from trypanosome cells of known morphologies. To this end, all extraction methods and primer regimes had some success and generated sequences linked to cell morphology. However, the methods employed differed in their ease and success rate. For all methods, the 18s rRNA was much easier to amplify and sequence than gGAPDH. This could be due to the original gene copy number in trypanosome cells. Trypanosomes have upwards of 100 copies of the 18s rRNA gene, yet only two copies of the glycosomal GAPDH gene (Stothard, 2000; Hamilton et al., 2004). This technique for isolating and amplifying DNA from single trypanosome cells means that the starting DNA concentration is very low. With more copies in the genome, the 18s rRNA gene should have a higher number of primer binding sites and should be easier to amplify and sequence, which was found in this study. Additionally, the low copy number of gGAPDH could make it more

vulnerable to amplifying contaminating trypanosome morphotypes than the 18s rRNA gene, which was also found in this study as three gGAPDH sequences resulted from contamination compared to one in the 18s trials.

Initially, it was thought that multiplexing both 18s rRNA and gGAPDH genes from individual cells would be valuable for confirming the morphological identification of sequences in both gene phylogenies. However, multiplexing proved difficult, and trials without multiplexing (A, B) had a much higher success rate for both the 18s rRNA gene (81%) and gGAPDH (40%) than trials with multiplexing (C, D, E; 18s 23%, gGAPDH 21%). Additionally, some variation was found in the ease of sequencing certain morphotypes and the success rate ranged from 21% to 56% at 18s and 17% to 57% at gGAPDH (Table 2). It is possible that the primers developed and used in this study could have favored certain morphotypes, however at least two isolates worked for all morphotypes attempted. Even though the success rate was relatively low in some combinations of extraction methods and primer regimes, all morphotypes investigated were able to be sequenced in a novel way that links the sequence data to the trypanosome bloodstream morphology. Additionally, both genes were sequenced from multiple trypanosome individuals from multiple frog species across different locations in Oklahoma, Arkansas, Wisconsin, and New Hampshire. Finally, both genes were successfully sequenced with multiplex PCR from the same individual cell at least once for each morphotype, bolstering the identity of morphotypes on each phylogeny.

Multiple morphotype infections are an extremely interesting part of amphibian trypanosome biology but they present a difficult challenge to studying trypanosome diversity (Desser, 2001). Studies are increasingly using genetic methods to investigate

amphibian trypanosome diversity, but methods that address the difficulties posed by multiple morphotype infections have only recently begun to be implemented (Spodareva et al., 2018). This chapter presents an improvement to the cloning techniques used by Spodareva et al. (2018) with a method that directly links the sequence data generated with trypanosome bloodstream morphology. The methods presented here offer a promising solution to overcome the difficulties of multiple morphotype infections and the data generated here has interesting consequences for the current amphibian trypanosome phylogeny, which is explored in Chapter III.

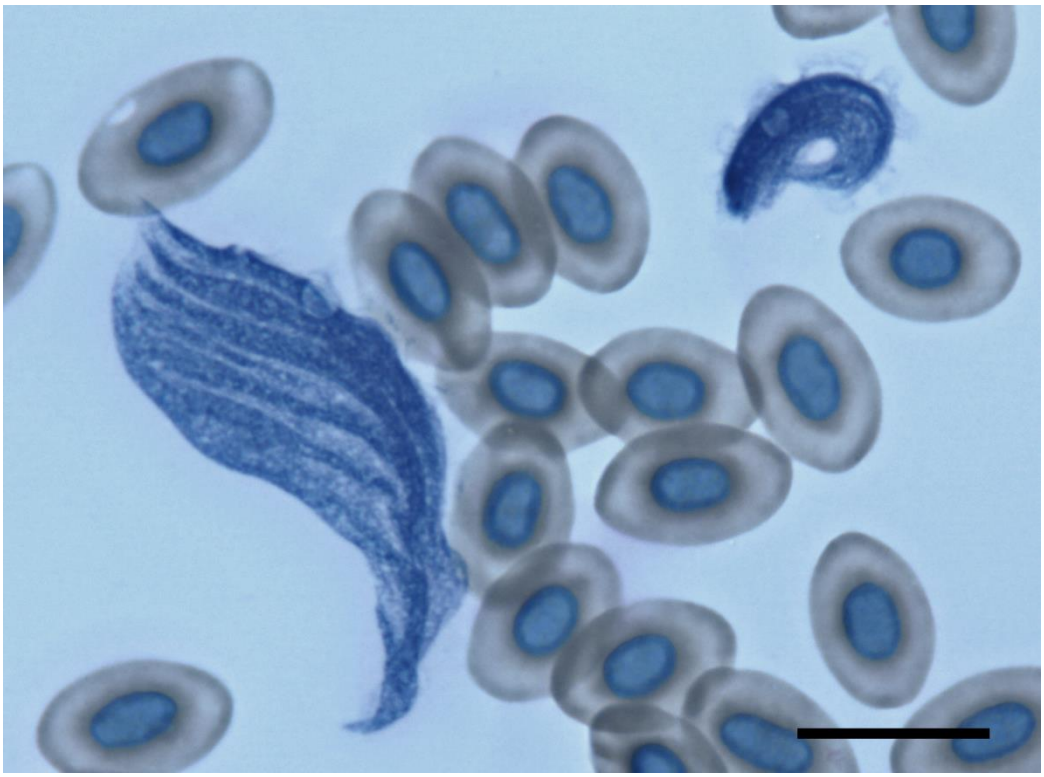

Figure 1. Photomicrograph of the R1 and R2 morphotypes coinfecting a single *Rana sphenocephala*. Multiple morphotype infections were common and necessitate methods to isolate morphotypes prior to amplification and sequencing. Scale bar = 20 µm.

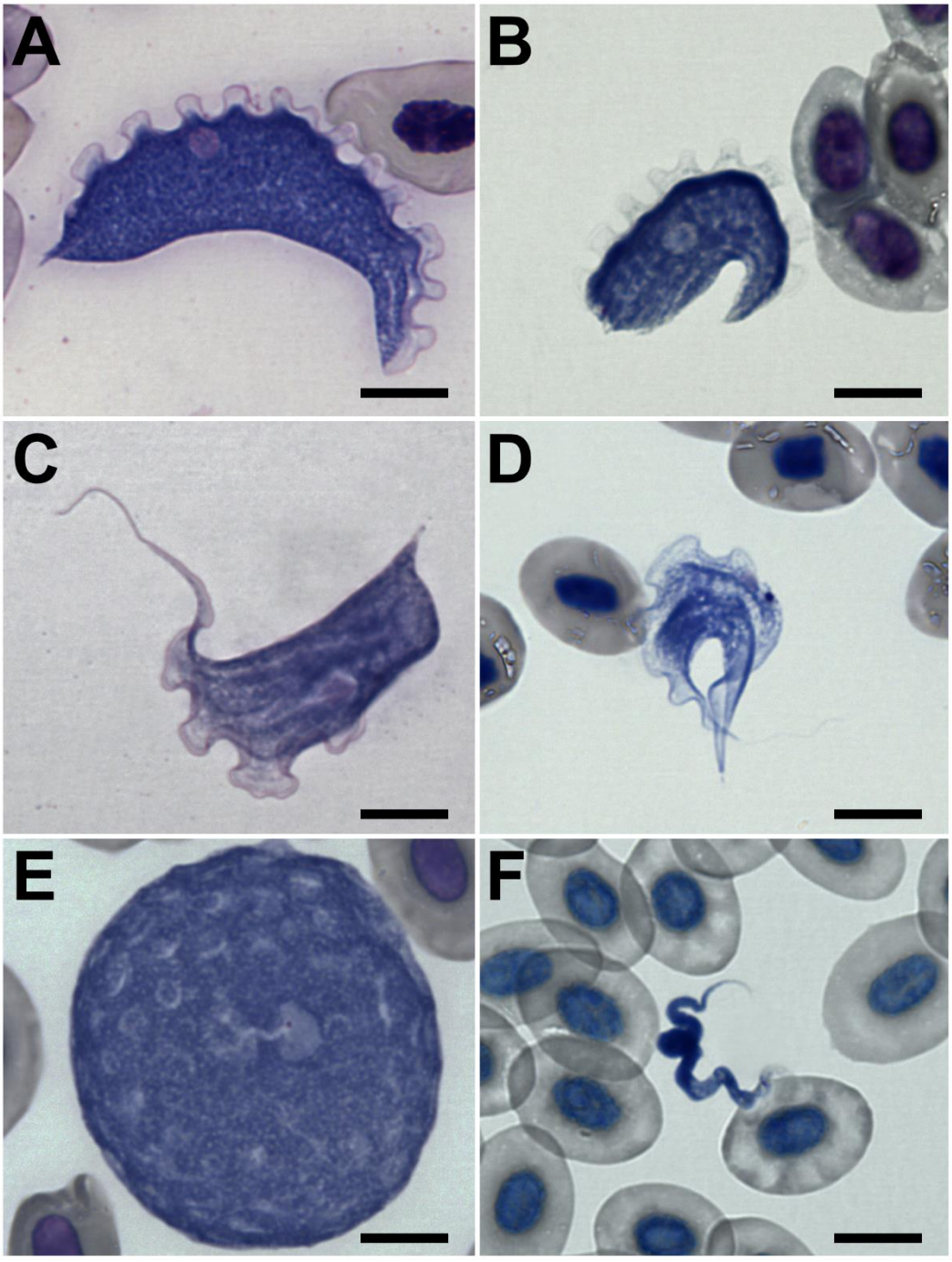

Figure 2. Photomicrographs of the 6 trypanosome morphotypes isolated in this study. **A.** Rl morphotype from *Rana clamitans*, **B.** R2 morphotype from *Rana sphenocephala*, **C.** *Trypanosoma* cf. *ranarum* from *Rana clamitans*, **D.** R3 morphotype from *Rana*

sphenocephala, **E.** *Trypanosoma* cf. *chattoni* from *Rana catesbeiana*, **F.** H3 morphotype from *Hyla cinerea*. Scale bars = 10 μm.

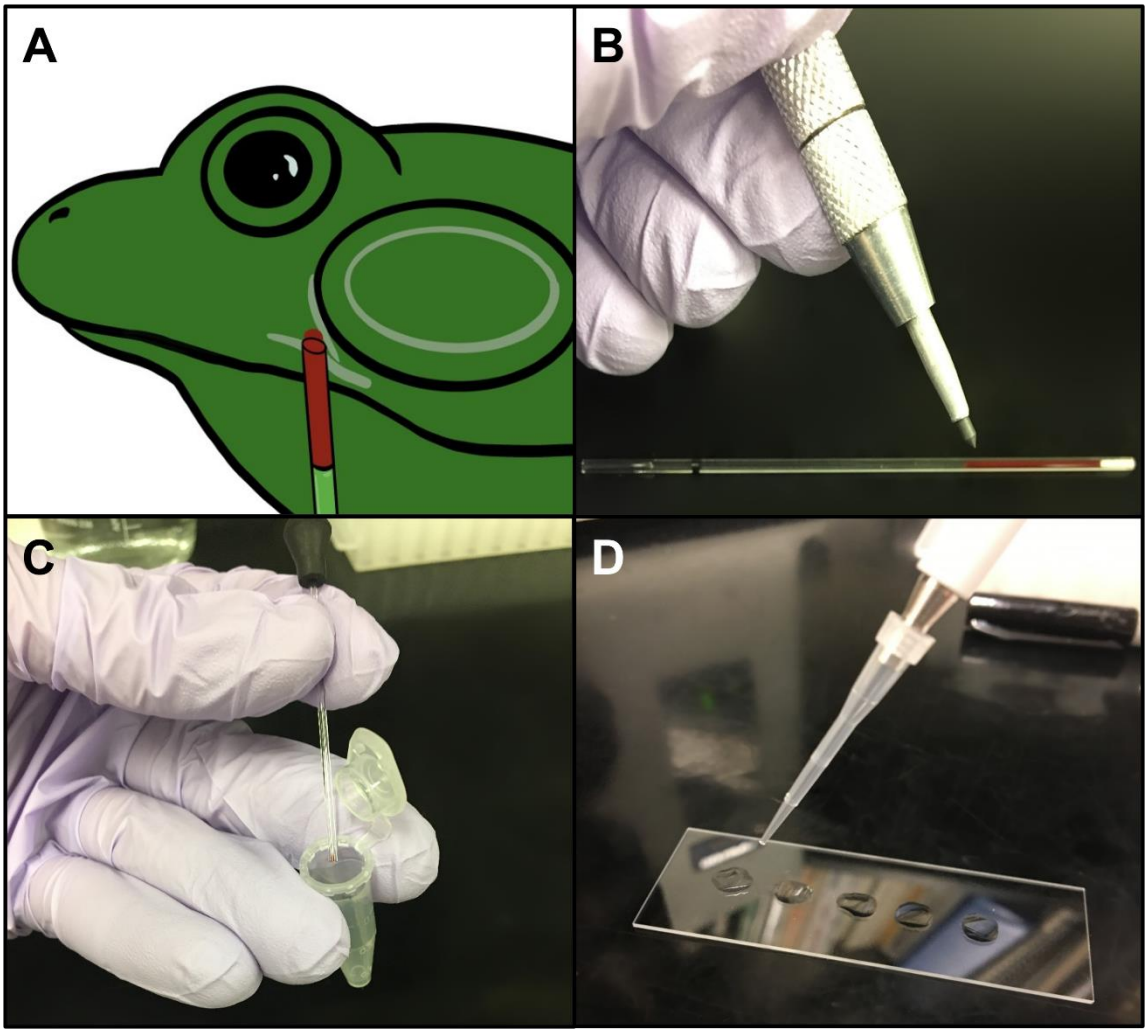

Figure 3. Blood collection and preparation to view and isolate trypanosomes. **A**. Diagram showing where the maxillary vein is punctured with a needle and blood is collected in a capillary tube. **B**. The capillary tube is centrifuged, separating red blood cells from plasma and concentration trypanosomes in the buffy coat layer. The capillary tube is scored with a glass scratcher just below the buffy coat layer. **C**. The tube is snapped and the buffy coat containing trypanosomes can be deposited into sodium citrate buffer, creating a stock for trypanosomes. **D**. The trypanosome stock is serially diluted in 20 µL drops of phosphate buffered saline.

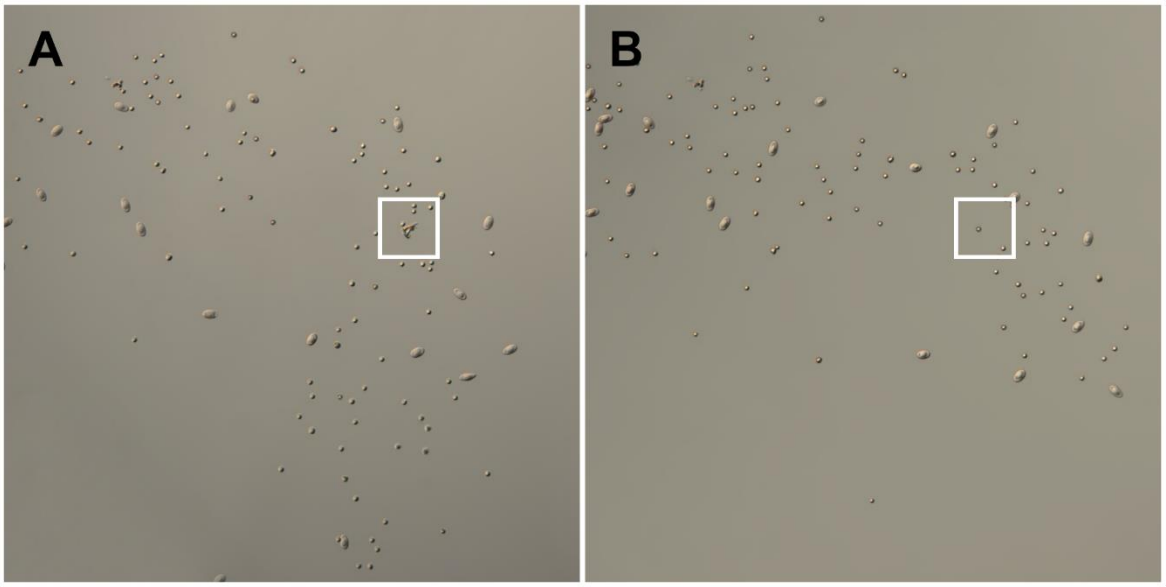

Figure 4. Photomicrographs of fresh green frog blood diluted in PBS buffer on a microscope slide and showing the location (white square) of before (**A**) and after (**B**) extraction of a live R1 morphotype trypanosome from the microscope slide. Both figures are at 200x magnification.

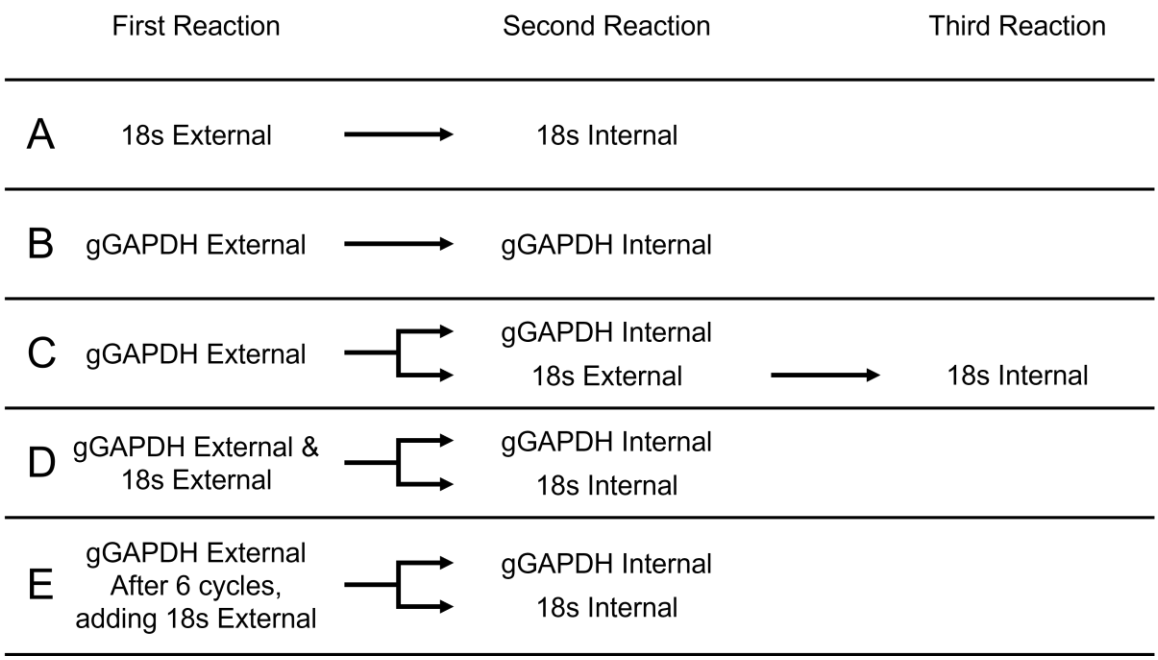

Figure 5. Schematic for five different (A-E) nested PCR primer combinations used to amplify the 18s rRNA and gGAPDH genes from individual trypomastigotes isolated from frog blood. Primer sequences are listed in the text.

Table 1. Sequencing success of the 18s rRNA and gGAPDH genes from isolated trypanosome cells organized by three different extraction methods and five different nested primer regimens. Data are presented as success/attempt (%).

Extraction Method	Primer Regimen	18s rRNA	gGAPDH
Modified Smaller Volume Extraction	A	6/6 (100%)	n/a
Modified Smaller Volume Extraction	B	n/a	3/5 (60%)
Modified Smaller Volume Extraction	C	6/23 (26%)	8/28 (29%)
	Subtotal	12/29 (41%)	11/33 (33%)
No Extraction, Initial Hot/Cold PCR cycles	A	16/18 (89%)	n/a
No Extraction, Initial Hot/Cold PCR cycles	B	n/a	4/11 (36%)
No Extraction, Initial Hot/Cold PCR cycles	D	5/8 (63%)	0/8 (0%)
No Extraction, Initial Hot/Cold PCR cycles	E	8/53 (15%)	9/53 (17%)
	Subtotal	29/79 (37%)	13/72 (18%)
Direct PCR Kit	A	9/14 (64%)	n/a
Direct PCR Kit	B	n/a	5/14 (36%)
	Subtotal	9/14 (64%)	5/14 (36%)
	Grand Total	50/122 (41%)	29/119 (24%)

Table 2. Sequencing success of the 18s rRNA and gGAPDH genes from isolated trypanosome cells organized by morphotype. Data are presented as success/attempt (%).

Morphotype	18s rRNA	gGAPDH
R1	19/45 (42%)	10/42 (24%)
R2	9/16 (56%)	4/16 (25%)
T. cf. *ranarum*	10/24 (42%)	4/23 (17%)
R3	3/14 (21%)	4/18 (22%)
T. cf. *chattoni*	7/16 (44%)	3/12 (25%)
H3	2/7 (29%)	4/7 (57%)
Total	50/122 (41%)	29/119 (24%)

CHAPTER III

INSIGHTS INTO AMPHIBIAN TRYPANOSOME DIVERSITY WITH THE ADDITION OF SEQUENCES MATCHED TO ISOLATE CELL MORPHOLOGY

ABSTRACT: Amphibians are commonly infected with multiple trypanosome morphotypes that are often assumed to represent pleomorphic stages of a single trypanosome species. These mixed infections make sequencing trypanosomes for genetic comparisons of morphological diversity difficult. In this study, I examined 15 amphibian species collected from nine locations across the central and eastern United States for their trypanosome diversity. In addition, I used a novel method to isolate and sequence individual trypanosome cells from amphibian blood to evaluate trypanosome genetic and morphological diversity. Of the fifteen amphibian species examined, six were found to be infected with trypanosomes. These included four species of true frogs (*Rana blairi*, *Rana catesbeiana*, *Rana clamitans*, and *Rana sphenocephala*), and two species of treefrogs (*Hyla avivoca* and *Hyla cinerea*). Twelve trypanosome morphotypes were recovered, six in true frogs and six in treefrogs. As expected, most trypanosome infected frogs were infected with multiple trypanosome morphotypes, with as many as five morphotypes occurring in an individual frog. Two pairs of morphotypes were suspected of being pleomorphic species based on coinfection frequency and morphological similarity.

However, all morphotypes were found to be genetically distinct. In fact, there is currently no genetic evidence from any study that has linked sequence data to trypanosome morphology that any amphibian trypanosome species is pleomorphic. Additionally, the removal of questionable sequences previously obtained from cultured trypanosome forms and commonly used in amphibian trypanosome phylogenetic analyses resulted in four clades of amphibian trypanosomes with general morphological similarities, strongly suggesting that amphibian trypanosome morphology is phylogenetically conserved across sampling locations in Europe and North America. This study suggests that with continued generation of sequences linked to morphology, the diversity and evolutionary history of amphibian trypanosomes can be better explored.

INTRODUCTION

The genus *Trypanosoma* (Trypanosomatida, Kinetoplasta) comprises more than 500 species of flagellated protozoa that infect the circulatory system of all classes of vertebrates (Roberts et al., 2013). However, most studies on trypanosomes have focused on a few species that infect mammals, primarily those that cause severe disease in humans and livestock (Bardsley and Harmsen, 1973; Hamilton et al., 2007; Espinosa-Álvarez et al., 2018; Spodareva et al., 2018). In contrast, trypanosomes of other vertebrate groups have largely been ignored in the scientific literature. This is particularly true of trypanosomes that infect amphibians, even though the first species representing the genus *Trypanosoma* were described from anurans (Bardsley and Harmsen, 1973; Spodareva et al., 2018). Currently, at least 70 species of *Trypanosoma* have been

described infecting amphibians worldwide, and in North America at least 26 species of trypanosomes have been reported infecting 36 amphibian species (Diamond, 1965; Bardsley and Harmsen, 1973; Martin and Desser, 1990; Desser, 2001; Bernal and Pinto, 2016).

Amphibians are interesting hosts for trypanosomes, because unlike other vertebrate groups, members of the class Amphibia are exposed to both terrestrial vectors such as blood feeding dipterans and aquatic vectors like leeches. In fact, previous studies have suggested amphibian trypanosomes are an evolutionary link between trypanosome species of terrestrial and aquatic vertebrate hosts (Vickerman, 2000; Spodareva et al., 2018). Additionally, amphibian trypanosomes are also some of the largest and most morphologically diverse species of *Trypanosoma* (Diamond, 1965; Woo, 1969; Barta and Desser, 1984, Desser, 2001). For example, some amphibian trypanosomes have "typical" trypanosome morphology and are long and slender with a free flagellum extending past the anterior portion of the cell (e.g. Fig. 7F). However, most amphibian trypanosomes are much wider than the typical trypomastigote form and vary in the presence or absence of the free flagellum (e.g. Figs. 7A-D). Additionally, some forms have such an atypical morphology that it is difficult to tell they are trypanosomes (Fig. 7E), and they can only be identified as trypanosomes by observing the kinetoplast and nucleus in stained preparations.

Although the morphological diversity and evolutionary relationships of amphibian trypanosomes are fascinating, the morphological diversity is difficult to characterize because amphibian infections commonly consist of multiple trypanosome morphotypes (Diamond, 1965; Bardsley and Harmsen, 1973; Desser, 2001; Spodareva et al., 2018).

For example, studies often find that 85-100% of frogs infected by trypanosomes are infected with two to five different trypanosome morphotypes (Diamond, 1965; Werner and Walewski, 1976; Jones and Woo, 1986; Attias et al., 2016; Spodareva et al., 2018). When observing these mixed trypanosome infections on amphibian blood smears, it is not clear whether the forms present in the bloodstream represent different species (genetic lineages) or a single pleomorphic species (one genetic lineage that takes more than one morphological form in the bloodstream). However, many authors have considered trypanosome morphotypes found infecting the same frog individual to represent a single species, often without any clear justification, and this has led to the assumption that most amphibian trypanosomes are pleomorphic (Fantham et al., 1942; Nigrelli, 1945; Diamond, 1965; Werner and Walewski, 1976, Desser, 2001).

Pleomorphism refers to changes in morphology through the development of trypanosome cells during their life cycle (Diamond, 1965; Desser, 2001). Technically, all trypanosomes are pleomorphic and change morphology when transmitted between vectors and vertebrate hosts (Vickerman, 1965; Roberts et al., 2013). In amphibian trypanosomes, this has been shown in experimental infections from trypanosome cultures. When culture forms are injected into a naïve frog, the individual trypomastigote cells start out as relatively small cells and over a period of about a month increase in size and develop to their adult morphological forms (Diamond, 1965; Martin and Desser, 1991; Desser, 2001). However, a pleomorphic trypanosome species refers to one that has multiple morphological stages in the bloodstream (Vickerman, 1965). Some of the most well studied and medically significant trypanosomes of humans (*Trypanosoma brucei* group) are pleomorphic in the bloodstream, with distinct trypomastigote morphologies

including slender forms and stumpy forms. These forms have important functions in the life cycle, where slender forms are proliferative in the bloodstream and stumpy forms are infective to the tsetse fly vector (Vickerman, 1965). Amphibians infected by multiple trypanosome morphotypes are often infected by specific pairs of morphologically similar morphotypes, and these associated forms have been commonly assumed to represent pleomorphic forms of the same species, like the slender and stumpy forms of *T. brucei* (Fantham et al., 1942; Nigrelli, 1944; Woo, 1969; Werner and Walewski, 1976). However, these assumptions have not been tested with controlled life cycle studies or genetic comparisons of morphotypes in mixed trypanosome infections of amphibian hosts, leading to a taxonomic nightmare where species descriptions are inconsistent in reports of pleomorphism and are often not usable for future comparisons (Desser, 2001).

The best demonstration of the problem comes from descriptions of the species *Trypanosoma rotatorium*. This trypanosome name has been reported from 21 different amphibian hosts and from all six continents having frogs (Bardsley and Harmsen, 1973). This species was reported to be pleomorphic with at least two forms by some authors (Fantham et al., 1942; Nigrelli, 1944; Woo, 1969; Werner and Walewski, 1976) and to consist of only one form by others (Diamond, 1965; Barta and Desser, 1984). Undoubtedly, many reports of *T. rotatorium* are not valid and do not refer to the original species. A recognized example is that researchers in North America used the name *Trypanosoma rotatorium* for a trypanosome that differs from the original morphological description in European amphibians (Diamond, 1965; Barta et al., 1989; Spodareva et al., 2018). Unfortunately, this trend is common for other amphibian trypanosome species as well, including *Trypanosoma chattoni*, which was originally described from Vietnam

from the Asian Toad, *Duttaphrynus melanostictus*, by Mathis and Léger (1911) yet has been reported in North and Central America (Diamond, 1965; Bardsley and Harmsen, 1973).

To overcome the taxonomic problems resulting from mixed morphotype infections, Desser (2001) argued for a specific list of information that needed to be characterized to describe amphibian trypanosome species. This included documenting the host associations and geographic localities, characterizing cell morphology and development in the bloodstream, and describing culture forms and vector stages of each trypanosome species by completing their life cycles in the laboratory. However, up to now, only two species, *T. pipentis* and *T. fallisi*, are reported to meet these characteristics. Since Desser (2001) published these criteria for identifying and describing amphibian trypanosome species based on morphological and life cycle data, technological advances have made obtaining genetic information much easier and genetic markers have been developed to help resolve the taxonomic conundrum of amphibian trypanosomes. However, the power of genetic methods is limited to the availability of sequences of identified trypanosomes for comparative purposes and the quality of the link between sequence data and the bloodstream morphological characteristics from which trypanosome species have been traditionally described (Diamond, 1965; Barta et al., 1989; Attias et al., 2016; Spodareva et al., 2018).

Establishing this link is a major challenge, as acquiring and interpreting sequence data from mixed infections is difficult. One problem is that if you directly sequence trypanosomes from frog blood containing a mixed infection, you can get messy chromatograms indicating there are multiple genotypes in the sample. Additionally, if

one of the multiple morphotypes is more numerous in the blood of their amphibian host, PCR can favor that genotype and result in clean chromatograms which look like a single genotype is present, hiding the true diversity of the infection (Shannon, unpublished observation). Another problem arises from sequencing cultured trypanosomes. Many amphibian trypanosomes sequences were obtained from cultured forms established from amphibian blood. However, as stated above, all trypanosomes drastically change their morphology from the vertebrate blood forms when cultured and it can be unclear which morphotype established in culture without doing controlled amphibian infections (Diamond, 1965; Bardsley and Harmsen, 1973; Martin and Desser, 1991; Martin et al., 1992; Attias et al., 2016). Therefore, the original bloodstream morphology is difficult if not impossible to confirm from sequences originating from trypanosome cultures.

To overcome these difficulties and obtain sequence data from individual trypanosome morphotypes, specific methods are needed. Spodareva et al. (2018) used cloning to separate and sequence gene copies amplified from multiple morphotype infections. This method provides clean sequence from each cloned bacterial colony, yet the origin of the sequence is usually unknown. Sequences must be assigned to morphotypes indirectly by repeating the cloning process on different frogs with different combinations of morphotypes. Additionally, PCR errors are exposed in this process, resulting in each clone sequence having 1-2 bases different at random positions. The assembly of cloned sequences into consensus sequences is then required to represent the taxa in phylogenetic comparisons (Brown, 2020).

I developed an improved method to link trypanosome morphology to sequence data by directly sequencing single cells with a known morphology (Chapter II). I

achieved this by diluting blood samples in PBS buffer down to small drops containing a single trypanosome cell, recording the cells' morphology, and directly amplifying and sequencing the 18s rRNA and gGAPDH genes from that specific cell (Chapter II). In this chapter, I use the 18s rRNA and gGAPDH sequence data generated in Chapter II to characterize the morphology and genetics of 6 of the 12 trypanosome morphotypes found in anurans examined from Arkansas, New Hampshire, Oklahoma, and Wisconsin, U.S.A. I then compare sequences of these 6 morphotypes with previous taxa in a phylogenetic context. In addition, I investigate the phylogenetic conservation of amphibian trypanosome morphology with a second 18s phylogeny that only includes sequences with confirmed trypomastigote morphology in the amphibian bloodstream.

MATERIALS AND METHODS

Collection of Specimens

During April through August of 2014-2021, 328 individuals of 14 anuran species and ten individuals of one caudatan species were collected and examined for blood protozoa. Sampling occurred in Arkansas, New Hampshire, Oklahoma, and Wisconsin (Table 3). Species sampled from Teal Ridge Aquatic Wetland, Stillwater, Oklahoma (36°06'03.3" N, 97°04'48.3" W) included *Acris blanchardi* (N=28), *Ambystoma texanum* (N=10), *Anaxyrus americanus* (N=2), *Anaxyrus woodhousii* (N=5), *Gastrophryne olivacea* (N=28), *Hyla chrysoscelis* (adults N=11, tadpoles N=13), *Pseudacris clarki* (N=5), *Rana catesbeiana* (N=13), *R. sphenocephala* (N=30). Species from Hennessey, Oklahoma (36°07'00.0" N, 97°53'56.0" W) included *R. blairi* (N=4) and *R. catesbeiana*

(N=2). Species from Guthrie, Oklahoma (35°48'38.4" N, 97°24'08.6" W) included *R. sphenocephala* (N=7). Species from Red Slough WMA, McCurtain Co. Oklahoma (33°44.897' N, 094°38.549' W) included *R. catesbeiana* (N=15), *R. clamitans* (N=7), and *R. sphenocephala* (N=1). Species from Little River NWR, McCurtain Co. Oklahoma (33°57.200' N, 094°42.166' W) included *H. avivoca* (N=9), *H. cinerea* (N=9), *R. clamitans* (N=2), and *R. sphenocephala* (N=2). Species from Blue Haze Vista, Arkansas (34°37'40.17" N, 94°14'44.4228" W) included *R. catesbeiana* (N =2) and *R. clamitans* (N=14). Nine of the *R. clamitans* were reported in McCallister et al. (2020). Species from Ouachita Mountains Biological Station, Arkansas (34°27'44.5" N, 93°59'54.2" W) included *H. cinerea* (N=5), *R. catesbeiana* (N=17), and *R. clamitans* (N=10). Additionally, eight *R. clamitans* were collected from Woodward Park, New London, New Hampshire (43°24'51" N, 71°59'32" W) and fifteen *R. clamitans* were collected from Muskego, Waukesha County, Wisconsin (42°51'13.1764" N, 88°7'22.944" W).

Amphibians were collected by hand or by dip-net. Adult and newly metamorphosed amphibians were placed in moist cotton bags, whereas all larval amphibians were placed in 18.9 L buckets filled with pond water and transported to the laboratory. In the laboratory, amphibians were double pithed and examined for blood protozoans within 12 hours of capture.

Blood Processing and Examination

For adult and newly metamorphosed amphibians, blood was drawn by puncturing the facial vein with a 26-gauge needle and collecting a drop of blood in capillary tubes

following the methods of Forzán et al. (2012). For tadpoles, the tail vein was punctured with a 26-gauge needle and blood was collected in capillary tubes, as described by Diamond (1965). For each amphibian individual, a drop of blood from a single capillary tube was deposited on a glass slide with a pipette bulb and a thin smear prepared. When possible, one capillary tube was centrifuged to observe live trypanosomes swimming and for isolation of single cells (See below).

Thin blood smears were air-dried and stained with the JorVet Dip Quick Stain Kit (Jorgensen Labs, CO). Stained slides were scanned at low power (10x objective) with an Olympus BX-51 upright research microscope for approximately 10 minutes to detect trypanosomes. When *Trypanosoma* spp. were found on smears, up to 20 trypomastigotes of each morphology were photographed with an Olympus 5-megapixel digital camera. Trypanosome cell dimensions and organelle positions were measured on photomicrographs (Fig. 6) using ImageJ (Schneider et al., 2012) calibrated with a stage micrometer (Reichert, NY). If possible, ten trypanosomes were photographed and measured from each infected frog, however not all measurements could be taken for all specimens because often organelles or flagella were not visible on each individual trypanosome. For the round form *T.* cf. *chattoni*, the maximum cell diameter was recorded for body length and the diameter perpendicular to the maximum diameter measurement was recorded for the body width.

Prevalence for trypanosome morphotypes was calculated according to Bush et al. (1997) and 95% confidence intervals were calculated for the number of frogs of each species sampled (Rohlf and Sokal, 1995). Morphotype richness within infected frogs was

calculated as the sum of trypanosome morphotypes per individual amphibian, excluding uninfected individuals, divided by the number of infected amphibians (Bush et al., 1997).

To determine whether morphotypes were morphologically distinct, measurements were tabulated and analyzed with Principal Component Analysis (PCA) in R version 4.1.2 using the prcomp function with scaled variables (R Core Team, 2021). Five metrics were used for PCA: body width (BW), body length (PA), area of the elliptical nucleus (NArea = π*LN*WN), and ratios of the kinetoplast to the posterior end of the cell body length over the body length (PK/PA), and nucleus to the posterior end of the cell body length over the body length (PN/PA). Trypanosomes from ranids and hylids were analyzed separately (Figs. 9 and 10).

Trypanosome Isolation and Sequencing

Trypanosomes were isolated from amphibian blood by dilution of plasma obtained by centrifuging infected blood in capillary tubes as described previously in Chapter II. Briefly, capillary tubes with frog blood were sealed with Cha-Seal (Kimble, NJ) and centrifuged for 1 minute at 4,000g, which concentrates trypanosomes and white blood cells in the buffy coat layer (Jones and Woo, 1989). The capillary tubes were scored with a glass scratcher just below the buffy coat layer, allowing the tube to be snapped at the scored location, and the buffy coat and plasma was dispensed into phosphate buffered saline (PBS) using a pipette bulb attached to the snapped capillary tube. Small samples (5 µL) of this stock solution of trypanosomes in buffer could then be further diluted in 20 µL drops of buffer on glass microscope slides and examined with a

microscope to find trypanosomes to isolate. When found, 2 µL were pipetted from the approximate area of the drop where a single trypanosome was observed and deposited into a new 5 µL drop of buffer. The new drop was then observed to see if transferring the trypanosome was successful. Most of the time multiple trypanosomes are transferred, but by repeating this process dilution of pipetting 2 µL samples with a trypanosome into new drops of buffer, one can make drops of buffer containing only a single trypanosome cell. These cells were then collected in 1-2 µL samples and transferred into 200 µL PCR tubes for DNA extraction, PCR amplification, and gene sequencing.

Extraction and Amplification of Isolated Trypanosome DNA

DNA was extracted and amplified directly from single cell isolates with the Platinum Direct PCR Universal Master Mix Kit (Thermofisher) with the following modifications. A stock lysis buffer containing 19.4 µL of lysis buffer and 0.6 µL proteinase K was prepared and 1-2 µL of this stock buffer was added to the 1-2 µL sample containing a single trypanosome for a total volume of 3 µL. This sample was incubated at room temperature for one minute, followed by one minute at 98°C on a thermal cycler. The sample was then returned to room temperature and PCR reagents were added and nested PCR was performed.

For amplification of the 18s rRNA gene, the first reaction was performed with external primers Tryp_18s_EF (5'-GATAACTTGGCGAAACGCC-3') and Tryp_18s_ER (5'-GCAATACTCGGTCCCAAGTG-3') with an annealing temperature of 58°C. For the second reaction, 1 µL of the first PCR product was used as the template for

the second, and internal primers Tryp_18s_IF (5'-AACCCATCCAATATCGAGTAAC-3') and Tryp_18s_IR (5'-GTTGCCCAAAATCTCACC-3') were used with an annealing temperature of 55°C. The internal and external primer sets were designed from an alignment of available frog trypanosome 18s rRNA sequences (Martin et al., 2002).

Amplification of glycosomal glyceraldehyde-3-phosphate dehydrogenase (gGAPDH) gene was also performed with nested PCR. The first reaction used the external primers Tryp_gGAPDH_EF (5'-GACATGAACACSGACGC-3') and Tryp_gGAPDH_ER (5'-GATGGAGCTRCGGTTGTC-3') with an annealing temperature of 55°C. The second reaction was performed with 1 µL of the first reaction as template, and the internal primers Tryp_gGAPDH_IF (5'-CGCGTACCAGATGAAGTACG-3') and Tryp_gGAPDH_IR (5'-CGGTTGTCRTTGATGAAGTC-3') with an annealing temperature of 55°C. These primers were designed using an alignment of available frog gGAPDH sequences (Hamilton et al., 2004).

PCR was performed with the Platinum Direct PCR Universal Master Mix Kit (Thermofisher) as follows: initial activation for 300s at 95°C, denaturation for 30s at 95°C, annealing for 30s at the appropriate temperature for the primer pair listed above, and extension for 60s at 72°C, repeated for 30-40 cycles before a final extension period of 420s at 72°C. The products of the nested PCRs were checked with gel electrophoresis for single bands of the appropriate size, 1200 base pairs for 18s rRNA and 800 for gGAPDH. If PCR was successful, the product was cleaned up with the Wizard® SV gel and PCR cleanup kit (Promega, WI), and submitted for Sanger sequencing at the Oklahoma State University Core Facility. The 18s rRNA gene fragments were sequenced

bidirectionally with primers Tryp_18s_IF, Tryp_18s_IR, as well as 827F and 662R from Maslov et al. (1996). The gGAPDH gene fragments were sequenced bidirectionally with primers Tryp_gGAPDH_IF and Tryp_gGAPDH_IR.

Phylogenetic Analyses

The 18s rRNA gene sequences obtained in this study were combined with the sequences used for the phylogenetic analyses in Attias et al. (2016) and Spodareva et al. (2018), which were accessed from GenBank. Sequences were aligned with the MUSCLE (Edgar, 2004) feature of MEGA X (Kumar et al., 2018). The alignment was visually inspected and corrected, resulting in a final alignment of 106 sequences with 1302 positions. The phylogeny was estimated using the Maximum Likelihood (ML) framework within MEGA X (Kumar et al., 2018). The TN93+G+I model (Tamura and Nei, 1993) was found to be the best fit (lowest BIC score of models tested, 20423.415) using the MEGA X model selection feature. Support values of nodes were assessed using 1000 bootstrap replications.

The 18s rRNA alignment used above had two important modifications. The first was that I generated consensus sequences for the clones sequenced by Spodareva et al. (2018). Spodareva et al. (2018) obtained sequences of amphibian trypanosomes from frogs with multiple infections by cloning partial 18s sequences, resulting in sequences for each morphotype but with PCR errors. To use their sequences in phylogenetic analyses, Spodareva et al. (2018) formed consensus sequences for each morphotype, but they only deposited raw sequences on GenBank. Therefore, I generated consensus sequences from

the sequences of each morphotype deposited on GenBank by Spodareva et al. (2018) with Geneious Prime 2021.1.1 using a 70% consensus threshold. The second important modification was a correction in how MUSCLE was aligning AF119810.1 *Trypanosoma ranarum*. This sequence has a gap of unknown data marked with 21 N's in the middle that actually represents 80 missing bases, and when misaligned creates a large branch length for this taxon that has been shown in many previous trypanosome phylogenies (Hamilton et al., 2007; Bernal and Pinto, 2016; Spodareva et al., 2018). When the gap of missing data is enlarged by 59 bases, the sequence is compared correctly to sequences generated in this study from trypanosomes with the same morphology as trypomastigotes from which the AF119810.1 *Trypanosoma ranarum* sequence was generated, and there are not nearly as many unique bases (see below).

The gGAPDH sequences obtained in this study were added to those from Hamilton et al. (2007), Attias et al. (2016), and Spodareva et al. (2018) and aligned with the MUSCLE (Edgar, 2004) feature of MEGA X (Kumar et al., 2018). The final alignment included 58 sequences and was 592 positions. The phylogeny was estimated using the ML framework within Mega X (Kumar et al., 2018). The T92+G model (Tamura, 1992) was found to be the best fit using the MEGA X model selection feature. Support values of nodes were assessed using 1000 bootstrap replications.

In addition to phylogenies, genetic distances were calculated to compare genetic variation within and between morphotypes in MEGA X (Kumar et al., 2018). The same alignments used for phylogenies were used for distances. For the 18s rRNA gene, distances were estimated using the TN93+G model with the pairwise deletion option

(Tamura and Nei, 1993, Table VI). For gGAPDH, distances were estimated using the T92+G model with the pairwise deletion option (Tamura, 1992, Table VII).

Many sequences included in the above phylogenies on amphibian trypanosomes included sequences that came from culture collections. These sequences are difficult if not impossible to track back to the original morphology in the bloodstream of their amphibian hosts because trypanosomes drastically change their morphology when cultured. As a result, I made an additional 18s phylogeny only using sequences obtained from cultured forms that could be linked to the morphology of trypomastigotes from the bloodstream of anurans. Cultured sequences were only included if there was published evidence demonstrating that experimentally infected anurans inoculated from cultured forms yielded infections of only trypomastigotes with the appropriate morphology for that particular species (Martin et al., 1992). Additionally, sequences were included from studies that demonstrated anurans were only infected with a single morphotype (Bernal and Pinto, 2016). The sequences in the aquatic clade and the terrestrial clade outgroup were the same from the original 18s phylogeny. The ML phylogeny was constructed with the partial 18s rRNA gene (1292 bp, -Ln = -7283.83) using the K2P+G+I model in MEGA X (Kumar et al., 2018). Support values of nodes were assessed using 1000 bootstrap replications.

For this additional 18s tree, I included the sequences obtained in Chapter II of this dissertation because they came from isolated cells that were identified before sequencing. I also included the consensus sequences of *T. loricatum*, *T.* sp. ring morphotype, *T. ranarum*, *T. rotatorium*, and *T.* sp. nautilus morphotype from Spodareva et al. (2018), which were obtained by sequencing clones made from mixed PCR products that could

then be tracked back to morphologies observed on blood smears. The two sequences of *T. tungarae* from Bernal and Pinto (2016) were also retained as they came from frogs assumed to be infected by only one trypanosome morphology. Finally, the sequences of *T. fallisi* and *T. ranarum* were retained because Martin et al. (1992) reinfected naïve frogs with these cultures and observed the correct bloodstream morphology in laboratory infected frogs.

The sequences I excluded did not have any confirmation of bloodstream morphology. For example, Martin et al. (1992) indicated that their identification of cultured forms of *T. rotatorium* (corresponding to sequences U39583.1 and AJ009161.1) was inferred from evidence other than bloodstream trypomastigote morphology because they were unable to infect frogs in the laboratory from *T. rotatorium* cultures. Therefore, I excluded U39583.1 and AJ009161.1 from this phylogeny. Additionally, sequences from culture forms of *T. chattoni* (KT765865.1 and AF119807.1) of Attias et al. (2016) and Martin et al. (2002) were excluded. The original cultures of *T. chattoni* were isolated from a single northern leopard frog, *Rana pipiens*, collected by Diamond (1965). Although Diamond (1965) was able to infect two frogs in the laboratory with culture forms of *T. chattoni* that produced blood forms resembling *T. chattoni* isolated from the blood of field collected frogs, many of the frogs collected from Anoka County were coinfected with *T. pipientis* and other amphibian trypanosomes. Previous phylogenetic analyses place 18s sequences for *T. chattoni* sister to amphibian trypanosome species that are morphologically similar to *T. pipientis* (long and skinny trypanosomes). Additionally, in the phylogenetic analyses in the present study, the *T. chattoni* sequences came out in distinct clades from all 18s and gGAPDH *T.* cf. *chattoni* sequences obtained in this study

from isolated cells. Therefore, it is not clear if Diamond (1965) established pure cultures of *T. chattoni*. Finally, the sequences of *T. neveulemairei*, *T. therezieni*, *T. mega*, and sequences from cultured trypanosomes from Attias et al. (2016) cannot be linked to forms from the bloodstream of frogs, because they were isolated for culturing without recording their morphology from the blood of their amphibian hosts.

RESULTS

Trypanosome Morphotype Prevalence

Of the fifteen amphibian species examined, six were found to be infected with trypanosomes (Table 3). These included four species in the family Ranidae, *Rana blairi*, *Rana catesbeiana*, *Rana clamitans,* and *Rana sphenocephala*, (Table 4) and two members of the Hylidae, *Hyla avivoca* and *Hyla cinerea* (Table 5). Twelve trypanosome morphotypes were recovered. Six were found in ranid frogs (R1-R4, *T.* cf. *ranarum*, and *T.* cf. *chattoni*, Fig. 7) and six morphotypes were unique to hylids (H1-H6, Fig. 8).

Of the ranid frogs, *Rana clamitans* had the highest prevalence (79%) and was infected with all six morphotypes found in ranids (Table 4). The most commonly observed trypanosome morphotype in ranids was the R1 form, which infected all ranids except *R. palustrus*. The R2 form was mainly found infecting leopard frogs *R. blairi* and *R. sphenocephala*, except for a single *R. clamitans* infection. *Trypanosoma* cf. *chattoni* and the *T.* cf. *ranarum* had similar prevalence in *R. catesbeiana* and *R. clamitans*, but *T.* cf. *chattoni* had a higher prevalence in *R. sphenocephala* than *T.* cf. *ranarum*. Lastly, the R3 and R4 forms were the least prevalent morphotypes infecting true frogs. The R3 form

was found in *R. catesbeiana, R. clamitans*, and *R. sphenocephala* while the R4 form was only found in *R. clamitans* and *R. sphenocephala* (Table 4).

For the hylid frogs, *Hyla cinerea* was most commonly infected species and the morphotypes infecting *H. cinerea* differed by collection site. *Hyla cinerea* collected in Oklahoma was infected with H1, H2, and H3 morphotypes; whereas *H. cinerea* sampled from Arkansas was infected with the H4, H5, and H6 morphotypes. A single *H. avivoca* of 12 collected in Oklahoma was infected with two morphotypes, H2 and H3 (Table 5).

Both ranids and hylids were often infected with multiple trypanosome morphotypes. Specifically, 59 of 88 (67%) infected ranids and 8 of 10 (80%) infected hylids were simultaneously infected with two or more trypanosome morphologies as observed on blood smears. In ranids, multiple infections were most common in *Rana sphenocephala* (19/23 infected frogs, 83%), followed by *R. catesbeiana* (12/18, 66%), *R. clamitans* (27/44, 61%), and *R. blairi* (1/3, 33%). The average infected ranid morphotype richness was 2.0 and was lowest 1.3 (range 1-2) for *R. blairi* and highest 2.1 (range 1-5) for *R. sphenocephala*. The maximum number of morphotypes found infecting a single frog was 5 and occurred in one *R. sphenocephala* and one *R. clamitans* (Table 3). In hylids, 7 of 9 (77%) *Hyla cinerea* and the single *Hyla avivoca* had at least 2 morphotypes. Average infected hylid trypanosome morphotype richness was 1.9; being 1.9 (range 1-3) in *H. cinerea* and 2.0 (range 1-2) in *H. avivoca* (Table 3).

In addition to finding multiple morphotypes in a single frog, specific morphotypes were often associated together in the same frog individuals. In ranids, all eleven frogs infected with the R3 morphotype were also infected with morphotype *T.* cf. *ranarum*.

Additionally, 75% (18/24) of ranids infected with the R2 morphotype were also infected with the R1 morphotype. These two pairs were interesting because they were also similar morphologically, the main difference was one form being larger than the other (Fig. 7). Lastly, 80% (35/44) of frogs infected with morphotype *T.* cf. *chattoni* were also infected with a morphologically distinct morphotype, R1 (Fig. 7). Morphotypes in hylids were also found together but the sample sizes are lower than the ranids. All 3 hylids infected with morphotype H1 were infected with morphotype H2 and 4 of 5 (80%) hylids infected with morphotype H3 were also infected with morphotype H2.

Descriptions of Trypanosome Morphology and Motility in Amphibian Blood

Trypanosomes of Ranids (Fig. 7)

R1 Morphotype (Fig. 7A)

Large, broad trypanosome with no free flagellum (PA 57.22 ± 7.38, BW 12.73 ± 3.87, Fig. 7A). Often appears flat like a sheet, or with longitudinal folds depending how cells rest when fixed on slides. Kinetoplast near the posterior end (PK/PA 0.17 ± 0.05), nucleus circular and about a third of the length of the cell from the posterior end (PN/PA 0.35 ± 0.05, Table 6). Both the kinetoplast and nucleus are off the midline of the cell, closer to the undulating membrane. The undulating membrane begins at the kinetoplast and ends at the anterior end of the cell. In live preparations of blood plasma, the undulating membrane flutters quickly, however the actual movement of the whole cell is gentle. Sometimes spinning and tumbling, the main direction of cell movement is perpendicular to the anterior-posterior axis, towards the undulating membrane.

R2 Morphotype (Fig. 7B)

Short, broad trypanosome (PA 34.76 ± 3.56, BW 10.6 ± 3.61, Fig. 7B) with a curved anterior end. Kinetoplast close to the posterior end of the cell (PK/PA 0.1 ± 0.05), nucleus circular and located about a third of the way from posterior to anterior end of cell body (PN/PA 0.36 ± 0.04). Both the kinetoplast and nucleus are off the midline of the cell, closer to the undulating membrane. Flagellum spans the length of the cell, terminating at the anterior end with no free flagellum. This form looks similar to morphotype R1 and differs only in the body length (PA), position of the kinetoplast (PK/PA), and curved anterior end (Table 6). In live preparations of blood plasma, the curved form moves toward the curved anterior end as the undulating membrane flutters along the length of the cell.

***Trypanosoma* cf. *ranarum* (Fig. 7C)**

Large, broad trypanosome with a free flagellum (PA 52.85 ± 7.11, BW 13.27 ± 3.73, Fig. 7C). Ends of cells come to a point, and the cell is often twisting to form an S or C shape. Kinetoplast about a third of the way from posterior to anterior end (PK/PA 0.33 ± 0.06), nucleus circular and just under halfway from the posterior end to anterior end of the cell body (PN/PA 0.45 ± 0.06). Both the kinetoplast and nucleus are off the midline of the cell, closer to the undulating membrane. The undulating membrane begins at the kinetoplast and extends into a free flagellum that was on average 14.75 ± 3.69 µm long (Table 6). When observed live in blood plasma, the free flagellum extends forward away from the cell and twists rapidly, pulling the rest of the cell body anteriorly in a spiral.

R3 Morphotype (Fig. 7D)

Medium sized trypanosome with a free flagellum (PA 46.07 ± 7.76, BW 7.19 ± 2.43, Fig. 7D). Both anterior and posterior ends taper to points. The kinetoplast is just under halfway (PK/PA 0.46 ± 0.06) from the posterior to the anterior end of the cell body, while the circular nucleus is located approximately halfway along the cell body (PN/PA 0.51 ± 0.05). Both the kinetoplast and nucleus are off the midline of the cell, closer to the undulating membrane. The flagellum extends past the anterior end of the cell (FF 12.03 ± 6.65). This form looks like a smaller version of *T.* cf. *ranarum*, with smaller body length (PA), body width (BW), and nucleus length and width (LN, WN). Additionally, the kinetoplast and nucleus are more anterior than in *T.* cf. *ranarum* (PK/PA, PN/PA, Table 6). In live blood plasma preparations, the posterior end generally stays straight, and the anterior end rotates as the flagellum pulls the cell body in a circular rotation.

***Trypanosoma* cf. *chattoni* (Fig. 7E)**

Unique trypanosome that is spherical with golf ball-like dimples around its surface. The diameter of this morphotype is similar in size to the cell lengths of the smaller morphotypes, such as the R2 and R4 morphotypes (PA 34.37 ± 7.46, BW 30.52 ± 6.94, Fig. 7E, Table 6). The nucleus and kinetoplast are near the center of the cell, and an internal flagellum extends from the kinetoplast. These cells are not motile in live preparations.

R4 Morphotype (Fig. 7F)

Small, slender trypanosome with a free flagellum (PA 31.67 ± 5.6, BW 2.18 ± 0.5, Fig. 7F). Kinetoplast about a fifth of the way from posterior to anterior of the cell

body (PK/PA 0.18 ± 0.09). The nucleus is oval in shape and located about two fifths of the way from posterior to anterior end of the cell body (PN/PA 0.42 ± 0.07). The flagellum extends past the anterior end of the cell (FF 15.54 ± 3.12) and is about half the length of the cell body (FF/PA 0.48 ± 0.11). This form is similar to the H6 slender morphotype form in hylids, but the kinetoplast and nucleus are closer to the posterior end in the R4 morphotype found in ranid hosts (Tables 6 and 7). In live blood plasma preparations, the cells writhe and twist without great progress in any specific direction.

Trypanosomes of Hylids (Fig. 8)

H1 Morphotype (Fig. 8A)

This long, slender trypanosome was the longest trypanosome found in this study and was often observed coiled up in a spiral (PA 74.98 ± 9.8, BW 5.08 ± 1.08, Fig. 8A). The kinetoplast was located near the posterior end of the cell body (PK/PA 0.11 ± 0.02). The nucleus is oval in shape and fills the whole cell width in its' position about a fifth of the way along the cell (PN/PA 0.2 ± 0.04, Fig. 8A). The flagellum extends past the anterior end of the cell and is on average about one third of the cell length 24.45 ± 3.18 (Table 7). This form spirals like a corkscrew in live blood plasma preparations.

H2 Morphotype (Fig. 8B)

Small, slender trypanosome with a free flagellum and a unique pre-flagellar extension that often rests such that the anterior end of the cell appears like the head of a horned goat or ibex (PA 34.82 ± 11.89, BW 3.83 ± 1.41, Fig. 8B). Kinetoplast near the

posterior end (PK/PA 0.14 ± 0.04) and nucleus positioned about a third from posterior to anterior end (PN/PA 0.34 ± 0.06). The flagellum extends past the anterior end of the cell and is quite variable in observed length, ranging from 18.37 to 30.05 µm with an average length of 19.41 ± 9.33 (Table 7). In blood plasma preparations, this form was observed rocking back and forth with its flagellum extending perpendicular to the cell at the anterior end.

H3 Morphotype (Fig. 8C)

Small, slender trypanosome with a free flagellum (PA 40.31 ± 5.05, BW 2.85 ± 0.78, Fig. 8C). Kinetoplast near the posterior end (PK/PA 0.14 ± 0.05) and nucleus positioned about a third from posterior to anterior end of the cell body (PN/PA 0.36 ± 0.07). Flagellum extends past the anterior end of the cell (FF 19.91 ± 3.03, Table 7). The H3 morphotype was very similar to the H2 morphotype but did not have the pre-flagellar extension observed in the H2 morphotype. In live blood plasma preparations, the cells writhe and twist without great progress in any specific direction.

H4 Morphotype (Fig. 8D)

Medium sized, broad trypanosome with a rounded posterior end (PA 40.92 ± 5.16, BW 15.17 ± 3.65, Fig. 8D). Kinetoplast positioned about a third of the length from posterior to anterior end of the cell body (PK/PA 0.31 ± 0.08). The nucleus is elongate in shape and just ahead of the kinetoplast (PN/PA 0.42 ± 0.09). Free flagellum is short (FF 10.94 ± 2.11, Table 7). This form was not observed alive in blood plasma, as all samples were obtained from fixed blood smears.

H5 Morphotype (Fig. 8E)

Small, broad trypanosome with a rounded posterior end (PA 30.01 ± 2.97, BW 11.69 ± 2.56, Fig. 8E). Kinetoplast near the posterior end of the cell body (PK/PA 0.13 ± 0.05). Nucleus elongate and about a third of the way from posterior to anterior end of the cell body (PN/PA 0.32 ± 0.08). Free flagellum about two thirds in length of the cell body length (FF 20.45 ± 4.79, FF/PA 0.7 ± 0.2). This form was similar to the H4 morphotype, but was smaller in cell length (PA), cell width (BW), and organelles were positioned more posterior in the cell body (PK/PA, PN/PA, Table 7). This form was not observed alive in the blood of frogs.

H6 Morphotype (Fig. 8F)

Small, slender trypanosome with a free flagellum (PA 37.3 ± 2.67, BW 2.74 ± 0.62, Fig. 8F). Kinetoplast distant from posterior end (PK/PA 0.4 ± 0.02). Nucleus a little past halfway between the posterior and anterior end of the cell body (PN/PA 0.57 ± 0.03). The flagellum extends past the anterior end of the cell and is about half the length of the cell (FF 21.34 ± 1.39, FF/PA 0.57 ± 0.06). This morphotype looked similar to the slender R4 form found in ranids, but the kinetoplast and nucleus were more anterior in this form (PK/PA, PN/PA, Tables 6 and 7). This form was not observed alive in frog blood plasma.

Trypanosome Morphology and Principal Component Analysis

The six morphotypes infecting ranids and six morphotypes infecting hylids were morphologically distinct (Fig. 9A and 10A). More specifically, they were easily separated

by cell size and/or the positions of the nucleus and kinetoplast along the midline of the cell. PCA showed clusters of morphotypes based on cell measurements (Figs. 9B-D and 10B-D). For the morphotypes infecting ranids, PC1 explained 37.65% of the variance and was most influenced by cell width (BW = -0.60) and nucleus area (NArea = -0.59). PC2 explained 35.92% of the variance and was most influenced by nucleus position (PN/PA = -0.70) and kinetoplast position (PK/PA = -0.61). PC3 explained 13.96% of the variance and was most influenced by cell length (PA = 0.77) and nucleus area (NArea = -0.47).

For the morphotypes infecting hylids, PC1 explained 42.97% of the variance and was most influenced by nucleus position (PN/PA = 0.60) and nucleus area (NArea = -0.48). PC2 explained 26.48% of the variance and was most influenced by cell width (BW = 0.55), nucleus area (NArea = 0.54), and kinetoplast position (PK/PA = 0.54). PC3 explained 23.58 % of the variance and was most influenced by cell length (PA = 0.68), cell width (BW = -0.64), and kinetoplast position (PK/PA = 0.31).

Phylogenetic Analyses of Trypanosome Morphotypes

Six of the twelve trypanosome morphotypes were successfully isolated and sequenced for both the 18s rRNA and gGAPDH genes. These included five morphotypes infecting ranid hosts, including R1, R2, R3, *T.* cf. *ranarum,* and *T.* cf. *chattoni* as well as one morphotype infecting a hylid, H3. Within-morphotype genetic distance was low regardless of host species or host sampling location from Oklahoma, Arkansas, or Wisconsin. Morphotype R1 was the most variable, with distances ranging from 0.0 – 0.9% (0 to 9/1110 bases) at 18s and 0.0 – 2.1% (0 to 12/590 bases) at gGAPDH. The

other five morphotypes were less variable and ranged between 0.0 – 0.3% (0 to 3/1111 bases) at 18s and 0.0 – 0.9% (0 to 5/590 bases) at gGAPDH. Between morphotype variation was much higher and ranged between 6.9 – 10.7% (72 to 109/1302 bases) at 18s and 8.7 – 12.3% (46 to 63/592 bases) at gGAPDH for all morphotype comparisons except for the comparisons between R1 and R2 morphotypes (18s: 0.8 – 1.6%, 9 to 17/1302 bases; gGAPDH: 2.5 – 4.4%, 14 to 24/592 bases), and R3 and *T.* cf. *ranarum* morphotypes (18s: 3.8 – 4.0%, 42 to 44/1302 bases; gGAPDH: 1.2 – 1.4%, 7 to 8/592 bases), which were closer to the within morphotype variation. These pairs were also found together commonly and had morphological similarities that are discussed further below.

In ML phylogenies for both 18s rRNA and gGAPDH genes, frog trypanosomes fell into four well supported clades, however the deeper relationships between these clades did not recover high bootstrap support, especially in the gGAPDH analysis (Figs. 11 and 12). The trypanosomes from aquatic hosts (fish and turtles) formed a clade within the frog trypanosomes, making frog trypanosomes paraphyletic. At 18s rRNA, the aquatic clade was sister to a group made up of the *T. loricatum* consensus sequence from Spodareva et al. (2018) and the sequences of the R1 and R2 morphotypes from this study (Clade A, Fig. 11). At gGAPDH, the aquatic clade was within the frog trypanosomes but there was low bootstrap support for its placement (Fig. 12).

Of the six trypanosome morphotypes sequenced in this study, three conform to morphology of previously sequenced trypanosomes from North American amphibians. The R1 morphotype observed in this study conforms to the morphology of *T. rotatorium* of Barta and Desser (1984), *T.* cf. *chattoni* conforms to the morphology of *T. chattoni* of

Diamond (1965), and *T.* cf. *ranarum* conforms to the morphology of *T. ranarum* of Barta and Desser (1984) and Spodareva et al. (2018). However, of these three morphotypes, only sequences from *T.* cf. *ranarum* were genetically similar to previous sequences of this species and came out in the same clade as previous *T. ranarum* sequences from North American and Europe (Fig. 11). Previous sequences for *T. rotatorium* and *T. chattoni* originated from cultures and it is suspected that these sequences may not correspond to the bloodstream morphologies they are assumed to represent (see below).

For the final phylogeny, and as mentioned above, sequences from amphibian trypanosome cultures were removed because they were difficult to track back to the original amphibian morphological bloodstream forms. This phylogeny yielded clades of trypanosomes with general morphological similarities (Fig. 13). Clade A included broad trypanosomes that did not have a free flagellum and included the *T. loricatum* consensus sequence from Spodareva et al. (2018) and sequences from the R1 and R2 morphotypes. Clade B included slender trypanosomes with free flagella, *T. tungarae* and the H3 morphotype. Clade C was more variable morphologically but generally contained broad trypanosomes with free flagella and included the spherical *T.* cf. *chattoni* from this study and the consensus sequences of the European *T. rotatorium* and the nautilus morphotype of Spodareva et al. (2018). Clade D contained broad trypanosomes with free flagella, including morphotype R3 and *T.* cf. *ranarum* from this study, *T. ranarum* and *T. fallisi* from North American anurans, and consensus sequences for the European *T. ranarum* and the ring morphotype of Spodareva et al. (2018). In all four clades, morphology was conserved independent of host species and geography, as trypanosomes from Europe nested with morphologically similar species from America. Additionally, in most

instances, European trypanosomes (blue lines) were found to be basal to trypanosomes from the Americas (red lines, Fig. 13).

DISCUSSION

Morphological Diversity and Coinfection of Amphibian Trypanosomes

I found a high morphological diversity of trypanosomes in this study including six morphotypes infecting ranid hosts and six morphotypes infecting hylid hosts (Diamond, 1965; Woo, 1969; Werner and Walewski, 1976; Barta and Desser, 1984; Desser, 2001; Spodareva et al., 2018). This finding is similar to previous research, for example, Woo (1969) found trypanosomes of seven morphotypes infecting four amphibian host species in Ontario, Canada, and Werner and Walewski (1976) found trypanosomes of eight morphotypes infecting seven amphibian host species in Michigan, USA. Additionally, in the current study, frogs were commonly infected with multiple morphotypes. On average infected frogs had two morphotypes with some frogs having as many as five morphotypes. These observations also support previous research on amphibian trypanosome diversity, with many studies reporting a large proportion of frogs having mixed morphotype infections (Diamond, 1965; Werner and Walewski, 1976; Jones and Woo, 1986, 1989; Spodareva et al., 2018). Most notably, Jones and Woo (1986) report all eight infected frogs in their study had mixed trypanosome infections and Spodareva et al. (2018) report that all 16 infected frogs they examined in their study were infected with multiple morphotypes. Furthermore, these mixed infections often consist of pairs of morphotypes that are commonly found coinfecting an individual frog host. In this study,

75% (18/24) of frogs with morphotype R2 also had morphotype R1 and 100% (11/11) of frogs infected with morphotype R4 were also infected with *T.* cf. *ranarum*. Other studies have found these associations as well, for example Werner and Walewski (1976) reported that in their study, 85% (52/61) of the anurans infected with round trypomastigote forms conforming to *T. chattoni* were co-infected with *T. rotatorium*.

In this study, the two morphotype pairs commonly associated together in the same frogs also had general morphological similarities. The R1 and R2 morphotypes are both broad trypanosomes that do not have a free flagellum (Fig. 7A & 7B), and the R3 and *T.* cf. *ranarum* morphotypes are both broad trypanosomes with free flagella (Fig. 7C & 7D). The pairs do differ in some measurements, as for example PCA demonstrated that the R1 morphotype differs from R2 morphotype in the body length (PA), position of the kinetoplast (PK/PA), and the curvature of the anterior end (Fig. 8). However, the general characteristics of the pairs are similar except for the general size, with a larger form and a smaller form, similar to the well documented slender and stumpy life cycle stages of the *T. brucei* group that infect mammal hosts (Vickerman, 1965; Roberts et al., 2013). Therefore, it would be logical to conclude that these morphologically similar morphotypes that almost always infect the same frog are pleomorphic forms of a single trypanosome species. Yet surprisingly, after isolating and sequencing these forms from mixed infections, each morphotype was genetically distinct (Figs. 11-13).

Inferences from Phylogeny with the Addition of Sequences Linked to Morphology

This study is the first to directly link amphibian trypanosome morphology to gene sequences obtained from frogs infected with multiple trypanosome morphologies. Additionally, this study provides novel sequence data for distinguishing North American trypanosomes from similar European forms sequenced by Spodareva et al. (2018). Many amphibian trypanosome species reported from North America were originally described infecting frogs in Europe and Asia (Diamond, 1965; Bardsley and Harmsen, 1973). The validity of European trypanosome species reported in North America have long been in contention, however sequence data for comparison have not been available until recently (Diamond, 1965; Barta et al., 1989; Spodareva et al., 2018). Spodareva et al. (2018) sequenced the first trypanosomes from European anurans and compared sequences of *T. rotatorium* and *T. ranarum* from their type host, *Pelophylax* kl. *esculentus*, in Europe to that of sequences of *T. rotatorium* and *T. ranarum* from North America. The addition of sequences of North American trypanosome morphotypes in this study enables further comparison of these species to their European counterparts. Additionally, because my sequences can be linked to bloodstream morphology, they allow for comparisons to previous sequences of North American trypanosomes originating from cultures. The next two sections cover comparisons of sequences from amphibian trypanosome taxa reported in North America and Europe and discuss issues that arise with the addition of these novel data.

Trypanosoma rotatorium in North America and Europe

Recently, Spodareva et al. (2018) argued that morphological comparisons and sequence divergence of *Trypanosoma rotatorium* in North America and Europe indicate that they are morphologically and genetically distinct. Based on the 18s phylogeny in this study, the *T. rotatorium* consensus sequence from Europe was also distinct from previous sequences of the North American *T. rotatorium*, and they occurred in different clades (Fig. 11). This is consistent with previous hypotheses that *T. rotatorium* from North American frogs represent a distinct species from *T. rotatorium* in European frogs (Diamond, 1965; Barta et al., 1989; Spodareva et al., 2018). However, until the current study, all sequences for the North American form of *T. rotatorium* used in previous phylogenetic analyses and generated by Maslov et al. (1996; U39583.1) and Stevens et al. (1998; AJ009161.1) were from cultures **(**B2-I and B2-II strains) of trypanosomes originally isolated from ranid frogs from Canada with multiple trypanosome infections (Martin et al., 1992). Importantly, Martin et al. (1992) indicated that their identification of *T. rotatorium* was inferred from evidence other than bloodstream trypomastigote morphology, as their attempts at infect naïve frogs using their culture forms (B2-I and B2-II) did not produce infections. Therefore, it is unclear if these sequences (U39583.1 and AJ009161.1) represent the North American *T. rotatorium*. Additionally, the R1 morphotype observed in this study conforms to the morphology of North American anuran trypanosomes previously identified as *T. rotatorium* by Barta and Desser (1984) and Martin et al. (1992). However, the sequences generated during this study from the R1 morphotypes were genetically distinct from sequences obtained from cultures of *T. rotatorium* from Martin et al. (1992), strongly suggesting that these cultures contained

some other anuran trypanosome. To determine what trypanosome Martin et al. (1992) cultured, additional trypanosomes from frogs in Ontario will have to be sequenced to compare to the sequences from cultures and the R1 morphotype in this study.

Interestingly, sequences obtained from the R1 morphotype during this study were sister to the R2 morphotype sequences and the consensus sequence of *T. loricatum* from Spodareva et al. (2018), forming a clade of morphologically similar anuran trypanosomes all without a free flagellum or an elongate nucleus (Fig. 11 - 13; Clade A). In fact, compared to the original *T. rotatorium* description, the North American *T. rotatorium* more closely resembles *T. loricatum*, a species described from the edible frog, *P.* kl. *esculentus* from Europe (França and Athias, 1906; Desser, 2001).

Although Mayer's (1843) original description of *T. rotatorium* is rather dubious, subsequent authors have clarified that *T. rotatorium* is a broad trypanosome with an elongate nucleus and a free flagellum (Laveran and Mesnil, 1901; França and Athias, 1906; Diamond, 1965; Barta et al., 1989). This morphological distinction is particularly important since no trypanosomes have been observed from North American anurans that have an elongate nucleus (Diamond, 1965; Barta et al., 1989). *Trypanosoma rotatorium* in North America has been described as a large, broad trypanosome with an undulating membrane spanning most of the cell body and terminating at the anterior end without a free flagellum (Fantham et al., 1942; Nigrelli et al., 1945; Diamond, 1965; Barta and Desser, 1984). Many authors acknowledge that *T. rotatorium* from North American anurans does not conform to the original description of *T. rotatorium* by Mayer in 1843 (Diamond, 1965; Bardsley and Harmsen, 1973; Barta et al., 1989; Martin et al., 2002; Spodareva et al., 2018). However, the name was often still used by North American

authors as a convention to report the same trypanosomes as previous research in North America (Martin et al., 2002). In my study, the R1 morphotype does not possess a free flagellum or an elongate nucleus and conforms to previous reports of North American anuran trypanosomes referred to as *T. rotatorium* (Diamond, 1965; Barta and Desser, 1984; Barta et al., 1989; Martin et al., 2002; Spodareva et al., 2018). Taken together, these morphological and genetic data strongly suggest that the North American R1 morphotype represents a distinct species from the European *T. rotatorium* and is one of three new species described in Chapter IV.

Trypanosoma ranarum in North America and Europe

In contrast to the clear morphological and genetic differences among North American and European anuran trypanosomes considered to represent *T. rotatorium*, the North American *T. ranarum* sequences were morphologically and genetically quite similar to the European *T. ranarum*. For example, sequences of *T.* cf. *ranarum*, which were genetically similar across the sampling sites in Oklahoma, Arkansas, and Wisconsin (18s: 0.0 – 0.2%, Fig. 11; gGAPDH: 0.0 – 0.2%, Fig. 12), were also similar to the sequences obtained from culture forms of *T. ranarum* originating from frogs in Canada (AF119810.1; 18s: 0.7 – 0.9%, Fig. 11) and the consensus sequence for European *T. ranarum* (18s: 0.9 – 1.1%, Fig. 11). The close genetic similarity between the European *T. ranarum* and the North American *T.* cf. *ranarum* is a novel finding. Spodareva et al. (2018) found long branches between these taxa, most likely due to the misalignment issues mentioned above.

Trypanosoma ranarum in Europe reported by Spodareva et al. (2018) and the North American *T.* cf. *ranarum* in this study are morphologically and genetically similar, however, the evidence is too premature to declare them conspecific at this point. There is currently only a single 18s consensus sequence for the European *T. ranarum*, which came from seven clones from three frogs, including two *P.* kl. *esculentus* from Ukraine and one *P. ridibundus* from Czechia (Spodareva et al., 2018). Additional sampling and sequencing using similar methods to those in Chapter II will have to be employed to link sequence data and morphology from different hosts across the type localities in Europe as well as North America to support or refute the specific status of the current reports. Additionally, gGAPDH sequences are needed to compare in addition to the 18s rRNA sequences, as the primary difference between the European *T. ranarum* and North American *T.* cf. *ranarum* 18s sequences were a gap of 19 bases (data not shown).

Trypanosoma ranarum was originally described from *P.* kl. *esculentus* from Germany by Lankester (1871) as a large, broad trypanosome with a free flagellum and a circular nucleus. The *T.* cf. *ranarum* and R3 morphotypes fit these general morphological characteristics and formed a clade with other broad anuran trypanosomes with a free flagellum and a circular nucleus (Fig. 13; Clade D). These included *T. fallisi* from North American toads, *Anaxyrus americanus*, *T. ranarum* from North American bullfrogs, *Rana catesbeiana*, and *T. ranarum* and an undescribed ring morphotype trypanosome from the edible frog, *P.* kl. *esculentus* from Europe. Importantly, previous sequences of the North American *T. fallisi* and *T. ranarum* were also generated from culture forms established by Martin et al. (1992). However, unlike *T. rotatorium* mentioned above, Martin et al. (1992) confirmed the identification of these trypanosomes by infecting naïve frogs in the

laboratory with culture forms of *T. fallisi* and *T. ranarum* and obtaining the correct morphology in the blood plasma of the infected frogs.

The R3 morphotype was also nested within Clade D, and it was unexpected to find greater morphological and genetic differences between the North American *T.* cf. *ranarum* and the R3 morphotype from the same individual frogs than between the North American *T.* cf. *ranarum* and *T. ranarum* in Europe, which infect geographically isolated frogs from different genera (*T.* cf. *ranarum* and R3 at 18s: 3.8 – 4.0%, 42 to 44/1302 bases vs *T.* cf. *ranarum* and European *T. ranarum* at 18s: 0.9% – 1.1%, 11 to 13/1302 bases). Based on the clear genetic and morphological differences between the *T.* cf. *ranarum* and R3 morphotypes and across multiple geographical localities, the R3 morphotype will also be described as a new species in a future publication.

Phylogenetic Conservation of Amphibian Trypanosome Morphology

Before the current addition of sequences of trypanosome with known morphology, previous phylogenetic analyses suggested that morphology may not be phylogenetically conserved for amphibian trypanosomes (Bernal and Pinto, 2016; Spodareva et al., 2018). This was primarily due to 18s sequences of the large, round trypanosome *T. chattoni* (AF119807.1 and KT765865.1) coming out as sister species to *T. tungarae* (KM406915.1 and KM406916.1), which is a long, skinny trypanosome (Bernal and Pinto, 2016; Spodareva et al., 2018). In the current study, the isolates of *T.* cf. *chattoni* sequenced from Oklahoma and Wisconsin were nested in a different clade than previously generated sequences from culture forms of *T. chattoni* and blood forms of

T. tungarae (Clade C, Fig. 11). Additionally, the 18s and gGAPDH sequences generated in this study for the H3 morphotype, a long and skinny trypanosome similar in morphology to *T. tungarae*, were nested in Clade B with the *T. chattoni* and *T. tungarae* (Figs. 11-12). Given their drastically different morphology to the other members of the clade, the *T. chattoni* sequences seem out of place.

Trypanosoma chattoni is a morphologically unique trypanosome that was originally described from the Asian toad, *Duttaphrynus melanostictus* (syn. *Bufo melanostictus*) in Vietnam by Mathis and Leger (1911). Its large, spherical shape has long bewildered parasitologists and many previous investigators have considered it a pleomorphic morphotype of other amphibian trypanosome species (Fantham et al., 1942; Nigrelli et al., 1945; Werner and Walewski, 1976). However, Diamond (1965) working in North America argued that his *T. chattoni* morphotype was a distinct species and distinct from other North American amphibian trypanosome species. In addition, he was able to establish a culture of *T. chattoni* morphotype from a single northern leopard frog collected in January 1950 from Anoka County, Minnesota. This culture was maintained in the laboratory for years before being deposited in the American Type Culture Collection **(**314, clone AC). This culture has been sequenced independently by two groups of researchers, Martin et al. (2002) provided a 18s rRNA sequence (AF119807.1) and Attias et al. (2016) provided the 18s (KT765865.1) and gGAPDH (KT765886.1) sequences.

Although Diamond (1965) was able to infect two leopard frogs from culture forms of *T. chattoni* which produced blood forms resembling *T. chattoni* in his laboratory reared frogs, he also indicated that many of the *T. chattoni* infected frogs he collected

from Anoka County, Minnesota were coinfected with *T. pipientis*. This is particularly interesting as both *T. tungarae* and the H3 morphotype sequenced in this study are morphologically similar to *T. pipientis*, which has also been described as a long and skinny trypanosome (Diamond, 1950). In the phylogenies generated during this study, these long, skinny trypanosomes nested within Clade B with the questionable *T. chattoni* sequences from culture (Figs. 11-13). Additionally, the *T.* cf. *chattoni* morphotype from multiple anuran species collected from multiple. geographical locations in the US during this study were 7.9 – 9.8% (60 to 76/1302 bases) different from the sequences obtained from *T. chattoni* from Diamond's (1965) cultures (Figs. 11-12). Taken together, these findings suggest Diamond (1965) may not have had pure cultures of *T. chattoni*, and perhaps the sequences are coming from the long, skinny *T. pipientis*. However, to truly resolve this issue, confirmed sequences from *T. pipientis* and *T. chattoni* morphotypes obtained from northern leopard frogs from Diamond's original localities in Anoka County, Minnesota are needed.

Potential Problems with Sequencing Trypanosome Cultures

Culturing amphibian trypanosomes is an incredibly useful tool for studying trypanosome biology and has been proposed as part of the standard tool kit for describing the diversity of these amphibian parasites (Desser, 2001). More recently, sequencing trypanosomes from previously cultured forms has become a way to obtain sequences for multiple amphibian trypanosomes from across the world and without the added costs of new biodiversity inventories to reisolate these species for molecular analyses (Maslov et

al., 1996 Stevens et al., 1998; Martin et al., 2002; Attias et al., 2016). However, when cultured, the morphology of the trypomastigotes from the blood of anuran hosts changes dramatically, which makes it difficult and impossible to link the morphology of culture forms to the morphotypes found in amphibian blood without doing frog laboratory infections (Attias et al., 2016). For example, Attias et al. (2016) observed six trypanosome morphotypes that commonly coinfected individual leptodactylid frogs from Brazil. These authors were successful at establishing in culture one of the six morphotypes observed in the blood of frogs. This trypanosome species was then described morphologically and genetically from its culture forms as *T. herthameyeri*. However, the authors stated that the trypomastigotes of *T. herthameyeri*, which occur in the blood of their amphibian hosts, still await descriptions based on the future discovery of a frog infected exclusively by this trypanosome species and by using genetic barcoding to match the blood trypomastigote form with the culture forms, or alternatively, by conducting experimental infection of laboratory-raised frogs using pure cultures of *T. herthameyeri* and recovering the trypomastigote stages for morphological descriptions (Attias et al. 2016).

As a result of the difficulty in linking sequences from cultured trypanosomes to the morphology of their trypomastigote stages in their amphibian hosts, I created an additional 18s phylogeny with these sequences removed (Fig. 13). This phylogeny yielded clades of trypanosomes with general morphological similarities. In all four clades, morphology was conserved independent of host species and geographic location, as trypanosomes from Europe fell out with morphologically similar species from America. Additionally, in most instances, European trypanosomes (blue lines) were

found to be basal to trypanosomes from the Americas (red lines, Fig. 13), suggesting the morphological lineages have existed before the continents split. In contrast to previous studies, my findings suggest that bloodstream amphibian trypanosome morphology may be phylogenetically conserved. However, there are not many taxa currently represented and additional sampling of different morphotypes from different hosts are needed to confirm these speculations. Furthermore, most amphibian trypanosomes studied and sequenced to date have been from North America and Europe, however the global morphological diversity of amphibian trypanosomes is impressive, with reports of trypanosome morphotypes that appear similar to and in some cases intermediate between the morphotypes in this study (Miyata and Yong, 1994; Netherlands et al. 2015). Continued study and generation of amphibian trypanosomes sequences linked to bloodstream morphology will be interesting additions to test the conservation of the four morphological clades found in this study.

CONCLUSIONS

While pleomorphism has been considered a major problem for amphibian trypanosome taxonomy, currently there is no genetic evidence that amphibian trypanosome species have multiple morphological forms in the bloodstream. Infections of multiple trypanosome morphotypes are common, and the close associations between forms in terms of coinfection frequency and morphology have undoubtedly led researchers to report morphotypes as a single, pleomorphic species (Fantham et al., 1942; Nigrelli et al., 1945; Diamond, 1965; Bardsley and Harmsen, 1973; Werner and Walewski, 1976; Jones

and Woo, 1986, 1989; Attias et al., 2016; Spodareva et al., 2018). Similarly, in this study pairs of trypanosome morphotypes that were morphologically similar and only differed in size were commonly observed coinfecting individual anurans. However, the implementation of a novel technique to isolate and amplify DNA from single trypanosome cells provided definitive evidence that these morphotypes were genetically distinct. Additionally, the sequences of morphotypes generated in this study were linked to their bloodstream morphology and discrepancies between previously sequenced species from cultures shed light on possible misrepresentations in previous analyses. The phylogenetic analysis using only sequences with confirmed bloodstream morphology formed clades of trypanosomes with general morphological similarities, suggesting that amphibian trypanosome morphology may be more conserved than previously thought. Overall, the methods presented in Chapter II provide a unique and novel technique to overcome the challenges of studying amphibian trypanosome diversity and with them we can begin to tease apart the relationships of this enigmatic group of parasites.

Table 3. Species, life stage, and numbers of amphibians collected and examined for trypanosomes.

Species Examined	Life Stage	Prevalence*	Avg. Morphotype Richness (range)
Ambystomatidae			
Ambystoma texanum	Adult	0/10 (0%) 0 - 31	-
Bufonidae			
Anaxyrus americanus	Adult	0/2 (0%) 0 - 84	-
Anaxyrus fowleri	Adult	0/2 (0%) 0 - 84	-
Anaxyrus woodhousii	Adult	0/5 (0%) 0 - 52	-
Hylidae			
Acris blanchardi	Adult	0/28 (0%) 0 - 12	-
Hyla avivoca	Adult	1/12 (8%) 0 - 38	2.0 (1-2)
Hyla cinerea	Adult	9/20 (45%) 23 - 68	1.9 (1-3)
Hyla chrysoscelis	Adult	0/11 (0%) 0 - 29	-
	Tadpole	0/13 (0%) 0 - 25	-
Pseudacris clarkii	Adult	0/5 (0%) 0 - 52	-
Microhylidae			
Gastrophryne olivacea	Adult	0/28 (0%) 0 - 12	-
Ranidae			
Rana blairi	Adult	3/6 (50%) 12 - 88	1.3 (1-2)
Rana catesbeiana	Adult	18/36 (50%) 33 - 67	1.9 (1-4)
Rana clamitans	Adult	44/56 (79%) 66 - 88	1.9 (1-5)
Rana palustrus	Adult	0/4 (0%) 0 - 60	-
Rana sphenocephala	Adult	23/39 (59%) 42 - 74	2.1 (1-5)
	Metamorph	3/31 (10%) 2 - 26	-
	Tadpole	0/30 (0%) 0 - 12	-
	Total	101/338 (30%)	

*Data in cells represent No. Infected/No. Examined (%), 95% Confidence Interval. Confidence intervals were calculated using the binomial distribution for the appropriate sample size.

Table 4. Ranid hosts infected with trypanosomes, their collection locations, and prevalence of trypanosome morphotypes. Numbers represent the no. infected/no. sampled followed by percent.

Species	Location	R1	R2	*T.* cf. *chattoni*	*T.* cf. *ranarum*	R3	R4	Total
Rana blairi	Hennessey, OK	2/6 (33%)	2/6 (33%)	-	-	-	-	3/6 (50%)
	Total	2/6 (33%)	2/6 (33%)	0/6 (0%)	0/6 (0%)	0/6 (0%)	0/6 (0%)	3/6 (50%)
Rana catesbeiana	Stillwater, OK	2/13 (15%)	-	2/13 (15%)	4/13 (31%)	1/13 (8%)	-	4/13 (31%)
	Hennessey, OK	-	-	-	-	-	-	0/2 (0%)
	Red Slough, OK	4/17 (24%)	-	6/17 (35%)	7/17 (41%)	1/17 (6%)	-	10/17 (59%)
	Blue Haze Vista, AR	1/2 (50%)	-	2/2 (100%)	-	1/2 (50%)	-	2/2 (100%)
	OMBS Pond, AR	2/2 (100%)	-	1/2 (50%)	-	-	-	2/2 (100%)
	Total	9/36 (25%)	0/36 (0%)	11/36 (31%)	11/36 (31%)	3/36 (8%)	0/36 (0%)	18/36 (50%)
Rana clamitans	Red Slough, OK	1/7 (14%)	-	1/7 (14%)	5/7 (71%)	1/7 (14%)	-	5/7 (71%)
	Little River, OK	1/2 (50%)	-	-	1/2 (50%)	1/2 (50%)	1/2 (50%)	1/2 (50%)
	Blue Haze Vista, AR	8/14 (57%)	1/14 (7%)	5/14 (36%)	1/14 (7%)	1/14 (7%)	-	10/14 (71%)
	OMBS Pond, AR	10/10 (100%)	-	6/10 (60%)	2/10 (20%)	1/10 (10%)	1/10 (10%)	10/10 (100%)
	New Hampshire	8/8 (100%)	-	6/8 (75%)	4/8 (50%)	-	-	8/8 (100%)
	Wisconsin	5/15 (33%)	-	3/15 (20%)	9/15 (60%)	2/15 (13%)	1/15 (7%)	10/15 (67%)
	Total	33/56 (59%)	1/56 (2%)	21/56 (38%)	22/56 (39%)	6/56 (11%)	3/56 (5%)	44/56 (79%)
Rana sphenocephala	Stillwater, OK	8/30 (27%)	10/30 (33%)	3/30 (10%)	5/30 (17%)	2/30 (7%)	1/30 (3%)	14/30 (47%)
	Stillwater, OK*	-	1/29 (3%)	-	-	-	-	1/29 (3%)*
	Stillwater, OK†	-	-	-	-	-	-	0/30 (0%)†
	Guthrie, OK	8/8 (100%)	8/8 (100%)	7/8 (88%)	-	-	-	8/8 (100%)
	Little River, OK*	1/2 (50%)*	1/2 (50%)*	1/2 (50%)*	1/2 (50%)*	-	2/2 (100%)*	2/2 (100%)*
	Hochatown, OK	1/1 (100%)	1/1 (100%)	1/1 (100%)	-	-	-	1/1 (100%)
	Total	17/39 (44%)	19/39 (49%)	11/39 (28%)	5/39 (13%)	2/39 (5%)	1/39 (3%)	23/39 (59%)
	Grand Total	61/137 (45%)	22/137 (16%)	43/137 (31%)	38/137 (28%)	11/137 (8%)	4/137 (3%)	88/137 (64%)

* - Data from newly metamorphosed frogs. Total and grand total do not include these data.
† - Data from tadpoles. Total and grand total do not include these data.

Table 5. Hylid hosts infected with trypanosomes, their collection locations, and prevalence of trypanosome morphotypes. Numbers represent the no. infected/no. sampled followed by percent.

Species	Location	H1	H2	H3	H4	H5	H6	Total
Hyla avivoca	Little River, OK	-	1/12 (8%)	1/12 (8%)	-	-	-	1/12 (8%)
	Total	0/12 (0%)	1/12 (8%)	1/12 (8%)	0/12 (0%)	0/12 (0%)	0/12 (0%)	1/12 (8%)
Hyla cinerea	Little River, OK	3/12 (25%)	5/12 (42%)	4/12 (33%)	-	-	-	6/15 (40%)
	OMBS, AR	-	-	-	2/5 (40%)	2/5 (40%)	1/5 (20%)	3/5 (60%)
	Total	3/20 (15%)	5/20 (25%)	4/20 (20%)	2/20 (10%)	2/20 (10%)	1/20 (5%)	9/20 (45%)
	Grand Total	3/32 (9%)	6/32 (19%)	5/32 (16%)	2/32 (6%)	2/32 (6%)	1/32 (3%)	10/32 (31%)

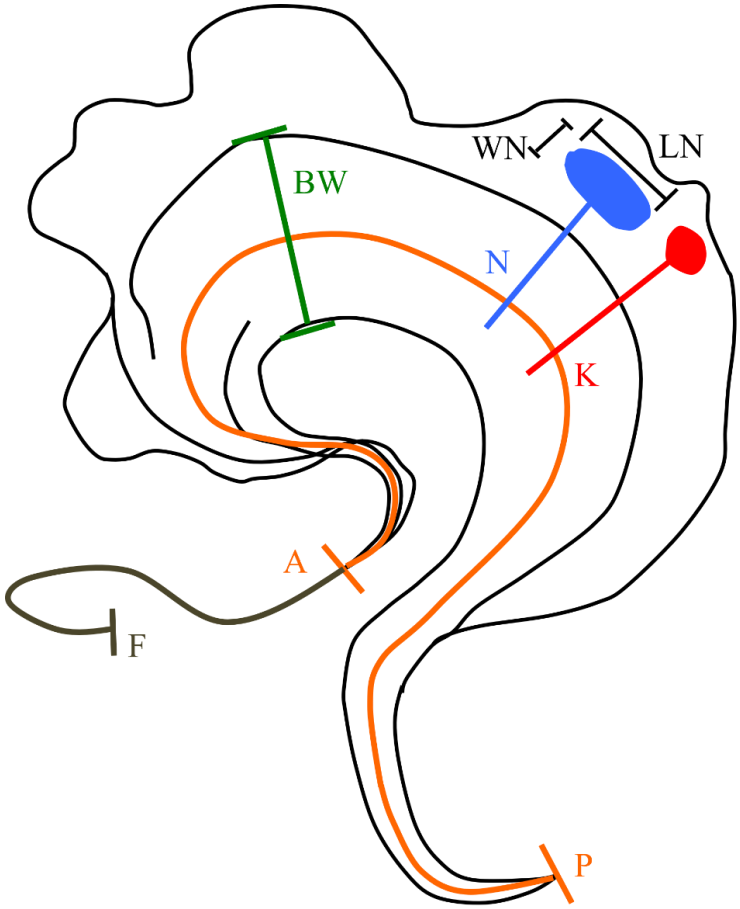

Figure 6. Key landmarks used to measure trypanosome morphology. The posterior end (P) was the end opposite the flagellum. Position of organelles was measured by the distance from either the center of the nucleus (N) or kinetoplast (K) to the posterior end (P), measured along the centerline of the cell (Orange line). The length of the nucleus (LN) was measured as its longest diameter, and the width of the nucleus (WN) was the diameter perpendicular to LN. Body width (BW) was measured at the cells widest point and did not include the undulating membrane. The free flagellum (F) was measured from when it extends past the cell at the anterior end (A) until the end of the flagellum. Specific measurements taken included: PF = total length including free flagellum, PA = body length excluding free flagellum, FF = length of free flagellum, BW = maximum body width excluding undulating membrane, LN = length of nucleus, WN = width of

nucleus, PK = distance from posterior end to kinetoplast, KN = distance from kinetoplast to center of nucleus, NA = distance from center of nucleus to anterior end, and PN = distance from posterior end to center of nucleus.

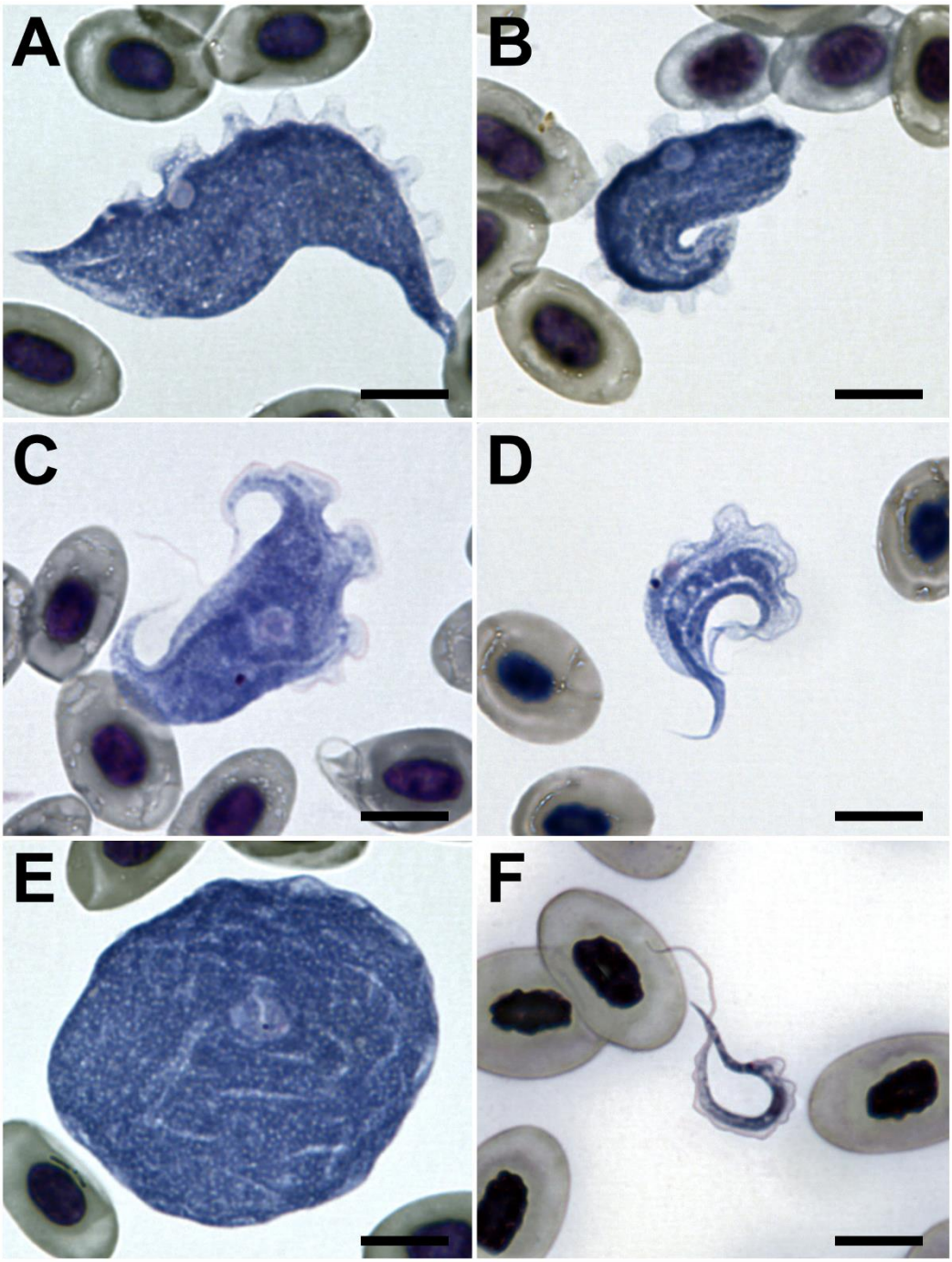

Figure 7. Photomicrographs of trypanosome morphotypes infecting ranid frogs, *Rana blairi*, *R. catesbeiana*, *R. clamitans*, and *R. sphenocephala*. **A.** R1 morphotype. **B.** R2 morphotype. **C.** *Trypanosoma* cf. *ranarum* morphotype. **D.** R3 morphotype, **E.** *Trypanosoma* cf. *chattoni* morphotype. **F.** R4 morphotype. Scale bars = 10 µm.

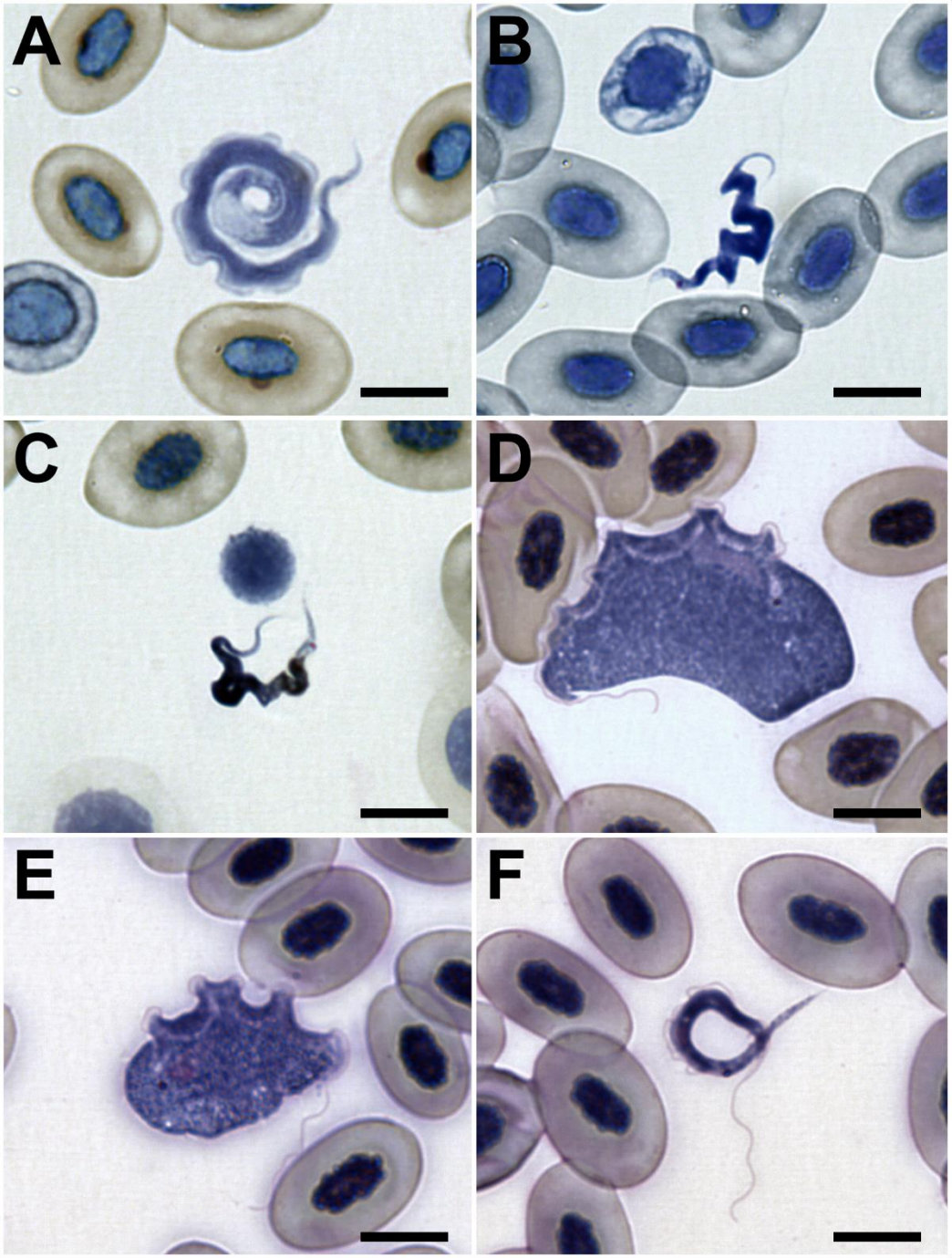

Figure 8. Photomicrographs of trypanosome morphotypes infecting hylid frogs, *Hyla cinerea* and *Hyla avivoca*. **A.** H1 morphotype. **B.** H2 morphotype. **C.** H3 morphotype. **D.** H4 morphotype. **E.** H5 morphotype. **F.** H6 morphotype. Scale bars = 10 µm.

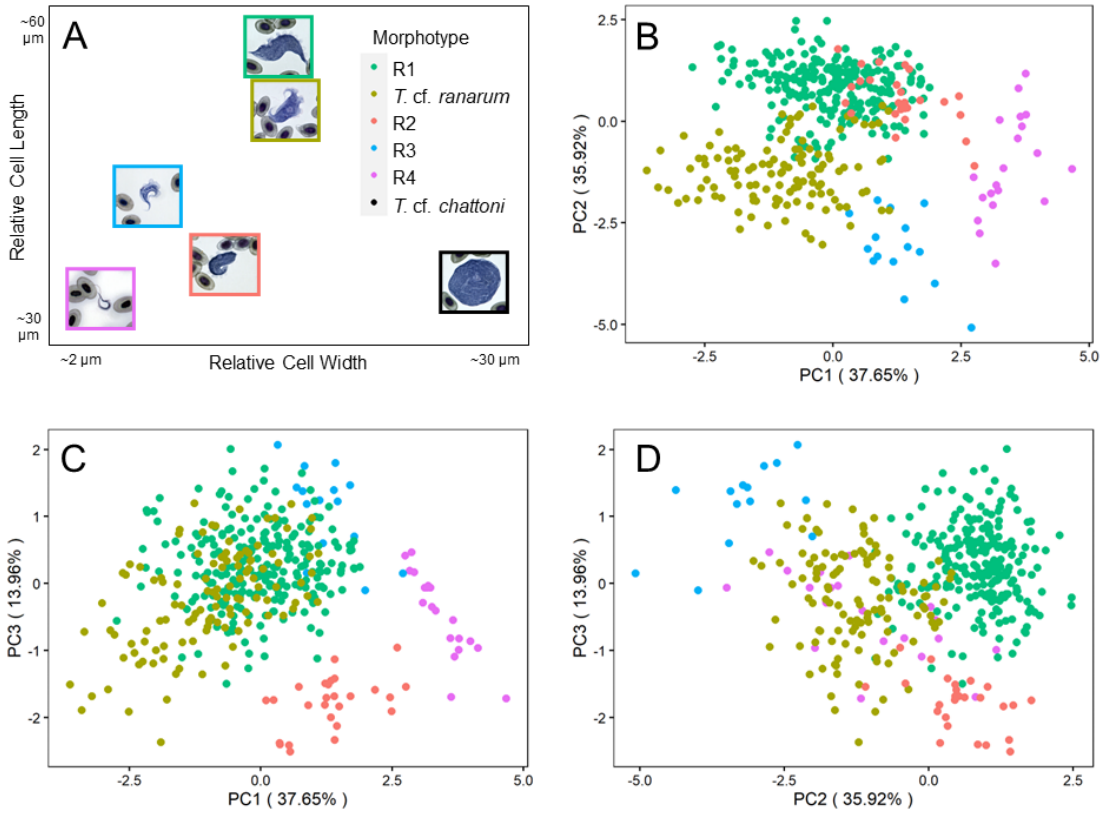

Figure 9. Plots comparing trypanosome morphotypes infecting ranid frogs. **A**. Pictures of morphotypes arranged by the average cell width and length. Picture border colors correspond to the same morphotypes in all plots. **B-D**. Principal component analyses (PCA) of measurements of the 5 morphotypes infecting ranids showing the first three principal components. *Trypanosoma* cf. *chattoni* was included in 3A to show the relative size but was excluded from 3B-3D because of its spherical shape. PC1 explained 37.65% of the variance and was most influenced by body width (BW = -0.60) and nucleus area (NArea = -0.59). PC2 explained 35.92% of the variance and was most influenced by nucleus position (PN/PA = -0.70) and kinetoplast position (PK/PA = -0.61). PC3 explained 13.96% of the variance and was most influenced by body length (PA = 0.77) and nucleus area (NArea = -0.47).

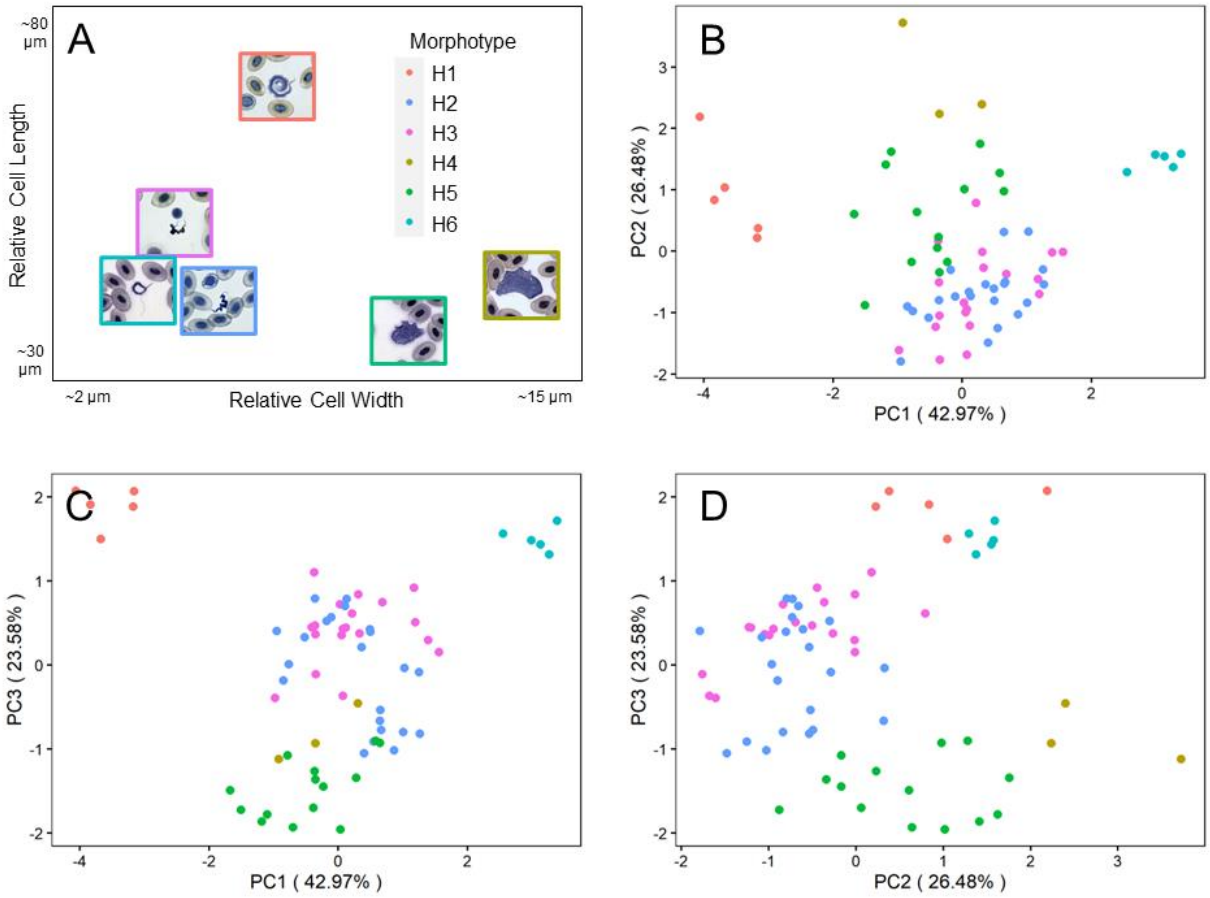

Figure 10. Plots comparing trypanosome morphotypes found infecting hylid frogs. **A**. Pictures of morphotypes arranged by the average cell width and length. Picture border colors correspond to the same morphotypes in all plots. **B-D**. Principal component analyses (PCA) of measurements of the 6 morphotypes infecting hylids showing the first three principal components. PC1 explained 42.97% of the variance and was most influenced by nucleus position (PN/PA = 0.60) and nucleus area (NArea = -0.48). PC2 explained 26.48% of the variance and was most influenced by body width (BW = 0.55), nucleus area (NArea = 0.54), and kinetoplast position (PK/PA = 0.54). PC3 explained 23.58 % of the variance and was most influenced by body length (PA = 0.68), body width (BW = -0.64), and kinetoplast position (PK/PA = 0.31).

Table 6. Dimensions of the six trypanosome morphotypes infecting ranids. All measurements are reported in micrometers (μm) as an average ± standard deviation followed by the range in parentheses.

	R1 n = 330	R2 n = 56	*T.* cf *ranarum* n = 193	R3 n = 18	R4 n = 20	*T.* cf. *chattoni* n = 133
PF	n/a	n/a	68.97 ± 6.84 (53 – 88.7)	55.67 ± 7.34 (47.3 – 66.7)	48.37 ± 6.44 (34 – 57.3)	n/a
PA	57.22 ± 7.38 (31.5 – 82.7)	34.76 ± 3.56 (27.1 – 46.5)	52.85 ± 7.11 (33.5 – 71.9)	46.07 ± 7.76 (26.8 – 59.7)	31.67 ± 5.6 (17.3 – 41)	34.37 ± 7.46 (19.7 – 56.1)
FF	n/a	n/a	14.75 ± 3.69 (4.4 – 23.2)	12.03 ± 6.65 (2.5 – 23)	15.54 ± 3.12 (8.7 – 20.7)	n/a
BW	12.73 ± 3.87 (5.5 – 26.8)	10.6 ± 3.61 (5.5 – 19.5)	13.27 ± 3.73 (6 – 28.3)	7.19 ± 2.43 (2.4 – 10.4)	2.18 ± 0.5 (1.6 – 4)	30.52 ± 6.94 (17 – 57.8)
LN	3.62 ± 0.58 (2.1 – 6.2)	3.55 ± 0.52 (2.3 – 4.5)	4.74 ± 1.04 (1.2 – 8.1)	2.44 ± 0.45 (1.8 – 3.3)	2.75 ± 0.61 (1.5 – 4.2)	5.16 ± 1.12 (2.4 – 7.4)
WN	3.03 ± 0.6 (1 – 4.8)	3.09 ± 0.56 (2 – 4.1)	3.82 ± 0.94 (1.4 – 6.7)	1.76 ± 0.49 (1.1 – 2.7)	1.45 ± 0.32 (1 – 2.1)	4.23 ± 0.86 (2.4 – 6.4)
PK	10.25 ± 3.44 (3 – 19.7)	3.55 ± 1.66 (1.3 – 7.3)	17.48 ± 4.13 (5.2 – 30.1)	21.12 ± 4.68 (12.9 – 28.6)	5.99 ± 3.39 (1.2 – 11.7)	n/a
KN	10.26 ± 3.54 (3.7 – 23.9)	9.08 ± 2.1 (3.9 – 12.6)	5.87 ± 1.35 (2.2 – 11)	3.39 ± 1.06 (2 – 5.6)	7.4 ± 1.37 (3.7 – 9.4)	n/a
NA	37.99 ± 5.91 (20.1 – 55.9)	22.95 ± 3.54 (15.9 – 31.1)	29.44 ± 5.01 (12.3 – 46.9)	24.47 ± 6.12 (10.6 – 34.4)	18.31 ± 3.69 (9 – 23.6)	n/a
PN	20.04 ± 3.63 (10.2 – 36.8)	12.52 ± 1.51 (8.8 – 15.7)	23.42 ± 4.55 (13.1 – 38)	22.73 ± 3.43 (16.1 – 28.4)	13.38 ± 3.47 (6.4 – 18.8)	n/a
PK/PN	0.51 ± 0.15 (0.15 – 0.85)	0.29 ± 0.14 (0.11 – 0.6)	0.75 ± 0.09 (0.39 – 1.02)	0.88 ± 0.08 (0.72 – 0.99)	0.42 ± 0.15 (0.16 – 0.63)	n/a
PK/PA	0.17 ± 0.05 (0.06 – 0.31)	0.1 ± 0.05 (0.04 – 0.21)	0.33 ± 0.06 (0.15 – 0.5)	0.46 ± 0.06 (0.34 – 0.64)	0.18 ± 0.09 (0.07 – 0.31)	n/a
PN/PA	0.35 ± 0.05 (0.21 – 0.58)	0.36 ± 0.04 (0.27 – 0.48)	0.45 ± 0.06 (0.28 – 0.69)	0.51 ± 0.05 (0.44 – 0.6)	0.42 ± 0.07 (0.27 – 0.56)	n/a
BW/PA	0.22 ± 0.07 (0.09 – 0.5)	0.3 ± 0.1 (0.16 – 0.57)	0.25 ± 0.08 (0.09 – 0.64)	0.16 ± 0.05 (0.07 – 0.23)	0.07 ± 0.03 (0.04 – 0.17)	0.89 ± 0.09 (0.53 – 1.17)
FF/PA	n/a	n/a	0.28 ± 0.08 (0.06 – 0.52)	0.33 ± 0.27 (0.05 – 0.86)	0.48 ± 0.11 (0.29 – 0.75)	n/a

Table 7. Dimensions of the six trypanosome morphotypes infecting hylids. All measurements are reported in micrometers (µm) as an average ± standard deviation followed by the range in parentheses.

	H1 n = 7	H2 n = 36	H3 n = 24	H4 n = 12	H5 n = 17	H6 n = 5
PF	92.8 ± 25.88 (74.5 – 111.1)	57.67 ± 9.65 (43.63 – 75.2)	58.99 ± 5.49 (49.5 – 65)	52.09 ± 6.33 (45.3 – 62.7)	50.37 ± 3.88 (45.2 – 58.1)	58.66 ± 2.8 (53.8 – 60.5)
PA	74.98 ± 9.8 (52.3 – 84.4)	34.82 ± 11.89 (17.3 – 55.9)	40.31 ± 5.05 (29.3 – 51.5)	40.92 ± 5.16 (32.3 – 50.4)	30.01 ± 2.97 (24 – 36)	37.3 ± 2.67 (33.1 – 40.5)
FF	24.45 ± 3.18 (22.2 – 26.7)	24.15 ± 3.81 (18.4 – 30.1)	19.91 ± 3.03 (12.8 – 22)	10.94 ± 2.11 (6.7 – 13.3)	20.45 ± 4.79 (9.9 – 26.2)	21.34 ± 1.39 (19.3 – 22.8)
BW	5.08 ± 1.08 (3.8 – 6.5)	3.83 ± 1.41 (1.9 – 6.9)	2.85 ± 0.78 (1.8 – 4.8)	15.17 ± 3.65 (11.3 – 24.4)	11.69 ± 2.56 (7.3 – 15.6)	2.74 ± 0.62 (2 – 3.6)
LN	4.95 ± 1.36 (1.9 – 6.3)	2.89 ± 0.69 (1.7 – 4.5)	2.64 ± 0.87 (1.4 – 4.3)	6.8 ± 2.28 (4 – 9.5)	3.99 ± 1.9 (2.4 – 8.3)	2.62 ± 0.13 (2.4 – 2.7)
WN	3.78 ± 0.78 (2.7 – 5.2)	1.65 ± 0.5 (1 – 3)	1.66 ± 0.49 (1.1 – 3)	2.18 ± 0.36 (1.9 – 2.7)	2.27 ± 0.35 (1.6 – 2.7)	1.52 ± 0.33 (1 – 1.8)
PK	8.35 ± 2.42 (4.3 – 11.1)	4.8 ± 2.01 (1.4 – 8.7)	5.54 ± 2.31 (1 – 9.8)	13.08 ± 4.2 (9.1 – 19)	3.78 ± 1.65 (1.4 – 7)	14.9 ± 1.23 (12.8 – 15.9)
KN	7.23 ± 2.24 (4.5 – 11)	7.1 ± 2.48 (3.2 – 13.8)	8.47 ± 2.36 (1.9 – 11.5)	5.18 ± 1.58 (2.9 – 6.3)	5.71 ± 1.86 (2.8 – 8.6)	6.84 ± 0.88 (5.7 – 7.7)
NA	59.95 ± 9 (38.7 – 68.7)	21.59 ± 8.26 (10.5 – 35.5)	25.78 ± 5.05 (14.2 – 34.9)	23.38 ± 3.02 (19 – 25.7)	20.17 ± 2.55 (14.9 – 23.8)	15.72 ± 2.15 (12.8 – 18.7)
PN	15.08 ± 1.85 (12.8 – 18.6)	10.72 ± 3.76 (5.2 – 18.8)	14.38 ± 3.22 (5.7 – 20)	17.73 ± 5.08 (13 – 24.9)	9.54 ± 2.58 (4.2 – 13.3)	21.24 ± 1.05 (19.6 – 22.2)
PK/PN	0.55 ± 0.15 (0.27 – 0.74)	0.4 ± 0.1 (0.23 – 0.6)	0.41 ± 0.13 (0.13 – 0.6)	0.73 ± 0.04 (0.7 – 0.77)	0.4 ± 0.13 (0.18 – 0.64)	0.7 ± 0.04 (0.65 – 0.76)
PK/PA	0.11 ± 0.02 (0.08 – 0.14)	0.14 ± 0.04 (0.04 – 0.2)	0.14 ± 0.05 (0.03 – 0.22)	0.31 ± 0.08 (0.25 – 0.42)	0.13 ± 0.05 (0.06 – 0.22)	0.4 ± 0.02 (0.38 – 0.42)
PN/PA	0.2 ± 0.04 (0.18 – 0.3)	0.34 ± 0.06 (0.2 – 0.46)	0.36 ± 0.07 (0.17 – 0.5)	0.42 ± 0.09 (0.35 – 0.56)	0.32 ± 0.08 (0.17 – 0.46)	0.57 ± 0.03 (0.53 – 0.6)
BW/PA	0.07 ± 0.02 (0.05 – 0.1)	0.14 ± 0.09 (0.04 – 0.31)	0.07 ± 0.02 (0.04 – 0.12)	0.38 ± 0.13 (0.24 – 0.76)	0.39 ± 0.1 (0.24 – 0.57)	0.07 ± 0.02 (0.05 – 0.1)
FF/PA	0.37 ± 0.08 (0.32 – 0.42)	0.89 ± 0.48 (0.33 – 1.6)	0.51 ± 0.1 (0.31 – 0.62)	0.27 ± 0.07 (0.16 – 0.4)	0.7 ± 0.2 (0.27 – 1.02)	0.57 ± 0.06 (0.48 – 0.63)

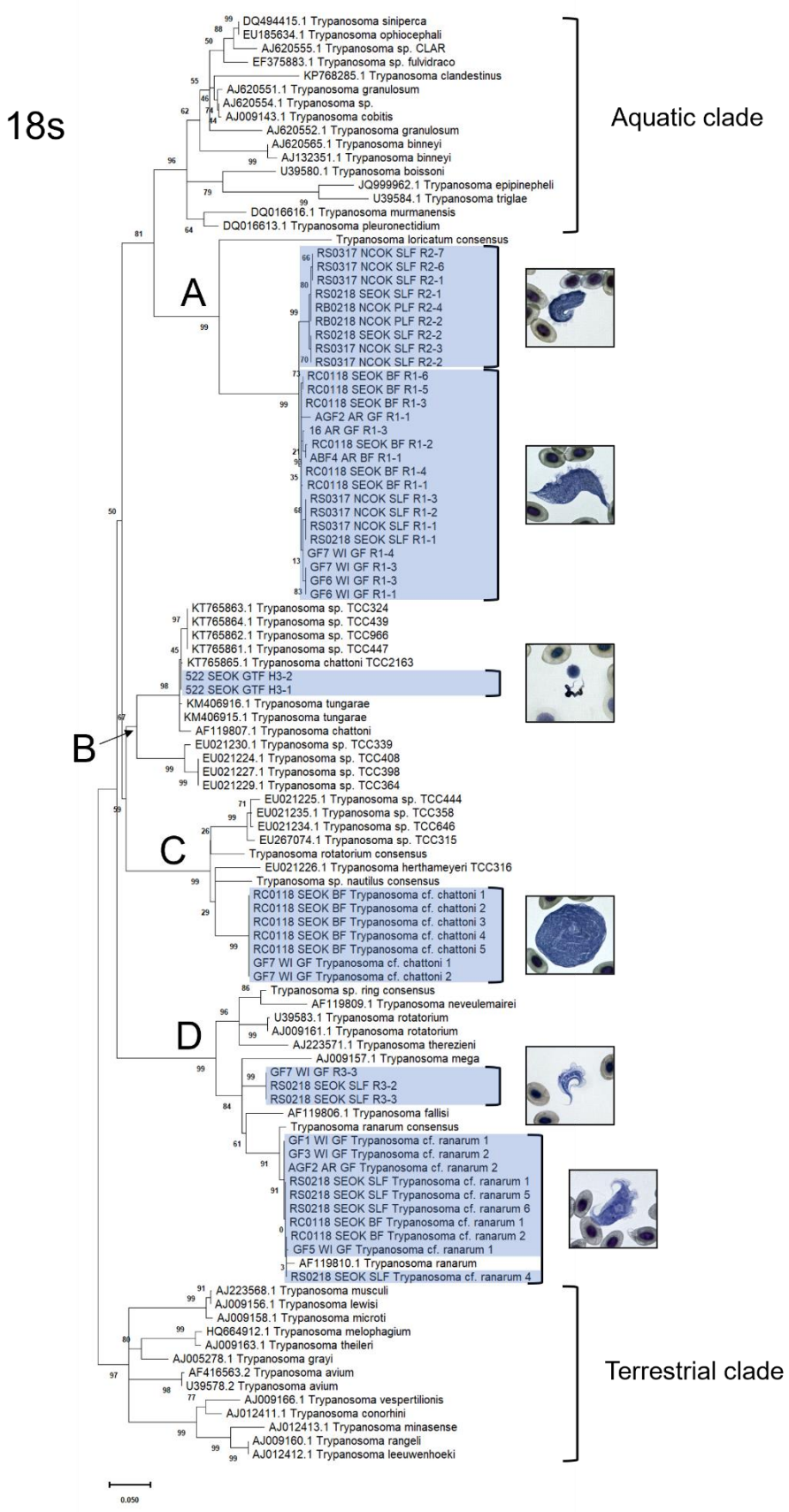
18s
Aquatic clade
Terrestrial clade
A
B
C
D
DQ494415.1 Trypanosoma siniperca
EU185634.1 Trypanosoma ophiocephali
AJ620555.1 Trypanosoma sp. CLAR
EF375883.1 Trypanosoma sp. fulvidraco
KP768285.1 Trypanosoma clandestinus
AJ620551.1 Trypanosoma granulosum
AJ620554.1 Trypanosoma sp.
AJ009143.1 Trypanosoma cobitis
AJ620552.1 Trypanosoma granulosum
AJ620565.1 Trypanosoma binneyi
AJ132351.1 Trypanosoma binneyi
U39580.1 Trypanosoma boissoni
JQ999962.1 Trypanosoma epipinepheli
U39584.1 Trypanosoma triglae
DQ016616.1 Trypanosoma murmanensis
DQ016613.1 Trypanosoma pleuronectidium
Trypanosoma loricatum consensus
RS0317 NCOK SLF R2-7
RS0317 NCOK SLF R2-6
RS0317 NCOK SLF R2-1
RS0218 SEOK SLF R2-1
RB0218 NCOK PLF R2-4
RB0218 NCOK PLF R2-2
RS0218 SEOK SLF R2-2
RS0317 NCOK SLF R2-3
RS0317 NCOK SLF R2-2
RC0118 SEOK BF R1-6
RC0118 SEOK BF R1-5
RC0118 SEOK BF R1-3
AGF2 AR GF R1-1
16 AR GF R1-3
RC0118 SEOK BF R1-2
ABF4 AR BF R1-1
RC0118 SEOK BF R1-4
RC0118 SEOK BF R1-1
RS0317 NCOK SLF R1-3
RS0317 NCOK SLF R1-2
RS0317 NCOK SLF R1-1
RS0218 SEOK SLF R1-1
GF7 WI GF R1-4
GF7 WI GF R1-3
GF6 WI GF R1-3
GF6 WI GF R1-1
KT765863.1 Trypanosoma sp. TCC324
KT765864.1 Trypanosoma sp. TCC439
KT765862.1 Trypanosoma sp. TCC966
KT765861.1 Trypanosoma sp. TCC447
KT765865.1 Trypanosoma chattoni TCC2163
522 SEOK GTF H3-2
522 SEOK GTF H3-1
KM406916.1 Trypanosoma tungarae
KM406915.1 Trypanosoma tungarae
AF119807.1 Trypanosoma chattoni
EU021230.1 Trypanosoma sp. TCC339
EU021224.1 Trypanosoma sp. TCC408
EU021227.1 Trypanosoma sp. TCC398
EU021229.1 Trypanosoma sp. TCC364
EU021225.1 Trypanosoma sp. TCC444
EU021235.1 Trypanosoma sp. TCC358
EU021234.1 Trypanosoma sp. TCC646
EU267074.1 Trypanosoma sp. TCC315
Trypanosoma rotatorium consensus
EU021226.1 Trypanosoma herthameyeri TCC316
Trypanosoma sp. nautilus consensus
RC0118 SEOK BF Trypanosoma cf. chattoni 1
RC0118 SEOK BF Trypanosoma cf. chattoni 2
RC0118 SEOK BF Trypanosoma cf. chattoni 3
RC0118 SEOK BF Trypanosoma cf. chattoni 4
RC0118 SEOK BF Trypanosoma cf. chattoni 5
GF7 WI GF Trypanosoma cf. chattoni 1
GF7 WI GF Trypanosoma cf. chattoni 2
Trypanosoma sp. ring consensus
AF119809.1 Trypanosoma neveulemairei
U39583.1 Trypanosoma rotatorium
AJ009161.1 Trypanosoma rotatorium
AJ223571.1 Trypanosoma therezieni
AJ009157.1 Trypanosoma mega
GF7 WI GF R3-3
RS0218 SEOK SLF R3-2
RS0218 SEOK SLF R3-3
AF119806.1 Trypanosoma fallisi
Trypanosoma ranarum consensus
GF1 WI GF Trypanosoma cf. ranarum 1
GF3 WI GF Trypanosoma cf. ranarum 2
AGF2 AR GF Trypanosoma cf. ranarum 2
RS0218 SEOK SLF Trypanosoma cf. ranarum 1
RS0218 SEOK SLF Trypanosoma cf. ranarum 5
RS0218 SEOK SLF Trypanosoma cf. ranarum 6
RC0118 SEOK BF Trypanosoma cf. ranarum 1
RC0118 SEOK BF Trypanosoma cf. ranarum 2
GF5 WI GF Trypanosoma cf. ranarum 1
AF119810.1 Trypanosoma ranarum
RS0218 SEOK SLF Trypanosoma cf. ranarum 4
AJ223568.1 Trypanosoma musculi
AJ009156.1 Trypanosoma lewisi
AJ009158.1 Trypanosoma microti
HQ664912.1 Trypanosoma melophagium
AJ009163.1 Trypanosoma theileri
AJ005278.1 Trypanosoma grayi
AF416563.2 Trypanosoma avium
U39578.2 Trypanosoma avium
AJ009166.1 Trypanosoma vespertilionis
AJ012411.1 Trypanosoma conorhini
AJ012413.1 Trypanosoma minasense
AJ009160.1 Trypanosoma rangeli
AJ012412.1 Trypanosoma leeuwenhoeki
0.050

Figure 11. Maximum Likelihood phylogenetic estimation of the partial 18s rRNA gene (1302 bp, -Ln = -8979.52) using the TN93+G+I model in MEGA X (Kumar et al., 2018). The tree shows four distinct anuran trypanosome clades (A-D) and is rooted with trypanosomes infecting terrestrial hosts. Values at nodes represent bootstrap support values, assessed with 1000 replications. Shaded boxes include morphotypes sequenced in this study and names include frog host ID, collection location (NCOK = North Central Oklahoma, SEOK = Southeast Oklahoma, AR = Arkansas, and WI = Wisconsin), host taxa (BF = *Rana catesbeiana*, GF = *Rana clamitans*, SLF = *Rana sphenocephala*, GTF = *Hyla cinerea*), morphotype name, and isolate number.

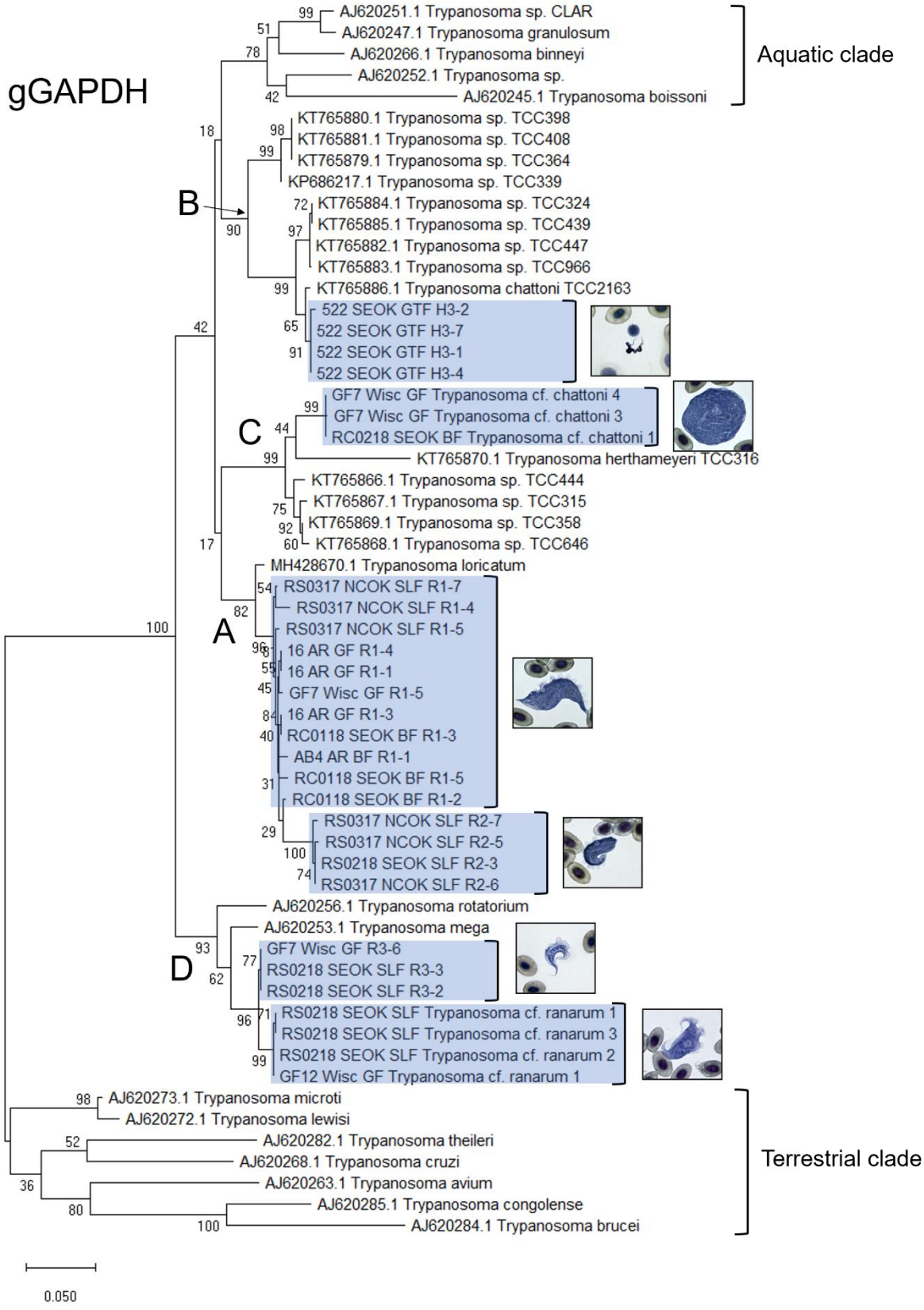
gGAPDH
AJ620251.1 Trypanosoma sp. CLAR
AJ620247.1 Trypanosoma granulosum
AJ620266.1 Trypanosoma binneyi
AJ620252.1 Trypanosoma sp.
AJ620245.1 Trypanosoma boissoni
Aquatic clade
KT765880.1 Trypanosoma sp. TCC398
KT765881.1 Trypanosoma sp. TCC408
KT765879.1 Trypanosoma sp. TCC364
KP686217.1 Trypanosoma sp. TCC339
B
KT765884.1 Trypanosoma sp. TCC324
KT765885.1 Trypanosoma sp. TCC439
KT765882.1 Trypanosoma sp. TCC447
KT765883.1 Trypanosoma sp. TCC966
KT765886.1 Trypanosoma chattoni TCC2163
522 SEOK GTF H3-2
522 SEOK GTF H3-7
522 SEOK GTF H3-1
522 SEOK GTF H3-4
GF7 Wisc GF Trypanosoma cf. chattoni 4
GF7 Wisc GF Trypanosoma cf. chattoni 3
RC0218 SEOK BF Trypanosoma cf. chattoni 1
C
KT765870.1 Trypanosoma herthameyeri TCC316
KT765866.1 Trypanosoma sp. TCC444
KT765867.1 Trypanosoma sp. TCC315
KT765869.1 Trypanosoma sp. TCC358
KT765868.1 Trypanosoma sp. TCC646
MH428670.1 Trypanosoma loricatum
RS0317 NCOK SLF R1-7
RS0317 NCOK SLF R1-4
A
RS0317 NCOK SLF R1-5
16 AR GF R1-4
16 AR GF R1-1
GF7 Wisc GF R1-5
16 AR GF R1-3
RC0118 SEOK BF R1-3
AB4 AR BF R1-1
RC0118 SEOK BF R1-5
RC0118 SEOK BF R1-2
RS0317 NCOK SLF R2-7
RS0317 NCOK SLF R2-5
RS0218 SEOK SLF R2-3
RS0317 NCOK SLF R2-6
AJ620256.1 Trypanosoma rotatorium
AJ620253.1 Trypanosoma mega
D
GF7 Wisc GF R3-6
RS0218 SEOK SLF R3-3
RS0218 SEOK SLF R3-2
RS0218 SEOK SLF Trypanosoma cf. ranarum 1
RS0218 SEOK SLF Trypanosoma cf. ranarum 3
RS0218 SEOK SLF Trypanosoma cf. ranarum 2
GF12 Wisc GF Trypanosoma cf. ranarum 1
AJ620273.1 Trypanosoma microti
AJ620272.1 Trypanosoma lewisi
AJ620282.1 Trypanosoma theileri
AJ620268.1 Trypanosoma cruzi
AJ620263.1 Trypanosoma avium
AJ620285.1 Trypanosoma congolense
AJ620284.1 Trypanosoma brucei
Terrestrial clade
0.050

Figure 12. Maximum Likelihood phylogenetic estimation of the partial glycosomal GAPDH gene (592 bp, -Ln = -4696.87) using the T92+G model in MEGA X (Kumar et al., 2018). The tree shows four distinct anuran trypanosome clades (A-D) and is rooted with trypanosomes infecting terrestrial hosts. Values at nodes represent bootstrap support values, assessed with 1000 replications. Shaded boxes include morphotypes sequenced in this study and names include frog host ID, collection location (NCOK = North Central Oklahoma, SEOK = Southeast Oklahoma, AR = Arkansas, and Wisc = Wisconsin), host taxa (BF = *Rana catesbeiana*, GF = *Rana clamitans*, SLF = *Rana sphenocephala*, GTF = *Hyla cinerea*), morphotype name, and isolate number.

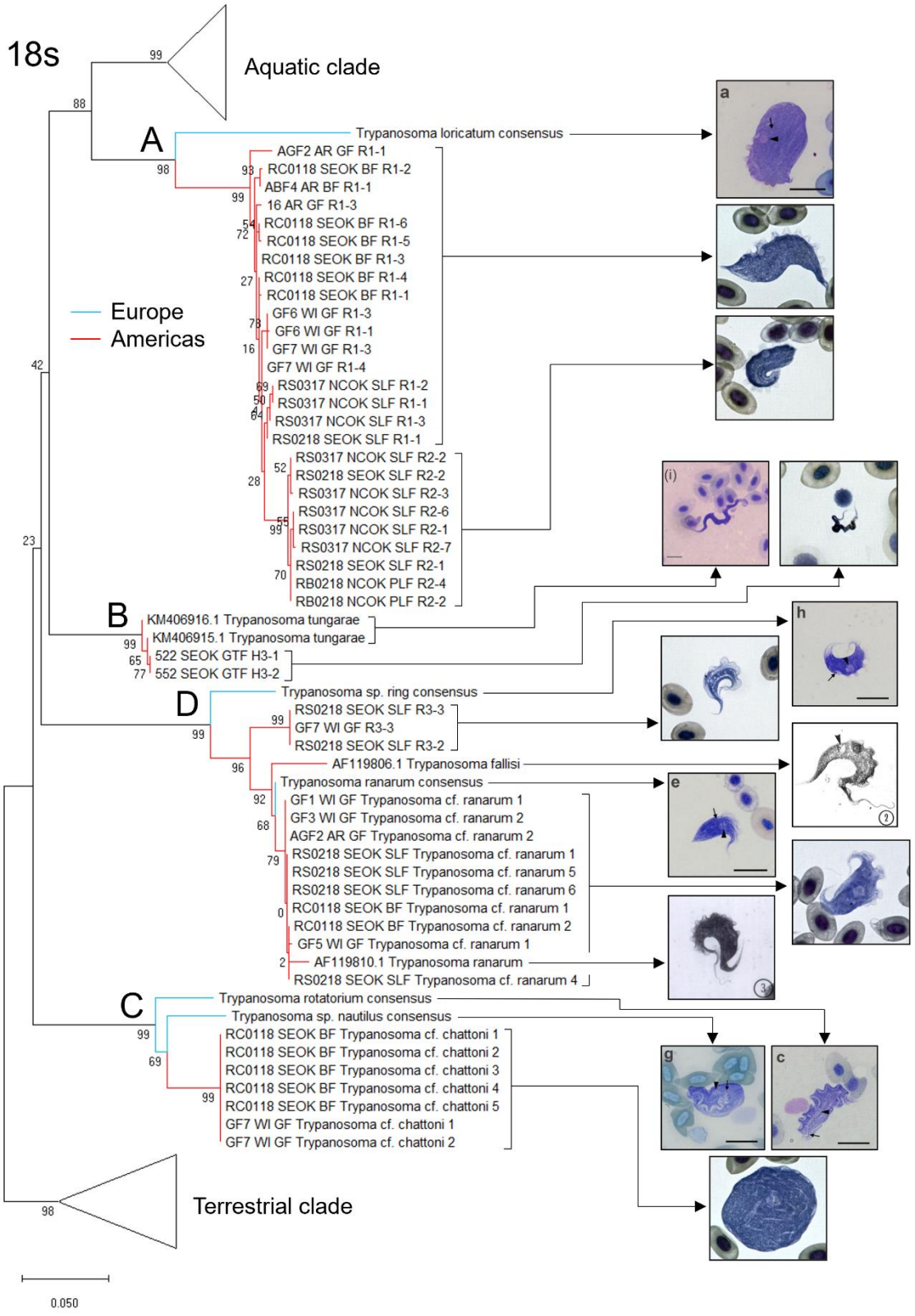
18s
Aquatic clade
Terrestrial clade
Europe
Americas
A
B
C
D
Trypanosoma loricatum consensus
AGF2 AR GF R1-1
RC0118 SEOK BF R1-2
ABF4 AR BF R1-1
16 AR GF R1-3
RC0118 SEOK BF R1-6
RC0118 SEOK BF R1-5
RC0118 SEOK BF R1-3
RC0118 SEOK BF R1-4
RC0118 SEOK BF R1-1
GF6 WI GF R1-3
GF6 WI GF R1-1
GF7 WI GF R1-3
GF7 WI GF R1-4
RS0317 NCOK SLF R1-2
RS0317 NCOK SLF R1-1
RS0317 NCOK SLF R1-3
RS0218 SEOK SLF R1-1
RS0317 NCOK SLF R2-2
RS0218 SEOK SLF R2-2
RS0317 NCOK SLF R2-3
RS0317 NCOK SLF R2-6
RS0317 NCOK SLF R2-1
RS0317 NCOK SLF R2-7
RS0218 SEOK SLF R2-1
RB0218 NCOK PLF R2-4
RB0218 NCOK PLF R2-2
KM406916.1 Trypanosoma tungarae
KM406915.1 Trypanosoma tungarae
522 SEOK GTF H3-1
552 SEOK GTF H3-2
Trypanosoma sp. ring consensus
RS0218 SEOK SLF R3-3
GF7 WI GF R3-3
RS0218 SEOK SLF R3-2
AF119806.1 Trypanosoma fallisi
Trypanosoma ranarum consensus
GF1 WI GF Trypanosoma cf. ranarum 1
GF3 WI GF Trypanosoma cf. ranarum 2
AGF2 AR GF Trypanosoma cf. ranarum 2
RS0218 SEOK SLF Trypanosoma cf. ranarum 1
RS0218 SEOK SLF Trypanosoma cf. ranarum 5
RS0218 SEOK SLF Trypanosoma cf. ranarum 6
RC0118 SEOK BF Trypanosoma cf. ranarum 1
RC0118 SEOK BF Trypanosoma cf. ranarum 2
GF5 WI GF Trypanosoma cf. ranarum 1
AF119810.1 Trypanosoma ranarum
RS0218 SEOK SLF Trypanosoma cf. ranarum 4
Trypanosoma rotatorium consensus
Trypanosoma sp. nautilus consensus
RC0118 SEOK BF Trypanosoma cf. chattoni 1
RC0118 SEOK BF Trypanosoma cf. chattoni 2
RC0118 SEOK BF Trypanosoma cf. chattoni 3
RC0118 SEOK BF Trypanosoma cf. chattoni 4
RC0118 SEOK BF Trypanosoma cf. chattoni 5
GF7 WI GF Trypanosoma cf. chattoni 1
GF7 WI GF Trypanosoma cf. chattoni 2
0.050

Figure 13. Maximum Likelihood phylogeny only using sequences for which there is good morphological data. Phylogeny was constructed with the partial 18s rRNA gene (1292 bp, -Ln = -7283.83) using the K2P+G+I model in MEGA X (Kumar et al., 2018). The tree shows four distinct anuran trypanosome clades (A-D) and is rooted with trypanosomes infecting terrestrial hosts. Values at nodes represent bootstrap support values, assessed with 1000 replications. Blue lines represent taxa from Europe, red lines represent taxa from North and Central America. Photomicrographs for trypanosomes of *T. loricatum*, *T.* sp. ring, *T. ranarum*, *T. rotatorium*, and *T.* sp. nautilus are from Spodareva et al. (2018). Photomicrographs of *T. tungarae*, *T. fallisi* and *T. ranarum* are from Bernal and Pinto (2016), Martin and Desser (1990), and Barta and Desser (1984) respectively.

CHAPTER IV

DESCRIPTION OF TRYPANOSOME SPECIES INFECTING RANID HOSTS IN THE CENTRAL UNITED STATES

ABSTRACT: Amphibian trypanosome diversity is difficult to characterize due to mixed infections and the possibility of pleomorphism. With the advancement of molecular technology and increases in affordability for gene sequencing, genetically determining pleomorphic species is now possible. However specific methods are required to link sequences generated from mixed trypanosome infections to trypanosome morphotype morphology. Using the methods detailed in Chapter II, trypanosome morphotypes infecting ranids were isolated and characterized morphologically and genetically at the 18s rRNA and gGAPDH loci. These techniques make critical links between sequence data and trypanosome morphology and suggest that morphotypes that were morphologically similar and often found infecting the same host were not pleomorphic species and were genetically distinct. In this chapter, three trypanosome species are formally described from the data presented in Chapters II and III. Given the difficulty of providing descriptions of trypanosomes that are reproducible and comparable for future parasitologists, I believe the most consistent way forward is to describe species based on sequence data linked to trypanosome cell morphology by sequencing single cells with known morphology.

INTRODUCTION

Amphibian trypanosomes contribute a large portion of trypanosome diversity, with at least 70 of the about 500 trypanosome species infecting vertebrate hosts described from amphibians (Bardsley and Harmsen, 1973; Desser, 2001; Roberts et al., 2013). However, characterizing amphibian trypanosome diversity is difficult because infected amphibian hosts are almost always infected with multiple trypanosome morphotypes (Diamond, 1965; Bardsley and Harmsen, 1973; Desser, 2001; Spodareva et al., 2018). When observing mixed infections on blood smears, it is not clear whether the forms present in the bloodstream represent different species (genetic lineages) or a single pleomorphic species (one genetic lineage that takes more than one morphological form in the blood stream). Historically, this has created a problem where some authors describe mixed infections as single pleomorphic species, and other authors describe the different morphotypes as distinct species (Desser, 2001). Therefore, the validity of many trypanosome species is questionable and until recently, methods to evaluate pleomorphic species have only included extensive life cycle studies and cell culturing (Desser, 2001). With the advancement of molecular technology and increases in affordability for gene sequencing, genetically determining pleomorphic species is now possible. However, mixed infections still pose significant challenges to acquire and interpret sequence data, and specific methods are needed to match sequence data with trypanosome morphology.

In Chapter II, novel methods to link trypanosome morphology to sequence data are detailed. These methods include isolating individual trypanosome cells and amplifying and sequencing the 18s rRNA and gGAPDH genes using nested PCR. Using these methods, five trypanosome morphotypes infecting ranids and one infecting a hylid

were characterized morphologically and genetically (Chapter III). Additionally, two pairs of these morphotypes were suspected of being pleomorphic species based on coinfection frequency and morphological similarity, similar to previous reports of pleomorphic trypanosome species, however with the methods in Chapter II, all morphotypes were found to be genetically distinct.

In this chapter, three trypanosome species are described from studies in Chapters II and III. These three trypanosome morphotypes were the most prevalent and were able to be sequenced from multiple frog hosts, species and/or across multiple locations sampled. Additionally, I describe *T.* cf. *ranarum*, a morphotype found in North America that morphologically conforms to *T. ranarum* originally described in Europe, however there were small genetic differences at the 18s rRNA and gGAPDH genes among morphotypes of this trypanosome species from European and North American anuran hosts (Chapter III).

Traditionally, trypanosomes have been described with morphological measurements and life cycle studies (Desser, 2001). The following descriptions include morphometrics and figures showing variation of the species, potentially allowing comparison to previous reports of trypanosome species in North American anurans. However, the trypanosomes described here are based on the 18s rRNA and gGAPDH sequence data which link the reports of these species across host and geographic ranges as well as across small morphological variation found between observations. Given the difficulty of providing descriptions of trypanosomes that are reproducible and comparable for future parasitologists, I believe the most consistent way forward is the

describe species based on sequence data linked to trypanosome cell morphology by sequencing single cells with known morphology.

MATERIALS AND METHODS

Sample Material and Morphotype Identification

Infected blood samples were obtained from five frog species, *Rana blairi*, *Rana catesbeiana*, *Rana clamitans*, *Rana sphenocephala*, and *Hyla cinerea* collected from Oklahoma, Arkansas, and Wisconsin, USA as described in Chapter II and Chapter III. Briefly, blood was collected in capillary tubes and blood smears on glass slides were created. Additionally, capillary tubes were centrifuged to concentrate trypanosomes at the buffy coat layer, which was then deposited into phosphate buffered saline for examination of live trypanosomes (Woo, 1969). Blood smears were stained with the JorVet Dip Quick Stain Kit (Jorgensen Labs, CO) and examined for trypanosomes with an Olympus BX-51 upright research microscope and when trypanosomes were found they were photographed with an Olympus 5-megapixel digital camera (Chapter III). Trypanosome cell dimensions and organelle positions were measured on photomicrographs as described in Chapter III (Table 8). In blood plasma preparations, live trypanosome general size, shape, and swimming behavior was observed and compared to morphology observed on slides to identify morphotypes (Supplementary Videos 1-4).

Trypanosome Isolation and Sequencing

Trypanosomes were isolated from amphibian blood by dilution of trypanosomes obtained by centrifuging infected blood in capillary tubes as described previously in Chapter II. Trypanosomes concentrated from blood samples by centrifugation were diluted in 5 µL drops of phosphate buffered saline until single trypanosome cells were isolated. The morphology of isolated cells was noted and then they were collected for DNA extraction, PCR, and gene sequencing of the 18s rRNA and gGAPDH genes (Chapter II).

RESULTS

Species Descriptions:

Trypanosoma desseri n. sp.

Fig. 14.

Diagnosis: Large, broad trypanosome with no free flagellum (PA 57.22 ± 7.38, BW 12.73 ± 3.87, Fig. 14; Table 8). Often appears flat like a sheet, or with longitudinal folds depending how cells rest when fixed on slides. Kinetoplast near the posterior end (PK/PA 0.17 ± 0.05), nucleus circular and about a third of the length of the cell from the posterior end (PN/PA 0.35 ± 0.05). Both the kinetoplast and nucleus are off the midline of the cell, closer to the undulating membrane. The undulating membrane begins at the kinetoplast and ends at the anterior end of the cell. In live preparations of blood plasma, the undulating membrane flutters quickly, however the actual movement of the whole

cell is gentle. Sometimes spinning and tumbling, the main direction of cell movement is perpendicular to the anterior-posterior axis, towards the undulating membrane (Supplementary Video 1).

Taxonomic Summary:

Type host: Rana sphenocephala.

Additional vertebrate hosts: Rana blairi, Rana catesbeiana, Rana clamitans.

Vector hosts: Unknown.

Type locality: Teal Ridge Aquatic Wetland, Stillwater, Oklahoma, (36°06'03.3" N, 97°04'48.3" W).

Distribution: Payne County, Oklahoma: Teal Ridge Aquatic Wetland (36°06'03.3" N, 97°04'48.3" W). Logan County, Oklahoma: (35°48'38.4" N, 97°24'08.6" W). Kingfisher County, Hennessey, Oklahoma (36°07'00.0" N, 97°53'56.0" W). McCurtain County, Oklahoma: Red Slough (33°44.897' N, 094°38.549' W), Little River NWR (33°57.200' N, 094°42.166' W). Polk County, Arkansas: Blue Haze Vista (34°37'40.17" N, 94°14'44.4228" W), Ouachita Mountains Biological Station (34°27'44.5" N, 93°59'54.2" W), Muskego, Waukesha County, Wisconsin (42°51'13.1764" N, 88°7'22.944" W), Woodward Park, New London, New Hampshire (43°24'51" N, 71°59'32" W).

Prevalence: Rana blairi (2/6, 33%), *Rana catesbeiana* (9/36, 25%), *Rana clamitans* (33/56, 59%), *Rana sphenocephala* (17/39, 44%).

Type material: Blood smears stained with DipQuik were deposited to the Harold W. Manter Laboratory of Parasitiology Collection, Lincoln, Nebraska. Gene sequences for the 18s rRNA and gGAPDH genes were deposited to GenBank, accession numbers (##### - #####).

Etymology: The species is named after Dr. Sherwin S. Desser for his numerous contributions to parasitology and protozoology, and especially for that of his work on amphibian trypanosomes. The work of Dr. Desser and his students on trypanosome taxonomy has set the foundation for studying amphibian trypanosomes in North America.

Remarks:

Trypanosoma desseri morphologically conforms to previous reports of *T. rotatorium* in North America, which has been described as a large, broad trypanosome with an undulating membrane spanning most of the cell body and terminating at the anterior end without a free flagellum (Fantham et al., 1942; Nigrelli et al., 1945; Diamond, 1965; Woo; 1969; Barta and Desser, 1984). However, many authors acknowledge that *T. rotatorium* from North American anurans does not conform to the original description of *T. rotatorium* by Mayer in 1843 from the edible frog, *Pelophylax* kl. *esculentus*, in Europe (Diamond, 1965; Bardsley and Harmsen, 1973; Barta et al., 1989; Martin et al., 2002; Spodareva et al., 2018). Mayer's (1843) original description of *T. rotatorium* is rather dubious, but subsequent authors have clarified that *T. rotatorium* is a broad trypanosome with an elongate nucleus and a free flagellum (Laveran and Mesnil, 1901; França and Athias, 1906; Diamond, 1965; Barta et al., 1989). Diamond (1965) first

pushed that no trypanosomes with elongate nuclei have been observed from North American anurans and therefore reports of *T. rotatorium* in North America are not valid (Diamond, 1965; Barta et al., 1989). However, the name *T. rotatorium* was still used by authors as a convention to report the same trypanosomes as previous research in North America (Martin et al., 2002).

Kudo (1922) first reported a broad trypanosome presumably infecting either *Rana pipiens* in Illinois and/or *Rana clamitans* from New York. Unfortunately, Kudo (1922) does not specify the locations sampled or host species which were infected with the broad trypanosome he identified as *Trypanosoma rotatorium*. However, Kudo's study was a survey for multiple parasitic protozoa in frogs and he mentions the above hosts and locations as his material. Figs. 30-33 of Kudo (1922) represent forms very similar to my observations of *T. desseri*, except for the free flagella extending past the anterior end of the cells. Kudo mentions that they are not always seen, so it is possible Kudo was observing multiple trypanosome species.

Fantham et al. (1942) surveyed frogs around Montreal, CA and reported *T. rotatorium* infecting *R. catesbeiana, R. clamatans*, and *R. pipiens*. Additionally, Nigrelli (1945) reported *T. rotatorium* from *R. catesbeiana* and *R. clamitans* in Connecticut, New York, New Jersey and Pennsylvania, USA. Both Fantham et al. (1942) and Nigrelli (1945) considered *T. rotatorium* to be polymorphic and include figures of rounded-up forms with internal or no flagella (pl. 2, figs. 16-17, Fantham et al., 1942; text figs. 3D and 3E, Nigrelli, 1945). Diamond (1965) first posited that these non-flagellated forms are a different species *T. chattoni*.

Woo (1969) reported a broad trypanosome infecting *Rana pipiens*, *R. clamitans*, and *R. catesbieana* in Ontario, Canada and identified it as *Trypanosoma rotatorium*. Barta and Desser (1984) also reported *T. rotatorium* from *R. clamitans*, *R. catesbieana*, and *R. septentrionalis* in Ontario. Drawings from Woo (Figs. 1-2, 1969) and photographs from Barta and Desser (Fig. 1, 1984) look very similar to *T. desseri*. They are large and broad cells (PA 66.2 and BW 20.0, Woo, 1969; PA 67.4 and BW 30.8, Barta and Desser, 1984) with similar kinetoplast and nucleus positions (PK/PA about 0.2, PN/PA about 0.35-0.4), and no free flagella.

I would like to synonymize my reports of *Trypanosoma desseri* (the R1 morphotype in Chapter III) with the reports of North American *T. rotatorium*. However, existing 18s rRNA sequences from cultures of *T. rotatorium* from North America (U39583.1 and AJ009161.1) are on average 8.2% (107/1302 bases) different from those generated in Chapter III for *T. desseri*, suggesting they are not the same species (Chapter III). The *T. rotatorium* sequences were generated by Maslov et al. (1996; U39583.1) and Stevens et al. (1998; AJ009161.1) from cultures **(**B2-I and B2-II strains) of trypanosomes originally isolated from ranid frogs with multiple trypanosome infections in Canada (Martin et al., 1992). Martin et al. (1992) indicated that their attempts to infect naïve frogs using their culture forms (B2-I and B2-II) did not produce infections. Therefore, the bloodstream morphology of their cultured trypanosomes was not verified, and it is unclear if these sequences (U39583.1 and AJ009161.1) represent the North American *T. rotatorium*. To determine what trypanosome Martin et al. (1992) cultured, additional trypanosomes from frogs in Ontario will have to be sequenced to compare to the sequences from cultures and *Trypanosoma desseri*.

In Chapter III, *Trypanosoma desseri* was commonly found coinfecting hosts with the morphologically similar *T. curvus* (see description below), however, *T. desseri* is larger (cell length 57.22 ± 7.38 compared to 34.76 ± 3.56) and the anterior end is not as markedly curved as in *T. curvus*. Additionally, the positions of the nucleus and kinetoplast are more central in *T. desseri* and the kinetoplast is very close to the posterior end in *T. curvus* (Table 8). The close association between *T. desseri* and *T. curvus* was originally thought to suggest they were life stages of a single trypanosome species, however genetic analysis of isolated cells of each species showed they are genetically distinct lineages (Chapter III).

When *T. desseri* was observed on stained slides and in live preparations from different frog host species, there was often morphological variation in cell lengths and widths. Sometimes a frog would have wider *T. desseri* and sometimes a different frog would have skinnier *T. desseri* (Fig. 14). Additionally, the cells found on slides might appear stretched or scrunched based on how they fell when the smear was prepared. Figure 14 is an example of this variation. When originally viewing these forms, I considered the possibility that they might vary genetically, however no such relationships were found (Chapter III). Additionally, principal components analyses of cell dimensions did not show different clusters when points were colored by host species or geographic collection location (data not shown). Although *T. desseri* was variable in cell length and width, consistent characters for this species include the lack of a free flagellum and the position of the kinetoplast and nucleus relative to the cell length (PK/PA 0.17 ± 0.05, PN/PA 0.35 ± 0.05).

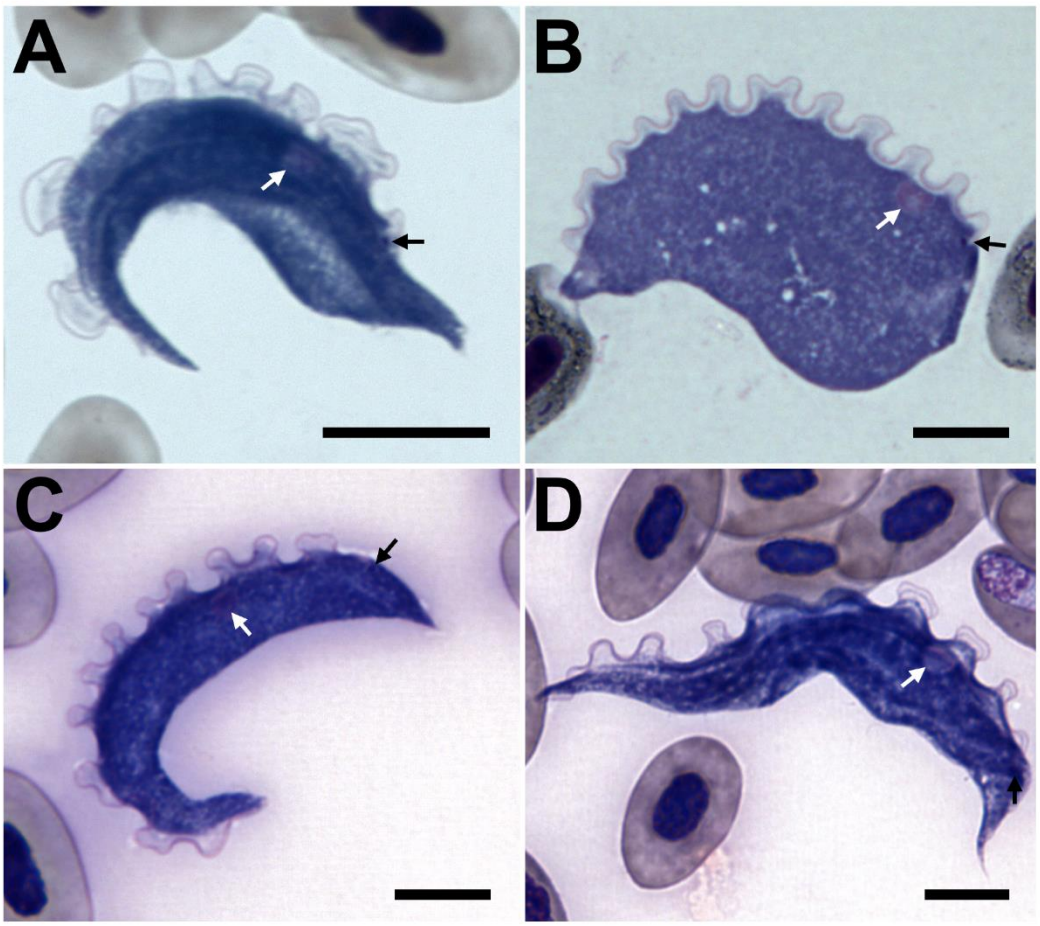

Figure 14. *Trypanosoma desseri* n. sp. on stained blood smears showing variation in cell length and width. **A-B.** Broader forms. **C-D**. More slender forms. Forms displaying this variation were found to be genetically identical or a few base pairs different at the 18s rRNA gene (Chapter III). Morphological characteristics consistent between forms include an undulating membrane beginning at the kinetoplast (black arrows), which is about 1/5th of the distance from posterior to anterior end and a nucleus (white arrows) about 2/5ths of the distance (Table 8). Additionally, the flagellum terminates at the anterior end not extending into a free flagellum. Scale bars = 10 µm.

Trypanosoma curvus n. sp.

Fig. 15.

Diagnosis: Short, broad trypanosome (PA 34.76 ± 3.56, BW 10.6 ± 3.61, Fig. 15; Table 8) with a curved anterior end. Kinetoplast close to the posterior end of the cell (PK/PA 0.1 ± 0.05), nucleus circular and about a third from posterior to anterior (PN/PA 0.36 ± 0.04). Both the kinetoplast and nucleus are off the midline of the cell, closer to the undulating membrane. Flagellum spans the length of the cell, terminating at the anterior end with no free flagellum. This form looks similar to *T. desseri* but differs in the body length (PA), position of the kinetoplast (PK/PA), and curved anterior end (Table 8). In live preparations of blood plasma, the curved form moves toward the curved anterior end as the undulating membrane flutters along the length of the cell (Supplementary Video 2).

Taxonomic Summary:

Type host: Rana sphenocephala.

Additional vertebrate hosts: Rana blairi, Rana clamitans,

Vector hosts: Unknown.

Type locality: Teal Ridge Aquatic Wetland, Stillwater, Oklahoma, (36°06'03.3" N, 97°04'48.3" W).

Distribution: Payne County, Oklahoma: Teal Ridge Aquatic Wetland (36°06'03.3" N, 97°04'48.3" W). Logan County, Oklahoma: (35°48'38.4" N, 97°24'08.6"

W). Kingfisher County, Hennessey, Oklahoma (36°07'00.0" N, 97°53'56.0" W). McCurtain County, Oklahoma: Little River NWR (33°57.200' N, 094°42.166' W). Hochatown (34°09'09.7" N, 94°45'05.6" W).

Prevalence: Rana blairi (2/6, 33%), *Rana clamitans* (1/56, 2%), *Rana sphenocephala* (19/39, 49%).

Type material: Blood smears stained with DipQuik were deposited to the Harold W. Manter Laboratory of Parasitiology Collection, Lincoln, Nebraska. Gene sequences for the 18s rRNA and gGAPDH genes were deposited to GenBank, accession numbers (##### - #####).

Etymology: The species is named for its characteristic curved anterior end.

Remarks:

To my knowledge, *Trypanosoma curvus* does not morphologically conform to any previously described *Trypanosoma* species. Its cell body length is smaller than most amphibian trypanosomes (PA 34.76 ± 3.56), yet it is relatively wide (BW 10.6 ± 3.61) and does not have a free flagellum (Table 8). A unique characteristic of *T. curvus* is how the wide posterior end tapers down to a curved anterior end resembling a cornucopia. The cornucopia shape has been used by previous authors to describe trypanosome morphology, but trypanosomes described as having this shape have differences relative to *T. curvus*. For example, Diamond (1965) mentions *T. ranarum* Type II forms as having a cornucopia shape, however the morphotypes he described 1) had free flagella extending

past the anterior end of the cell and 2) were widest in the anterior portion of the cell (near the free flagellum), and tapered to a point at the posterior end, which is the opposite of *T. curvus* which is widest at the posterior end of the cell (see Diamond, 1965, Fig. 51). Additionally, Laveran and Mesnil (1907) refer to a cornucopia form of *T. rotatorium* infecting frogs in Europe, however their form has a free flagellum and is larger than *T. curvus*.

In this study, *Trypanosoma curvus* n. sp. was primarily found infecting semi-terrestrial leopard frogs, *Rana blairi* and *Rana sphenocephala*, and was found on only one occasion infecting the semi-aquatic *Rana clamitans* (Chapter III). One could speculate that this species is adapted to more terrestrial frogs, and perhaps is transmitted by a more terrestrial vector such as a blood feeding dipteran.

Trypanosoma curvus was almost always found (75%, 18 of 24 frogs) coinfecting frogs with the larger yet morphologically similar *T. desseri*. The morphological similarity and frequent coinfections of *T. desseri* and *T. curvus* were originally thought to suggest they were life stages of a single trypanosome species, however genetic analysis of isolated cells of each species showed they are genetically distinct lineages (Chapter III).

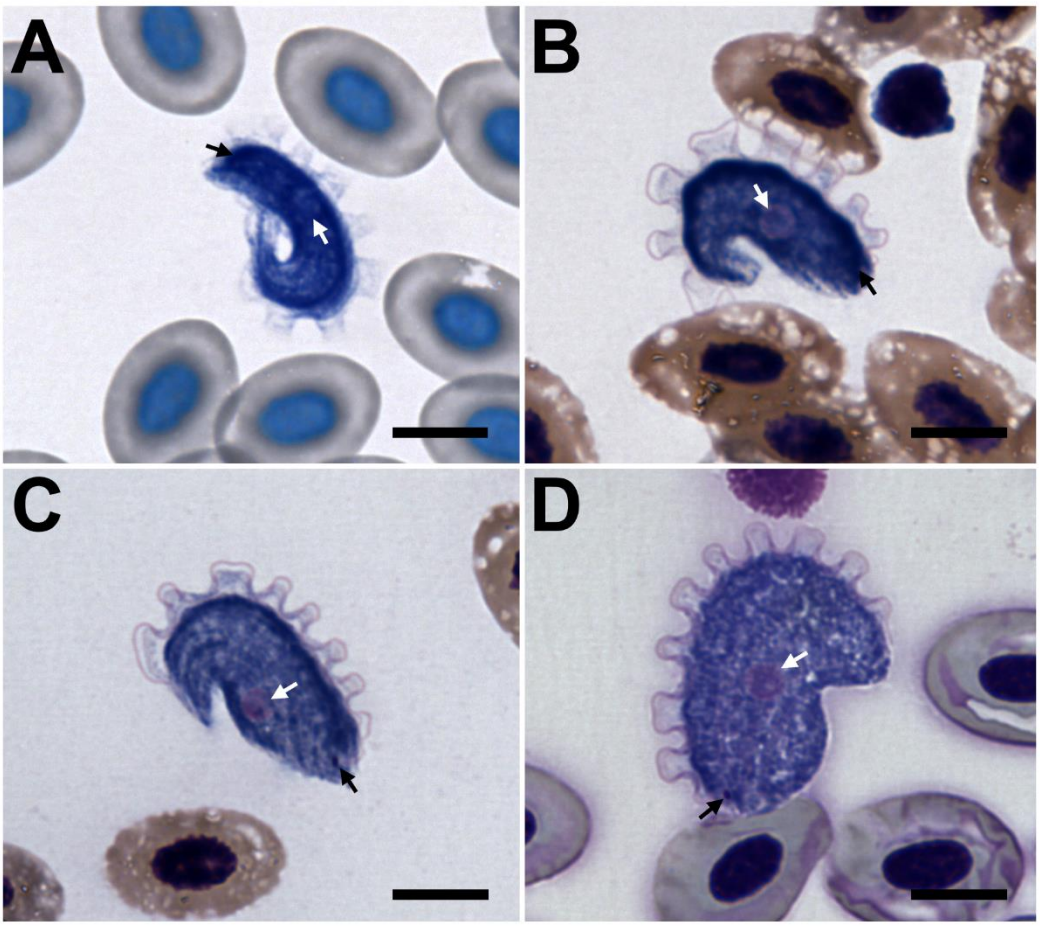

Figure 15. *Trypanosoma curvus* n. sp. on stained blood smears showing variation in cell width. **A.** More slender form. **B-C**. Intermediate width forms. **D.** Broad form. Consistent characteristics include an undulating membrane beginning at the kinetoplast (black arrows), which is very close to the posterior end of the cell. The nucleus (white arrows) is about 1/3rd of the distance from the posterior end to the anterior end. Flagellum terminates at the anterior end not extending into a free flagellum. Scale bars = 10 µm.

Trypanosoma louisdiamondi n. sp.

Fig. 16

Diagnosis: Medium sized trypanosome with a free flagellum (PA 46.07 ± 7.76, BW 7.19 ± 2.43, Fig. 16; Table 8). Both anterior and posterior ends taper to points. The kinetoplast is just under halfway (PK/PA 0.46 ± 0.06) from the posterior end to the anterior, while the circular nucleus is halfway along the cell (PN/PA 0.51 ± 0.05). Both the kinetoplast and nucleus are off the midline of the cell, closer to the undulating membrane. The flagellum extends past the anterior end of the cell (FF 12.03 ± 6.65). This form looks like a smaller version of *T.* cf. *ranarum* (see redescription of North American form below), with smaller body length (PA), width (BW), and nucleus (LN, WN). Additionally, the kinetoplast and nucleus are more anterior than *T.* cf. *ranarum* (PK/PA, PN/PA, Table 8). In live blood plasma preparations, the posterior end generally stays straight, and the anterior end rotates as the flagellum pulls it in a circle (Supplementary Video 3).

Taxonomic Summary:

Type host: Rana sphenocephala

Additional vertebrate hosts: Rana catesbeiana, Rana clamitans

Vector hosts: Unknown.

Type locality: Teal Ridge Aquatic Wetland, Stillwater, Oklahoma, (36°06'03.3" N, 97°04'48.3" W).

Distribution: Payne County, Oklahoma: Teal Ridge Aquatic Wetland (36°06'03.3"N, 97°04'48.3" W). McCurtain County, Oklahoma: Red Slough (33°44.897' N, 094°38.549' W), Little River NWR (33°57.200' N, 094°42.166' W). Polk County, Arkansas: Blue Haze Vista (34°37'40.17" N, 94°14'44.4228" W), Ouachita Mountains Biological Station (34°27'44.5" N, 93°59'54.2" W). Muskego, Waukesha County, Wisconsin (42°51'13.1764" N, 88°7'22.944" W).

Prevalence: Rana catesbeiana (3/36, 8%), *Rana clamitans* (6/56, 11%), *Rana sphenocephala* (2/39, 5%).

Type material: Blood smears stained with DipQuik were deposited to the Harold W. Manter Laboratory of Parasitiology Collection, Lincoln, Nebraska. Gene sequences for the 18s rRNA and gGAPDH genes were deposited to GenBank, accession numbers (##### - #####).

Etymology: This species is named after Dr. Louis S. Diamond in recognition for his research on amphibian trypanosome biology.

Remarks:

Trypanosoma louisdiamondi n. sp. was found infecting ranid hosts yet was not as common as other species. Additionally, *T. lousidiamondi* was always found infecting frogs with the morphologically similar morphotype *T.* cf. *ranarum*. The close association and morphological similarity of *T. lousidiamondi* and *T.* cf. *ranarum* was originally thought to suggest these species were life stages of a single trypanosome species,

however genetic analysis of isolated cells of each species showed they are genetically distinct lineages (Chapter III).

Trypanosoma louisdiamondi n. sp. looks similar to *T. schmidti* of Diamond (1965) but is much smaller. In this study, *T. louisdiamondi* had an average total cell length including flagellum of 55.67 ± 7.34, while *T. schmidti* is 99.5 ± 6.95 (Diamond, 1965). Interestingly, Diamond (1965) describes that upon inoculation of frogs with *T. schmidti* from cultures, juveniles of *T. schmidti* resemble the adult forms but are about half of the size. However, it is doubtful that all observations of *T. lousidiamondi* in the current study were immature forms, as this species was found eleven times across Oklahoma, Arkansas, Wisconsin, and New Hampshire, and larger versions of this species were not observed.

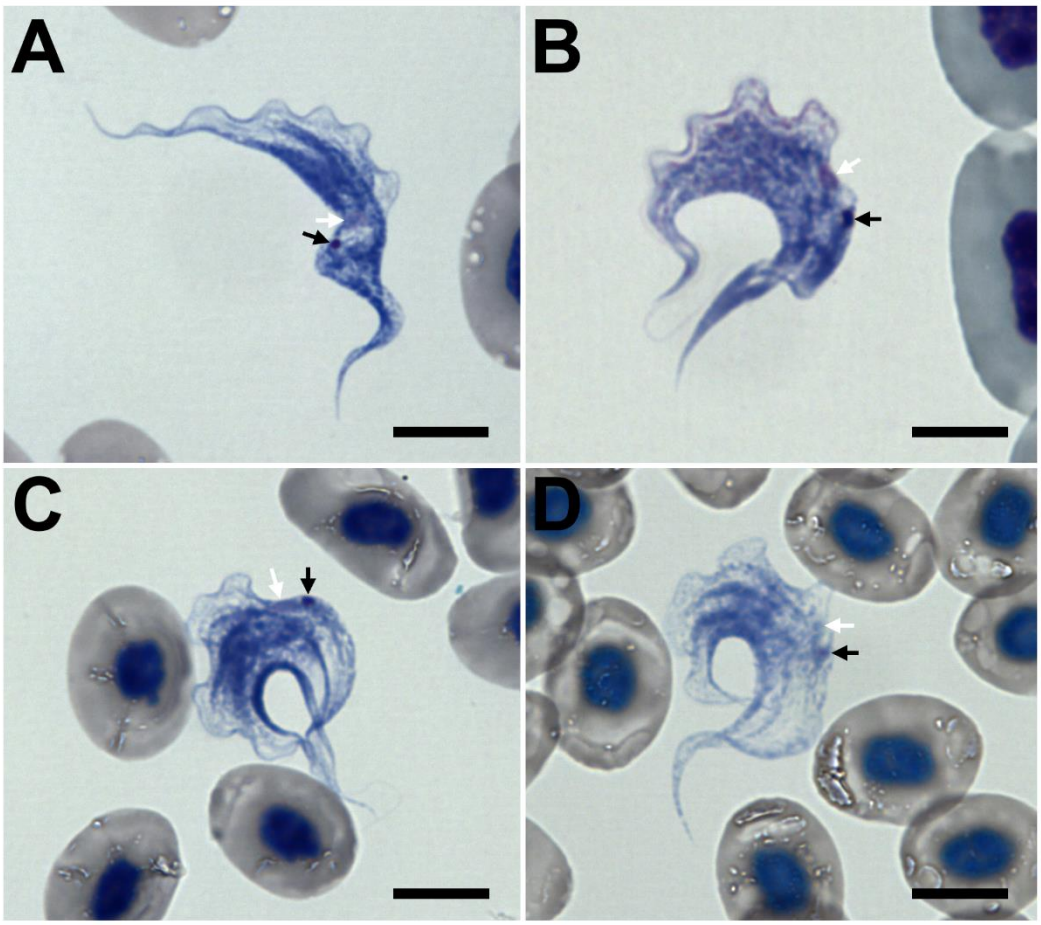

Figure 16. *Trypanosoma louisdiamondi* n. sp. on stained blood smears. This species is more morphologically consistent than other species in this study. Note the undulating membrane beginning at the kinetoplast (black arrows), just under halfway from the posterior end to anterior end, while the nucleus (white arrows) is near halfway along the cell. The flagellum extends past the anterior end of the cell. Scale bars = 10 µm.

Trypanosoma cf. *ranarum*

Fig. 17.

Diagnosis: Large, broad trypanosome with a free flagellum (PA 52.85 ± 7.11, BW 13.27 ± 3.73, Fig. 17; Table 8). Ends of cells come to a point, and the cell is often twisting to form an S or C shape. Kinetoplast about a third of the way from posterior to anterior end (PK/PA 0.33 ± 0.06), nucleus circular and just under halfway from posterior to anterior (PN/PA 0.45 ±0.06). Both the kinetoplast and nucleus are off the midline of the cell, closer to the undulating membrane. The undulating membrane begins at the kinetoplast and extends into a free flagellum 14.75 ± 3.69 microns long. When observed live in blood plasma, the free flagellum extends forward away from the cell and twists rapidly, pulling the rest of the cell anteriorly in a spiral (Supplementary Video 4).

Taxonomic Summary:

Vertebrate hosts in North America: Rana catesbianae, Rana clamitans, and *Rana sphenocephala*

Vector hosts: Unknown.

Distribution: Payne County, Oklahoma: Teal Ridge Aquatic Wetland (36°06'03.3" N, 97°04'48.3" W). McCurtain County, Oklahoma: Red Slough (33°44.897' N, 094°38.549' W), Little River NWR (33°57.200' N; 094°42.166' W). Polk County, Arkansas: Blue Haze Vista (34°37'40.17" N, 94°14'44.4228" W), Ouachita Mountains Biological Station (34°27'44.5" N, 93°59'54.2" W), Muskego, Waukesha County,

Wisconsin (42°51'13.1764" N, 88°7'22.944" W), Woodward Park, New London, New Hampshire (43°24'51" N, 71°59'32" W).

Prevalence: Rana catesbeiana (11/36, 31%), *Rana clamitans* (22/56, 39%), *Rana sphenocephala* (5/39, 13%).

Type material: Blood smears stained with DipQuik were deposited to the Harold W. Manter Laboratory of Parasitiology Collection, Lincoln, Nebraska. Gene sequences for the 18s rRNA and gGAPDH genes were deposited to GenBank, accession numbers (##### - #####).

Remarks:

Trypanosoma ranarum (Lankester, 1871), to which this species *Trypanosoma* cf. *ranarum* conforms, was originally described by Lankester from *P.* kl. *esculentus* in Germany. Since description, *T. ranarum* has been reported in North America and Europe, however the synonymy of these reports is not yet clear and because of this I have opted to designate the reports of this species in this study as *T.* cf. *ranarum* (Bardsley and Harmsen, 1973; Barta and Desser, 1984; Spodareva et al., 2018).

Trypanosoma cf. *ranarum* morphologically conforms to *Trypanosoma ranarum* reported by Spodareva et al. (2018) from European anurans. However, despite genetic similarities of 0.9 - 1.1% at 18s rRNA, the evidence is too premature to declare these reports conspecific at this point (Chapter III). There is currently only a single 18s consensus sequence for the European *T. ranarum*, which came from seven clones from

three frogs, including two *P.* kl. *esculentus* from Ukraine and one *P. ridibundus* from Czechia (Spodareva et al., 2018). Additional sampling and sequencing using similar methods to those in Chapter II will have to be employed to link sequence data and morphology from different hosts across the type localities in Europe as well as North America to support or refute the specific status of the current reports (Chapter III).

In North America, Stebbins (1907) described *Trypanosoma clamatae* from *Rana clamatans* presumably from Long Island, New York. He considered *T. clamatae* to have two forms, a larger broad form (Figs. 4-8, Stebbins, 1907) and a smaller slender form (Figs. 1-3, Stebbins, 1907). Based on recent investigations, these forms most likely represent distinct species and based on morphology in the plates, the larger form conforms to *Trypanosoma* cf. *ranarum*. Diamond (1965) reported two forms of *Trypanosoma ranarum* infecting *Rana pipiens* collected in Minnesota, USA. My forms are morphologically similar to Diamond's *T. ranarum* type II forms in terms of their general form (plates 52 and 53) and measurements (Table 5 of Diamond, 1965). Woo (1969) reported a broad trypanosome with a free flagellum infecting *Rana pipiens, R. clamitans,* and *R. catesbieana* in Ontario, Canada and identified it as *Trypanosoma ranarum*. Woo reports two forms of *T. ranarum,* a broader form and a slenderer form. These forms have similar kinetoplast and nucleus positions and both are within my concept of *Trypanosoma* cf. *ranarum*. Werner and Walewski (1976) report finding *T. ranarum* infecting various ranid frogs in Michigan, USA, however they do not provide any morphological data. They do report data from trypanosome species infecting toads, and these forms do have morphological similarities to *Trypanosoma* cf. *ranarum* of this study. However, the forms of Werner and Walewski (1976) were found be host-specific

to toads by later investigations and were synonymized with *T. fallisi* (Werner et al., 1988; Martin and Desser, 1990). Additionally, *T. fallisi* is genetically distinct from *T. ranarum* at 18s rRNA (Chapter III; Martin et al., 2002). Barta and Desser (1984) reported *T. ranarum* infecting *R. catesbeiana*, *R. clamitans*, and *R. septentrionalis* in Ontario, Canada. Their measurements of the body length, body width, and flagella as well as their Fig. 3 conform to my concept of *Trypansoma* cf. *ranarum*.

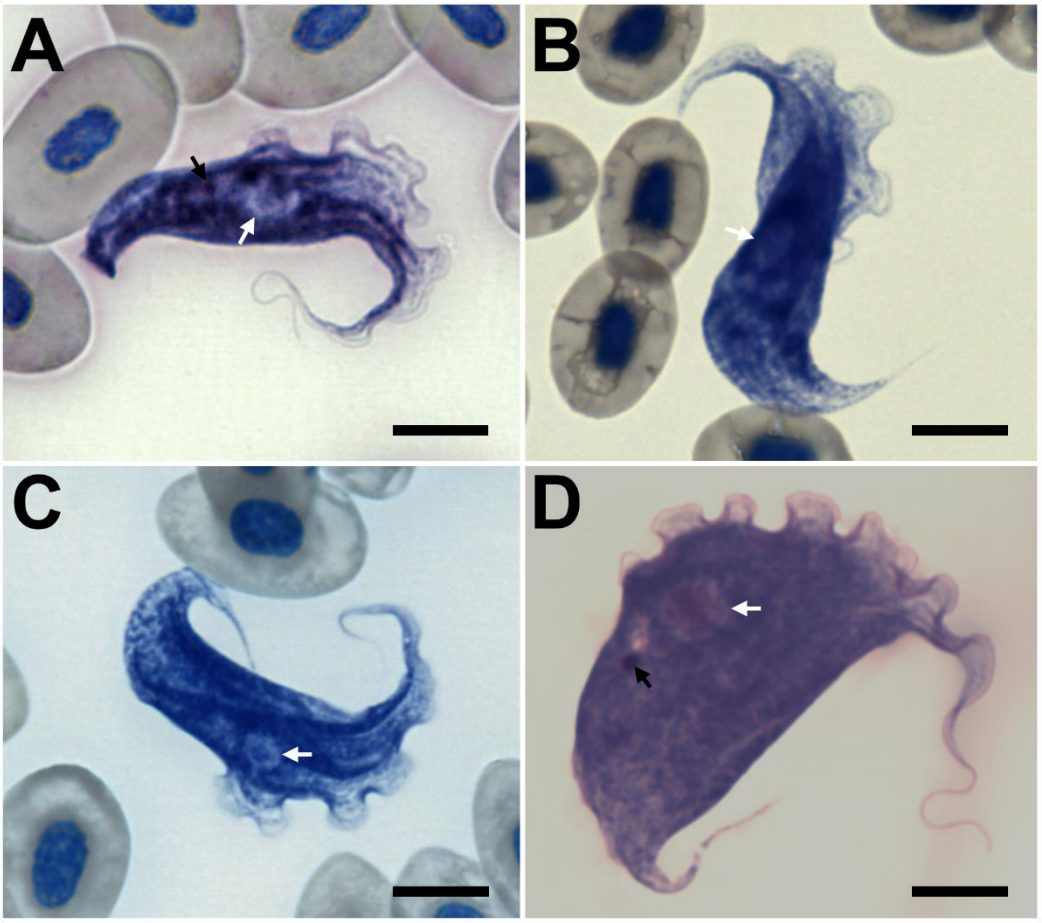

Figure 17. *Trypanosoma* cf. *ranarum* on stained blood smears showing variation in cell length and width. **A.** More slender form. **B-C.** Intermediate width forms. **D.** Broad form. Consistent characteristics include an undulating membrane beginning at the kinetoplast (black arrows), which is about 1/3rd of the cell length from posterior to anterior end. The nucleus (white arrows) is about half of the distance from the posterior end to the anterior end. The undulating membrane begins at the kinetoplast and extends into a free flagellum 14.75 ± 3.69 microns long. Scale bars = 10 µm.

DISCUSSION

Mixed infections and the possibility for pleomorphic species have been a major challenge to describing the diversity of amphibian trypanosomes (Bardsley and Harmsen, 1973; Desser, 2001). Data generated on amphibian trypanosomes without discerning the identity and number of forms present in a trypanosome infection runs the risk of adding confusion rather than clarity. An example is investigated in Chapter III, when previous studies found evidence suggesting trypanosome morphology was not phylogenetically conserved. However, phylogenetic analyses in Chapter III that excluded sequences without confirmed bloodstream morphology yielded clades of trypanosomes with general morphological similarities, suggesting that amphibian trypanosome morphology may be more conserved than previously thought. The methods outlined in Chapter II provide the ability to link sequence data to trypanosome cell morphology, which is a powerful tool to identify the forms in mixed trypanosome infections and elucidate pleomorphic species. Future studies on amphibian trypanosomes can use the techniques in Chapter II to sequence new trypanosomes cells and compare the 18s rRNA and gGAPDH gene sequences to the species described here. Further study including sequencing isolated cells is needed to describe the remaining eight morphotypes reported in Chapter III.

I argue that combining morphological measurements linked to sequence data is the way forward in describing the diversity of trypanosomes in anurans, allowing for studies on life cycles, development, and host parasite interactions on known species. Additionally, the continued generation of sequences linked to morphology will test the consistency of morphology as a character to identify species and define the morphological limits of trypanosome species. The current research provides hope that

with careful considerations of possible pitfalls (mixed infections and pleomorphism) we can reliably identify these organisms and uncover the hidden diversity of amphibian trypanosomes.

Table 8. Dimensions of the four trypanosome species. All measurements are reported in micrometers (μm) as an average ± standard deviation followed by the range in parentheses.

	Trypanosoma desseri n. sp. n = 330	*Trypanosoma curvus* n. sp. n = 56	*Trypanosoma louisdiamondi* n. sp. n = 18	*Trypanosoma* cf. *ranarum* n = 193
PF	n/a	n/a	55.67 ± 7.34 (47.3 – 66.7)	68.97 ± 6.84 (53 – 88.7)
PA	57.22 ± 7.38 (31.5 – 82.7)	34.76 ± 3.56 (27.1 – 46.5)	46.07 ± 7.76 (26.8 – 59.7)	52.85 ± 7.11 (33.5 – 71.9)
FF	n/a	n/a	12.03 ± 6.65 (2.5 – 23)	14.75 ± 3.69 (4.4 – 23.2)
BW	12.73 ± 3.87 (5.5 – 26.8)	10.6 ± 3.61 (5.5 – 19.5)	7.19 ± 2.43 (2.4 – 10.4)	13.27 ± 3.73 (6 – 28.3)
LN	3.62 ± 0.58 (2.1 – 6.2)	3.55 ± 0.52 (2.3 – 4.5)	2.44 ± 0.45 (1.8 – 3.3)	4.74 ± 1.04 (1.2 – 8.1)
WN	3.03 ± 0.6 (1 – 4.8)	3.09 ± 0.56 (2 – 4.1)	1.76 ± 0.49 (1.1 – 2.7)	3.82 ± 0.94 (1.4 – 6.7)
PK	10.25 ± 3.44 (3 – 19.7)	3.55 ± 1.66 (1.3 – 7.3)	21.12 ± 4.68 (12.9 – 28.6)	17.48 ± 4.13 (5.2 – 30.1)
KN	10.26 ± 3.54 (3.7 – 23.9)	9.08 ± 2.1 (3.9 – 12.6)	3.39 ± 1.06 (2 – 5.6)	5.87 ± 1.35 (2.2 – 11)
NA	37.99 ± 5.91 (20.1 – 55.9)	22.95 ± 3.54 (15.9 – 31.1)	24.47 ± 6.12 (10.6 – 34.4)	29.44 ± 5.01 (12.3 – 46.9)
PN	20.04 ± 3.63 (10.2 – 36.8)	12.52 ± 1.51 (8.8 – 15.7)	22.73 ± 3.43 (16.1 – 28.4)	23.42 ± 4.55 (13.1 – 38)
PK/PN	0.51 ± 0.15 (0.15 – 0.85)	0.29 ± 0.14 (0.11 – 0.6)	0.88 ± 0.08 (0.72 – 0.99)	0.75 ± 0.09 (0.39 – 1.02)
PK/PA	0.17 ± 0.05 (0.06 – 0.31)	0.1 ± 0.05 (0.04 – 0.21)	0.46 ± 0.06 (0.34 – 0.64)	0.33 ± 0.06 (0.15 – 0.5)
PN/PA	0.35 ± 0.05 (0.21 – 0.58)	0.36 ± 0.04 (0.27 – 0.48)	0.51 ± 0.05 (0.44 – 0.6)	0.45 ± 0.06 (0.28 – 0.69)
BW/PA	0.22 ± 0.07 (0.09 – 0.5)	0.3 ± 0.1 (0.16 – 0.57)	0.16 ± 0.05 (0.07 – 0.23)	0.25 ± 0.08 (0.09 – 0.64)
FF/PA	n/a	n/a	0.33 ± 0.27 (0.05 – 0.86)	0.28 ± 0.08 (0.06 – 0.52)

CHAPTER V

MORPHOLOGICAL AND MOLECULAR CHARACTERIZATION OF *HEPATOZOON* SPECIES INFECTING FROGS AND SNAKES ACROSS THE CENTRAL AND EASTERN UNITED STATES

ABSTRACT: The genus *Hepatozoon* Miller, 1908 (Apicomplexa: Adeleorina) are intracellular blood parasites that are vector transmitted between diverse vertebrate hosts including frogs and snakes. Species identification based on forms in vertebrate blood is difficult because there are usually not many morphological characters to distinguish species and gamonts of genetically different isolates can be morphologically indistinguishable. Traditionally, *Hepatozoon* spp. have been distinguished by characters other than bloodstream gamont morphology, such as pathology to host erythrocytes and/or developmental stages in the invertebrate vector. However, recent molecular studies are finding these traditional distinctions do not correlate with gene sequence data. Specifically, *H. catesbianae* and *H. clamatae* are closely related species that infect North American anurans that are morphologically indistinguishable and have been distinguished by fragmentation of the host erythrocyte nucleus. However, this character does not correlate with specific genotypes of these infections. In this study, anurans from the United States with fragmented and unfragmented infections are morphologically and

molecularly characterized at three loci, CO3, ITS-1, and 18s rRNA, and their genotypes and fragmentation effects are compared. Of the three ranid species found infected with *Hepatozoon* spp., *Rana catesbeiana, R. clamitans*, and *R. sphenocephala*, only *R. clamitans* had infected erythrocytes with fragmented nuclei. Similar to previous studies, genotypes of *Hepatozoon* spp. from *R. clamitans* did not correlate with the presence or absence of fragmentation. Additionally, *Hepatozoon* cf. *sipedon* is reported and characterized from three snake species collected in Oklahoma and Arkansas. Infected erythrocytes in these snakes displayed variation in cytoplasm clearing. While frog *Hepatozoon* spp. infecting frogs were in a single clade on the 18s rRNA phylogeny, *Hepatozoon* spp. infecting snakes were found in multiple clades with other hosts including lizards, small mammals, and frogs, suggesting snakes may be capturing *Hepatozoon* spp. from their prey. The possibilities for life cycle evolution of *Hepatozoon* spp. infecting snakes are discussed.

INTRODUCTION

The genus *Hepatozoon* Miller, 1908 (Apicomplexa: Adeleorina) includes intracellular protozoan parasites that infect erythrocytes, leukocytes, and hepatocytes of mammals, birds, reptiles, and amphibians (Smith, 1996; Kim et al., 1998). Hemophagous arthropods including ticks, mites, lice, fleas, reduviid bugs, sandflies, tsetse flies, and mosquitoes have been reported as vectors and definitive hosts for *Hepatozoon* spp. (Smith, 1996). *Hepatozoon* species are reported to have either two-host or three-host life cycles. In two-host life cycles, gamogany (sexual reproduction) occurs in the invertebrate definitive host, forming oocysts (Desser et al., 1995; Smith, 1996). The oocyst then

undergoes sporogany (asexual reproduction) producing sporocysts containing sporozoites (Levine, 1988). Transmission to the vertebrate host occurs by ingestion of an infected arthropod. Sporozoites invade the internal organs such as the liver, where merogony (asexual reproduction) takes place, leading to the release of merozoites that infect erythrocytes or leukocytes and develop to gamonts (Smith, 1996). When the appropriate hematophagous invertebrate host ingests blood with gamonts from an infected vertebrate, gamonts travel to the hemocoel or malphigian tubules and undergo sexual reproduction (gamogony) followed by asexual reproduction (sporogony) forming sporozoites and completing the life cycle (Smith, 1996).

Three-host lifecycles involve the addition of a dizoic cyst stage in the liver and/or lungs of an insectivorous vertebrate transfer host. The transfer host typically ingests an arthropod infected with sporozoites, and the sporozoites infect the liver and/or lungs and develop into dizoic cysts (Smith, 1996). When this transfer host is ingested by a suitable predator host, the cysts pass over and infect the predators' organs where they undergo two rounds of merogany. This produces merozoites that infect circulating erythrocytes where they develop into gamonts that are ingested by the hematophagous arthropod. Gametogenesis, fertilization, and sporogony occur in the arthropod and the life cycle continues when the arthropod is ingested by the transfer host (Smith et al., 1994; Smith, 1996). A more complicated life cycle is described for *H. domerguei* where a lizard transfer host has both gamonts in circulating erythrocytes and dizoic cysts in its organs (Landau et al., 1972). This lizard is then able to infect both blood-feeding arthropods and the predator snake intermediate host.

Hepatozoon spp. Infecting Amphibians

Currently, 48 species of *Hepatozoon* have been described from amphibians around the world (Smith, 1996; Harris et al., 2014, Netherlands et al., 2018). In North America, five species of *Hepatozoon* are known to infect amphibians. Stebbins (1904, 1905) described *H. catesbianae* in bullfrogs (*Rana catesbeiana*) and *H. clamatae* in green frogs (*Rana clamatans*) from New York. Additionally, Lehmann (1959a; 1959b; 1960) described three species of *Hepatozoon* in anurans from California including *H. sonomae* and *H. boyli* infecting the foothill yellow-legged frog (*Rana boylii*) and *H. aurora* infecting the northern red-legged frog (*Rana aurora*). The only other reports of *Hepatozoon* spp. infecting amphibians in North America include *H. catesbianae* and *H. clamatae* in bullfrogs, green frogs and northern leopard frogs (*Rana pipiens*) from Ontario, Canada, *H. catesbianae* and *H. clamatae* in bullfrogs and green frogs in Nova Scotia, Canada, and *H. clamatae* in green frogs and northern leopard frogs from Illinois (Kudo, 1922; Barta and Desser, 1984; Desser et al., 1995; Kim et al., 1998; Boulianne et al., 2007). More recently, it has become the practice to forgo naming *Hepatozoon* species without molecular data. Stenberg and Bowerman (2008) reported a *Hepatozoon* sp. from the Oregon spotted frog (*Rana pretiosa*) from Oregon and McAllister et al. (2020) reported *Hepatozoon* spp. from green frogs in Arkansas. Additionally, Léveillé et al. (2021) reported three genotypes of *Hepatozoon* spp. in Ontario, genotype A (corresponding to *H. catesbeiana*) infecting bullfrogs and green frogs, genotype B (corresponding to *H. clamatae*) in bullfrogs, green frogs, and northern leopard frogs, and genotype C (designated *Hepatozoon* sp.) that was only found in northern leopard frogs.

The life cycles for *Hepatozoon catesbianae* and *H. clamatae* were elucidated by Desser et al. (1995) and Kim et al. (1998), respectively. Briefly, gametogenesis, fertilization, and sporogony of both species occur in the malpighian tubules of the mosquito *Culex territans*. When a frog ingests an infected mosquito, sporozoites invade frog liver cells and form meronts. These meronts release merozoites that infect erythrocytes and develop into gamonts. *Culex territans* then feeds on the frog and ingest circulating gamonts, which migrate to the malpighian tubules and mate forming oocysts that undergo sporogony and the life cycle continues. More recently, Harkness et al. (2010) was able to infect *Culex pipiens*, a bird/mammal feeding mosquito, with *H. clamatae* in the laboratory, suggesting that amphibian *Hepatozoon* species may not be specific to their mosquito vector hosts. Clearly other species of mosquitoes must serve as vectors for anuran *Hepatozoon* spp. because frogs are infected in California which is outside of the range of *C. territans* (Lehman, 1959a; 1959b; 1960; Darsie and Ward, 2005).

Traditionally, *Hepatozoon clamatae* has been differentiated from *H. catesbianae* by the effect on the host erythrocyte nucleus, as *H. clamatae* fragments the erythrocyte nucleus while *H. catesbianae* does not (Fig. 18; Desser et al. 1995; Kim et al. 1998; Boulianne et al., 2007; Léveillé et al. 2021). Additionally, *H. clamatae* (fragmented infections) have been primarily found infecting *Rana clamitans* while *H. catesbianae* (unfragmented infections) are mainly found in bullfrogs *R. catesbeiana*, and hence the *Hepatozoon* spp. were named for their hosts (Desser et al. 1995; Kim et al. 1998; Boulianne et al., 2007). However, recent molecular studies found no genetic correlation with the erythrocyte nucleus fragmentation character, as sequences of Genotypes A and B

originated from both infections with fragmented nuclei and unfragmented nuclei (Boulianne et al., 2007; Léveillé et al. 2021). The biological significance of this character and its occurrence across different host frog species and across *Hepatozoon* genotypes remains unexplained.

Hepatozoon spp. Infecting Snakes

In addition to amphibians, at least 123 species of *Hepatozoon* have been described infecting snakes worldwide (Smith, 1996; Cook et al., 2018). In North America, Telford (2009) recognized 18 *Hepatozoon* spp. infecting snakes that have sufficient life cycle information available. The most studied of these species include *Hepatozoon rarefaciens*, *H. fusifex*, and *H. sipedon*. *Hepatozoon rarefaciens* naturally infects indigo snakes (*Drymarchon corais*) in Mexico and was experimentally transmitted to *Boa constrictor* and *Pituophis c. catenifer* via lab raised *Culex tarsalis* mosquitoes (Ball et al., 1967; Telford, 2009). *Hepatozoon fusifex* was described from natural populations of *Boa constrictor* near Colima, Mexico and sporogany was observed in the hemocoel of ticks (*Amblyomma dissimile*) attached to the boas upon capture (Ball et al., 1969). Additionally, *H. fusifex* developed in diverse vertebrate and invertebrate hosts when exposed experimentally. The mosquitoes *C. tarsalis* and *Aedes togoi* became infected with mature oocysts after feeding on infected boas. Additionally, feeding infected mosquitoes to lizards, *Anolis carolinensis* and *Sceloporus occidentalis*, and the snake *Pituophis c. catenifer* resulted in development and the presentation of gamonts in circulating red blood cells (Booden et al., 1970; Oda et al., 1971; Telford, 2009). *Hepatozoon sipedon* was described from northern watersnakes, *Nerodia sipedon*, in

Ontario, Canada (Smith et al., 1994). The life cycle for *H. sipedon* includes three hosts, the northern water snake, *Nerodia sipedon*, the northern leopard frog *Rana pipiens*, and either of two mosquitoes *Culex pipiens* or *Culex territans* (Smith et al., 1994).

In general, snakes become infected with *Hepatozoon* spp. when they ingest either an invertebrate containing sporozoites, or a vertebrate containing dizoic cysts in the liver or lungs (Smith, 1996; Telford, 2009, Zechmeisterova et al., 2021). However, snakes do not commonly feed on hematophagous invertebrates, and the most plausible mode of transmission involves ingesting vertebrates such as frogs, lizards, and rodents containing dizoic cysts (Smith, 1996; Sloboda et al., 2007; Zechmeisterova et al., 2021). However, three-host life cycles have not been demonstrated for many snake *Hepatozoon* species. Additionally, numerous studies by Telford et al. (2001; 2004; 2005; 2008) report finding oocysts or sporocysts of *Hepatozoon* spp. in the proboscides of mosquitoes, suggesting transmission via direct inoculation of the blood during mosquito feeding is possible (Telford, 2009). Congenital transmission has also been reported, where infected pregnant female snakes give birth to offspring that are also infected (Lowichik and Yaeger, 1987; Kauffman et al., 2017).

Most *Hepatozoon* spp. were described and named for the host they were found infecting, and experimental lab infections have generally demonstrated low host-specificity and potentially wide host ranges (Booden et al., 1970; Oda et al., 1971; Landau et al., 1972; Sloboda et al., 2007; Telford, 2009). Genetic data is increasingly becoming available for *Hepatozoon* spp. and is a promising way to evaluate species associations. However, sequence data are only available for two species of *Hepatozoon* from frogs (*H. clamatae* and *H. catesbianae*) and one species from a snake (*H. sipedon*)

in North America. The goal of this study was to survey frogs and snakes in central USA for *Hepatozoon* species and sequence the 18s rRNA, CO3, and ITS-1 genes to provide a basis for genetic species identification of *Hepatozoon* spp. in North America.

MATERIALS AND METHODS

Collection of Specimens

During April through August of 2014-2019, 250 anurans, ten caudatans, and six snakes were collected and examined for blood protozoa from Arkansas, New Hampshire, Oklahoma, and Wisconsin (Table 9). Species sampled from Teal Ridge Aquatic Wetland, Stillwater, Oklahoma (36°06'03.3" N, 97°04'48.3" W) included *Acris blanchardi* (N=28), *Ambystoma texanum* (N=10), *Anaxyrus americanus* (N=2), *Anaxyrus woodhousii* (N=5), *Gastrophryne olivacea* (N=28), *Hyla chrysoscelis* (adults N=11, tadpoles N=13), *Pseudacris clarki* (N=5), *Rana catesbeiana* (N=13), *R. sphenocephala* (N=30). Species from Hennessey, Oklahoma (36°07'00.0" N, 97°53'56.0" W) included *R. blairi* (N=4) and *R. catesbeiana* (N=2). Species from Guthrie, Oklahoma (35°48'38.4" N, 97°24'08.6" W) included *R. sphenocephala* (N=7). Species from Red Slough WMA, McCurtain Co. Oklahoma (33°44.897' N, 094°38.549' W) included *R. catesbeiana* (N=15), *R. clamitans* (N=7), and *R. sphenocephala* (N=1). Species from Little River NWR, McCurtain Co. Oklahoma (33°57.200' N, 094°42.166' W) included *H. avivoca* (N=9), *H. cinerea* (N=9), *R. clamitans* (N=2), and *R. sphenocephala* (N=2). Species from Blue Haze Vista, Arkansas (34°37'40.17" N, 94°14'44.4228" W) included *R. catesbeiana* (N =2) and *R. clamitans* (N=14). Nine of the *R. clamitans* were reported in McCallister et al. (2020). Species from Ouachita Mountains Biological Station, Arkansas (34°27'44.5" N,

93°59'54.2" W) included *H. cinerea* (N=5), *R. catesbeiana* (N=17), and *R. clamitans* (N=10). Additionally, eight *R. clamitans* were collected from Woodward Park, New London, New Hampshire (43°24'51" N, 71°59'32" W) and fifteen *R. clamitans* were collected from Muskego, Waukesha County, Wisconsin (42°51'13.1764" N, 88°7'22.944" W).

Amphibians from all locations were collected by hand or by dip-net. Adult and newly metamorphosed amphibians were placed in moist cotton bags; whereas all larval amphibians were placed in 18.9 L buckets filled with pond water and transported to the laboratory. In the laboratory, amphibians were double pithed and examined for blood protozoans within 12 hours of capture. Snakes were caught by hand and euthanized by an overdose of with an intraperitoneal injection of sodium pentobarbital. Additionally, the single *Nerodia rhombifer* was road kill found dead on the side of the road in Stillwater, Oklahoma.

Blood Processing and Examination

For adult and newly metamorphosed amphibians, blood was drawn from the facial vein with a 26-gauge needle and collected in capillary tubes following Forzán et al. (2012). Blood was drawn from the heart of euthanized snakes with a 22-gauge needle and collected into capillary tubes. For each amphibian and snake individual, blood from a single capillary tube was deposited on a glass slide with a pipette bulb and a thin smear prepared. Additionally, 200 µL of blood from each amphibian and snake was fixed in 100% ethanol in 1.5 ml Eppendorf tubes and stored at -80 °C for molecular analyses.

Thin blood smears were air-dried and stained with the JorVet Dip Quick Stain Kit (Jorgensen Labs, CO). Stained slides were scanned at high power (100x objective) with an Olympus BX-51 upright research microscope for approximately 10 minutes to detect intracellular parasites infecting host red blood cells. When *Hepatozoon* spp. gamonts were found on smears, 10 to 20 specimens of each stage were photographed with an Olympus 5-megapixel digital camera. Parasite cell dimensions were measured on photomicrographs using ImageJ (Schneider et al., 2012) calibrated with a stage micrometer (Reichert, NY). Gamont length and width as well as the gamont nucleus length and width were measured from each cell. Gamont length was measured along the midline of the cell, and the gamont width was measured from the cell's widest point. The gamont nucleus length was the long axis of the nucleus and the width was perpendicular to the length measurement.

DNA Extraction

DNA was extracted from ethanol preserved frog blood by thawing and drying 20 μL in a Thermolyne dri-bath heated to 56°C for approximately 30 minutes to evaporate ethanol. Then the DNeasy Blood and Tissue Kit (Qiagen, CA) was used following the recommended protocol for samples of nucleated blood.

PCR Amplification and Sequencing

The 18s ribosomal RNA, internal transcribed spacer region 1 (ITS-1), and cytochrome oxidase subunit 3 (CO3) genes were amplified from extracted DNA samples

by PCR using previously published primers as well as new primers made from alignments of available sequences (Table 10). For all gene targets, 25 µL PCR reactions were performed using the Platinum Green Hot Start PCR Master Mix Kit (Invitrogen, Carlsbad, CA). The PCR program was as follows: initial activation for 300s at 95°C, annealing for 30s at the appropriate temperature for the primer pair in Table 10, and extension for 60s at 72°C, repeated for 30-40 cycles before a final extension period of 420s at 72°C. PCR success was determined by running 4 µL of PCR product on a 1% agarose gel and only single, solid bands were prepped for sequencing using the Promega Wizard DNA Purification Kit (Promega, WI). Sanger sequencing of PCR amplicons was performed with the primers in Table 10 on an Applied Biosystems 3730 capillary sequencer at the Oklahoma State University core facility. Forward and reverse chromatograms were aligned and inspected in MEGA X (Kumar et al., 2018). All sequences had 100% identity between forward and reverse chromatograms.

Phylogenetic Analyses

Gene sequences of the 18s rRNA, ITS-1, and CO3 genes were obtained from GenBank. Each gene alignment was created using the MUSCLE (Edgar, 2004) feature of MEGA X (Kumar et al., 2018). For the 18s rRNA gene, sequences from Karadjian et al. (2015) were combined with more recently sequenced *Hepatozoon* spp. 18s rRNA available on GenBank. However, to obtain reasonable support values, only sequences greater than 1170 base pairs in length were retained. The final alignment had 126 sequences and 1090 positions after gaps were removed. The phylogeny was estimated using the Maximum Likelihood (ML) framework within MEGA X (Kumar et al., 2018).

The HKY+G+I model (Hasegawa et al., 1985) was found to be the best fit using the MEGA X modeltest feature. Support values of nodes were assessed using 1000 bootstrap replications.

The ITS-1 gene alignment included 27 sequences with 93 positions after removal of gaps. ITS-1 sequences from Kim et al. (1998) and Smith et al. (1999) were not included in the alignment as they were reported to contain errors due to early sequencing technology (Boulianne et al., 2007, T. Smith pers. comm.) The ML tree was created with the T92 model (Tamura, 1992), as it was the best fit. Support values of nodes were assessed using 1000 bootstrap replications.

The 17 cytochrome oxidase subunit 3 (CO3) gene sequences obtained in this study were aligned with additional CO3 sequences from *Hepatozoon* spp. obtained from GenBank. Of these, nine CO3 sequences were in records of full mitochondrial genomes and only the CO3 gene sequences were used for these analyses. The alignment was made with the MUSCLE feature and involved 31 nucleotide sequences with 581 positions and included all codon positions. The ML tree was created with the GTR + G model (Nei and Kumar, 2000), as it was the best fit. Support values of nodes were assessed using 1000 bootstrap replications.

For all three genes, p-distances were calculated using pairwise comparisons between sequences using MEGA X (Kumar et al., 2018).

RESULTS

Parasite Prevalence and Morphology in Anurans

Of all amphibians sampled, three species were infected with *Hepatozoon* spp. gamonts (Table 9). Prevalence was highest in *Rana clamitans* at 50% (28 of 56), followed by 22% (8 of 36) in *Rana catesbeiana*, and 10% (4 of 39) in *Rana sphenocephala* (Table 9, Fig. 18). Host erythrocyte nuclei were only fragmented in *Rana clamitans*, which represented 64% (18 of 28) of *R. clamitans* infections (Table 9). Additionally, infections in *R. clamitans* displayed varying degrees of fragmentation, including fully fragmented nuclei (ten infections), cells with nuclei split into two lobes (six infections), and nuclei that appeared to have been liquified (two infections; Fig. 19).

Mature and immature *Hepatozoon* sp. gamonts were found infecting the three *Rana* species (Fig. 18A-C, Table 11). Immature gamonts are smaller than mature gamonts and arise earlier in infection (Kim et al., 1998). One *R. clamitans* and one *R. sphenocephala* contained both mature and immature gamonts, while one *R. catesbeiana* was infected by immature gamonts exclusively. Length and width measurements of mature gamonts were similar from all frog hosts, as were immature gamonts from different frog hosts (Table 11). Additionally, measurements were similar for gamonts infecting red blood cells with fragmented and unfragmented nuclei and measurements of mature and immature gamonts were similar between genotypes (Tables 12 and 13).

Parasite Prevalence and Morphology in Snakes

Five of the six snakes collected were infected with *Hepatozoon* sp. gamonts, including both the individual *Nerodia rhombifer* and *Thamnophis proximus* examined and three of the four *Agkistrodon contortrix* (Fig. 18D, Table 9). Infected snake erythrocytes often displayed a clearing of the cytoplasm, which varied in extent from no observed clearing to total clearing of the entire cell (Fig. 20). Examples of all extents of clearing were observed in all three snake species. Most infected cells had an intermediate clearing (Fig. 20B-C).

Phylogenetic Analyses of Anuran *Hepatozoon* Genotypes

At the CO3 gene locus, the sequences obtained in this study fell into three clades with *Hepatozoon* spp. genotypes previously identified by Léveillé et al. (2021) from *Hepatozoon* spp. infecting frogs in Ontario, Canada (Fig. 21). Nine sequences from this study were identical to *Hepatozoon catesbianae* (KF894962.2) and can be designated Genotype A. Five sequences had very close similarity (0 – 0.3% of 629 bases) to *Hepatozoon clamatae* (MN245241.1 and MN310689.1) and can be assigned to Genotype B. Three sequences were near Genotype C (MN245143.1 and MN310690.1), but with low bootstrap support and a slightly larger sequence divergence (1.0-1.2% of 629 bases). Therefore, these sequences are considered a distinct genotype, Genotype D (Fig. 21). The average difference between genotypes varied from 0.7% (A to C) to 2.7% (B to D) different over the 629 bases.

In general, the genetic differences found between amphibian *Hepatozoon* spp. sequences at ITS-1 and 18s rRNA were much smaller than the differences found at CO3. Sequences differed by only one or two bases at 18s and ITS-1, while larger variation of 5 to 17 bases was found between sequences at CO3. For this reason, the genotype identity of samples at CO3 is used in the next paragraphs to compare samples at ITS-1 and 18s rRNA phylogenies (Figs. 22 - 24).

The ITS-1 phylogeny recovered two groups for the *Hepatozoon* sp. genotypes sequenced in this study, designated as clades 1 and 2 (Fig. 22). Samples identified as Genotype A at CO3 formed Clade 1 on the ITS-1 phylogeny and included *H. catesbianae* from Léveillé et al. (2021; MN244528.1) and Boulianne et al. (2007; DQ856589-91). Samples identified as Genotype B and D were identical at ITS-1 and formed Clade 2 with *H. clamatae* from Léveillé et al. (2021; MN244529.1) and Boulianne et al. (2007; DQ856584-88). Clade 1 was two bases different (4.3%) than Clade 2 over the 93 base ITS-1 gene. Genotype C of Léveillé et al. (2021; MN244530.1) was one base different (2.2%) than Clade 1 sequences over the 93 base pair gene and was designated Clade 3 (Fig. 22).

The 18s phylogeny recovered similar topology to previous work (Fig. 23, Karadjian et al., 2015, Maia et al., 2016). Our *Hepatozoon* sp. sequences came out in a monophyletic group with previous sequences of *Hepatozoon catesbianae* and *Hepatozoon clamatae* from Ontario, Canada (Fig. 24; Barta et al., 2012; Léveillé et al., 2021). This group was nested within a group containing sequences for *Hepatozoon* spp. infecting frogs throughout the world and *Hepatozoon* spp. infecting natricine snakes, which often feed on frogs. Much like the ITS-1 phylogeny, the 18s rRNA phylogeny

recovered two groups for the *Hepatozoon* sp. genotypes sequenced in this study (Fig. 24). Also similar to ITS-1, samples identified as Genotype A at CO3 formed Clade 1 and included sequences of *H. catesbianae* from Léveillé et al. (2021; MN244528.1) and *H.* cf. *catesbeiana* and *H.* cf. *clamatae* from Barta et al. (2012; HQ224954.1, HQ224962.1). Samples identified as Genotype B and D at CO3 were identical except for three isolates that showed single base pair differences across the 1090 base gene segment. Clade 1 sequences were one base different than Clade 2 sequences. Interestingly, the sample from NH2 was Genotype A at CO3 and Clade 2 (matching Genotype B/D samples) at 18s rRNA. NH2 was a mixed infection of both fragmented and unfragmented cells and it appears different genotypes were amplifying at different loci (Table 14).

When comparing the effect on the host erythrocyte nucleus with sample CO3 genotype, *Hepatozoon* spp. infections that only showed unfragmented nuclei were predominantly Genotype A (7 of 9, 77%) with two samples Genotype C (2 of 9, 22%; Table 14). Samples from infections with only fragmented nuclei were mostly Genotype B (3 of 4, 75%) with one sample Genotype A (1 of 4, 25%). Mixed infections where unfragmented, fragmented, two lobed, and melted nuclei were observed showed a variation of all three genotypes (Table 14).

Phylogenetic Inferences on *Hepatozoon* spp. in Snakes

While frog *Hepatozoon* spp. infecting frogs were in a single clade on the 18s rRNA phylogeny, *Hepatozoon* spp. infecting snakes were found in multiple clades with other hosts including lizards, small mammals, and frogs (Fig. 24). The sequences generated in this study from *Thamnophis proximus*, *Nerodia rhombifer*, and *Agkistrodon*

contortrix were identical and were four bases (0.37%) different from the previous 18s rRNA sequence of *H. sipedon* from Barta et al. (2012; JN181157.1). The single CO3 sequence from *T. proximus* was on average 18.2% different from the frog *Hepatozoon* genotypes and came out in the outgroup with *Hepatozoon spp.* from mammals.

DISCUSSION

Morphological and Phylogenetic Relationships of *Hepatozoon* spp. infecting Anurans

In this study, only *Rana clamitans* was infected with *Hepatozoon* spp. gamonts that fragmented the host erythrocyte nucleus. Similar to previous studies, the extent of fragmentation varied in *R. clamitans* infections, spanning from unfragmented nuclei, nuclei beginning to fragment but split into only two lobes, and fully fragmented nuclei (Kim et al., 1998; Fig. 19). Additionally, two infected *R. clamitans* displayed host erythrocyte nuclei that appeared liquified or melted, where the nucleus seemed to fill the available space in the erythrocyte cytoplasm (Fig. 19D). To my knowledge, this specific effect on the host erythrocyte nucleus has not been previously reported in *Hepatozoon* spp. infections (Kim et al., 1998; Smith, 1996).

The fragmented infections in *Rana clamitans* came from multiple *Hepatozoon* genotypes, including one sample that sequenced as Genotype A, which represented most unfragmented infections in *R. catesbeiana* and *R. sphenocephala* (Table 14). This seems to suggest the nuclear fragmentation is unique to *R. clamitans*. However, previous studies have found fragmented nuclei in *R. catesbeiana* and *R. pipiens* in addition to *R. clamitans*

(Kim et al., 1998; Boulianne et al., 2007; Léveillé et al., 2021). Yet interestingly, previous studies also found fragmented infections more commonly in *R. clamitans* than other host frog species (Kim et al., 1998; Boulianne et al., 2007; Léveillé et al., 2021). Currently, it remains unclear why some *Hepatozoon* spp. infections distort and fragment the host erythrocyte nucleus. Léveillé et al. (2021) found a mixed genotype infection that fragmented the nuclei of *R. catesbeiana*. Clearly more sequencing is needed to investigate the possibility of genotype/host interactions explaining fragmentation in bullfrogs.

Rana sphenocephala constitutes a new host record for *Hepatozoon* sp. All four *R. sphenocephala* infections were unfragmented and the single infection sequenced from a *R. sphenocephala* came out as Genotype A at CO3, which corresponds to *Hepatozoon catesbianae* as defined by Léveillé et al. (2021; Fig. 21).

Gamont morphology was similar between cells from different hosts (Table 11), fragmentation character (Table 12), and genotype (Table 13). This supports previous research that amphibian *Hepatozoon* spp. in North America cannot be differentiated by gamont dimensions. Other characteristics such as gamogany and sporogonic development in the definitive mosquito vector and/or the effect on the host erythrocyte nucleus have been used to delineate *Hepatozoon* species (Desser et al., 1995; Smith, 1996; Kim et al., 1998). However, recent molecular studies including the current study show that the traditional differentiation of *Hepatozoon catesbianae* and *Hepatozoon clamatae* by the effect on host erythrocyte nucleus has been somewhat of an oversimplification, and the character is not correlated with *Hepatozoon* genotypes (Boulianne et al., 2007; Léveillé et al. 2021).

The three genotypes reported by Léveillé et al. (2021) from CO3 gene sequences did not fall out with erythrocyte nuclear fragmentation. Genotype A was identified as *Hepatozoon catesbianae* (KF894962.2) from the blood of *Rana clamitans*, yet the sequences originated from both fragmented and unfragmented infections. Genotype B was identified as *Hepatozoon clamatae* (MN245241.1 and MN310689.1) and also came from both fragmented and unfragmented infections in *R. clamitans* and *R. pipiens*. Genotype C (MN245143.1 and MN310690.1) was designated as *Hepatozoon* sp. and was only found in *Rana pipiens* from unfragmented infections (Léveillé et al., 2021). Additionally, Léveillé et al. (2021) found mixed infections of Genotype A and B in *R. catesbeiana* and *R. clamitans*.

I found similar results with genotypes originating from infections with both fragmented and unfragmented host erythrocyte nuclei (Table 14). Additionally, I also found mixed infections of fragmented and unfragmented host erythrocytes, which came out as different genotypes at different genes. This suggests that there are multiple genotypes in these samples. Which genotype gets sequenced should depend on the proportions of each genotype in the sample and the annealing affinities of the primers for the different genes. Three samples originating from one *R. catesbeiana* and two *R. clamitans* had a sequence distinct from the three genotypes found by Léveillé et al. (2021), and I designated these samples Genotype D (Fig. 21). These infections were unfragmented with one sample having a mix of cells with unfragmented nuclei and cells that appeared melted (Table 14; Fig. 19D).

In general, only small genetic differences of one or two bases were found between genotypes at 18s and ITS-1. Larger variation of 5 to 17 bases was found between

genotypes at CO3. These findings corroborate Léveillé et al. (2021) who asserted CO3 was a good gene for DNA barcoding *Hepatozoon* spp.

Recently developed single cell isolation and sequencing techniques outlined in Chapter II could potentially shed light on the confusion of nuclear fragmentation and mixed genotype *Hepatozoon* infections. These techniques were shown to link sequence data with morphology of trypanosome cells from mixed infections, providing convincing evidence that trypanosome morphotypes in mixed infections were distinct genetic lineages (Chapter II). Identifying, isolating, and sequencing single erythrocytes containing *Hepatozoon* gamonts with different extents of nuclear fragmentation could provide useful data regarding mixed *Hepatozoon* infections and may clarify inconsistencies between genotypes and nuclear fragmentation characteristics, which may simply be resulting from current methods that sequence *Hepatozoon* spp. from whole blood (Kim et al., 1998; Boulianne et al., 2007; Léveillé et al., 2021).

Morphological and Phylogenetic Relationships of *Hepatozoon* spp. Infecting Snakes

The gamonts of *Hepatozoon* cf. *sipedon* infecting the three snake species (*Thamnophis proximus*, *Nerodia rhombifer*, and *Agkistrodon contortrix*) were morphologically similar to each other and to previous reports of *Hepatozoon sipedon* (Fig. 18D; Smith et al., 1994). Additionally, varying degrees of cytoplasm clearing were observed in these snake infections, which have also been reported previously for *H. sipedon* (Fig. 20; Smith et al., 1994). Genetically, the three isolates were identical at 18s rRNA and ITS-1 (Fig. 22 and 23). Unfortunately, amplification of the CO3 gene was only successful from one snake, *T. proximus*, and currently no other CO3 sequences are

available from snake *Hepatozoon* spp. (Fig. 21). For the 18s rRNA gene, isolates in this study were four bases (0.37%) different from the previous sequence of *H. sipedon* from Barta et al. (2012; JN181157.1). *Hepatozoon* spp. isolates from frogs were identical to previously sequenced genotypes, suggesting exact matches may be reasonable for species identification. Therefore, because of the four base pair difference to the previous sequence of *H. sipedon*, I designate the isolates infecting snakes in this study as *H.* cf. *sipedon*. Additional CO3 sequences from *Hepatozoon* spp. infecting snakes should shed light on this distinction and may prove a better locus for differentiating *Hepatozoon* spp. of snakes just as it has been found for anuran *Hepatozoon* genotypes (Léveillé et al., 2021).

In the 18s rRNA phylogeny in this study, many *Hepatozoon* spp. infecting snakes were found to have close genetic similarity to *Hepatozoon* spp. infecting likely prey sources. This trend has been noticed by previous authors and occurrence of *Hepatozoon* species in snakes has been proposed to be driven by ecological interactions between the snake predators and their prey (Sloboda et al., 2007; Tome et al., 2013). Specific examples include *Hepatozoon domerguei* infecting *Madagascarophis colubrinus* (KM234646.1) and *Ithycyphus oursi* (KM234648.1) were identical to that of *Hepatozoon domerguei* infecting *Furcifer* sp. chameleon (KM234649.1), on which these snakes prey (Crottini et al., 2010; Maia et al., 2014). Additionally, *Psammophis* spp. prey on lizards, and specifically *P. sibilans* feeds on *Quedenfeldtia moerens*, which had very similar 18s sequences (KC696567.1, HQ734809.1; Tome et al., 2013). *Hepatozoon* spp. infecting generalist feeding snakes *M. colubrinus*, *Python regius*, and *Elaphe carinata* came out in

the clade with *Hepatozoon* spp. from *Abrothrix* spp. rodents, however this clade is not well resolved.

Experimental evidence suggests there is low host specificity for *Hepatozoon* spp. infecting snakes at all hosts in their life cycle: first intermediate hosts (Booden et al., 1970; Landau et al., 1970; Landau et al., 1972; Smith et al., 1996; Paperna and Lainson, 2004), second intermediate hosts (Ball et al., 1967; Booden et al., 1970; Landau et al., 1972; Smith, 1996; Telford et al., 2004; Sloboda et al., 2007), and mosquito vectors (Ball et al., 1967; Landau et al., 1972; Wozniak and Telford, 1991; Smith, 1996). However, in nature snake hosts seem to have specific parasites (Telford et al., 2001; Sloboda et al., 2007). Snakes vary in the specificity of their diet, yet the experimentally determined low host specificity of *Hepatozoon* spp. suggests that the avenues available for snakes to acquire *Hepatozoon* spp. come from *Hepatozoon* species of their prey. While we do not know most *Hepatozoon* spp. life cycles, all known life cycles of *Hepatozoon* spp. include a blood feeding invertebrate definitive host. Snakes probably seldom ingest blood feeding invertebrates, except perhaps accidentally if they are feeding on their prey. This limits snakes to acquire *Hepatozoon* spp. via host capture and addition of the snake host to existing two-host *Hepatozoon* species. Exceptions could arise from findings of congenital vertical transmission of *Hepatozoon* sp. in live-bearing snakes and reports of *Hepatozoon* sporozoites in mosquito proboscides, suggesting transmission via direct inoculation of the blood during mosquito feeding is possible (Lowichik and Yaeger, 1987; Telford et al., 2001; 2004; 2005; 2008; 2009; Kauffman et al., 2017).

Taken together, the occurrence of snake *Hepatozoon* species within multiple clades of *Hepatozoon* species infecting frogs, mammals, and squamates, the low host

specificity of *Hepatozoon* species in snakes, and the inability of snakes to feed on mosquitoes and other definitive host vectors of *Hepatozoon* species, strongly suggests that snakes are prone to host capturing a diverse assemblage of *Hepatozoon* species that have evolved and are transmitted within their prey (Fig. 24; Sloboda et al., 2007; Tome et al., 2012; 2013). Given these possibilities, the *Hepatozoon* spp. infecting snakes represent a remarkable study system for studying parasite life cycle evolution. Continued sequence generation and life cycle studies on *Hepatozoon* spp. are promising to yield interesting examples of parasites diversifying within the ecological interactions of their hosts.

Table 9. Prevalence of *Hepatzoon* spp. infecting amphibians and reptiles collected in Arkansas, New Hampshire, Oklahoma and Wisconsin. Data in cells represent No. Infected/No. Examined (%), 95% Confidence Interval. Confidence intervals were calculated using the binomial distribution for the appropriate sample size.

	Host Red Blood Cell Nucleus		
Species Examined	Unfragmented	Fragmented	Overall
Ambystomatidae			
Ambystoma texanum	0/10 (0%) 0 - 31	0/10 (0%) 0 - 31	0/10 (0%) 0 - 31
Bufonidae			
Anaxyrus americanus	0/2 (0%) 0 - 84	0/2 (0%) 0 - 84	0/2 (0%) 0 - 84
Anaxyrus fowleri	0/2 (0%) 0 - 84	0/2 (0%) 0 - 84	0/2 (0%) 0 - 84
Anaxyrus woodhousii	0/5 (0%) 0 - 52	0/5 (0%) 0 - 52	0/5 (0%) 0 - 52
Hylidae			
Acris blanchardi	0/28 (0%) 0 - 12	0/28 (0%) 0 - 12	0/28 (0%) 0 - 12
Hyla avivoca	0/12 (0%) 0 - 26	0/12 (0%) 0 - 26	0/12 (0%) 0 - 26
Hyla cinerea	0/20 (0%) 0 - 17	0/20 (0%) 0 - 17	0/20 (0%) 0 - 17
Hyla chrysoscelis	0/11 (0%) 0 - 29	0/11 (0%) 0 - 29	0/11 (0%) 0 - 29
Pseudacris clarkii	0/5 (0%) 0 - 52	0/5 (0%) 0 - 52	0/5 (0%) 0 - 52
Microhylidae			
Gastrophryne olivacea	0/28 (0%) 0 - 12	0/28 (0%) 0 - 12	0/28 (0%) 0 - 12
Ranidae			
Rana blairi	0/6 (0%) 0 - 46	0/6 (0%) 0 - 46	0/6 (0%) 0 - 46
Rana catesbeiana	8/36 (22%) 10 - 39	0/36 (0%) 0 - 10	8/36 (22%) 10 - 16
Rana clamitans	10/56 (18%) 9 - 30	18/56 (32%) 20 - 46	28/56 (50%) 36 - 64
Rana sphenocephala	4/39 (10%) 3 - 24	0/39 (0%) 0 - 9	4/39 (10%) 3 - 24
Colubridae			
Agkistrodon contortrix	3/4 (75%) 19 - 99	n/a	3/4 (75%) 19 - 99
Nerodia rhombifer	1/1 (100%) 3 - 100	n/a	1/1 (100%) 3 - 100
Thamnophis proximus	1/1 (100%) 3 - 100	n/a	1/1 (100%) 3 - 100
Total	33/266 (12%) 9 - 17	12/266 (5%) 2 - 8	45/266 (17%) 13 - 22

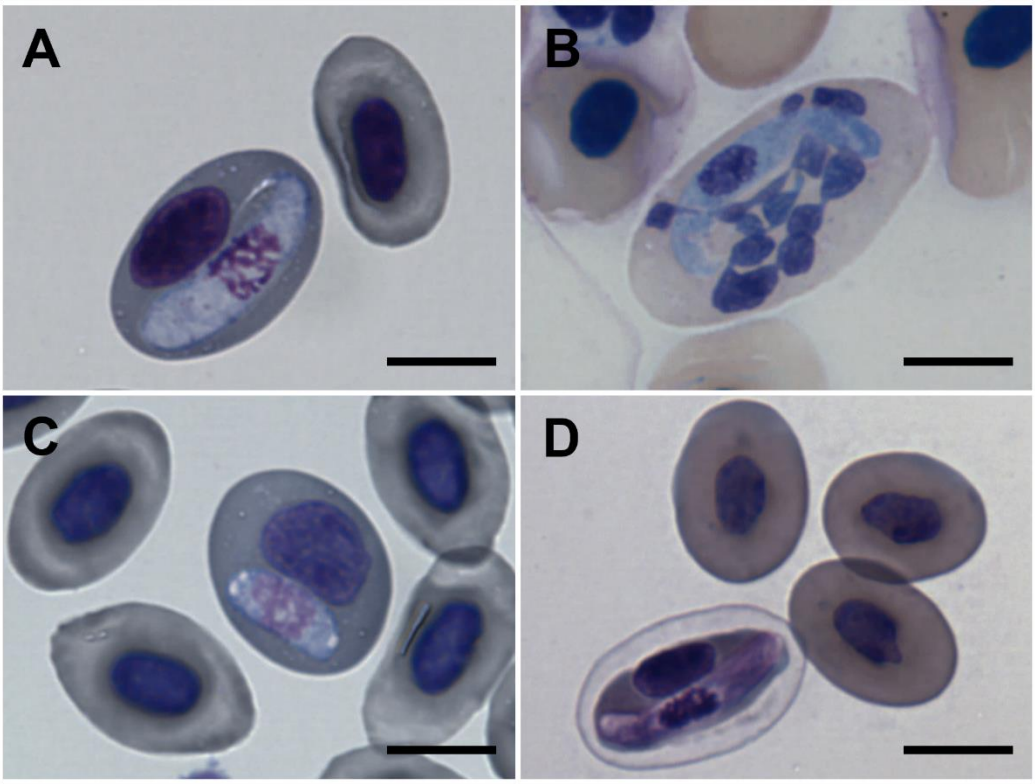

Figure 18. Photomicrographs of *Hepatozoon* spp. cells. **A.** *Hepatozoon* sp. gamont infecting the frog *Rana sphenocephala*. Note the nucleus of the host red blood cell is not fragmented. **B.** *Hepatozoon* sp. gamont infecting the frog *Rana clamitans*. Note the fragmented nucleus of the host red blood cell. **C.** *Hepatozoon* sp. immature gamont/merozoite infecting *Rana sphenocephala*. **D.** *Hepatozoon* sp. infecting the snake *Thamnophis proximus* with cleared cytoplasm. Scale bars = 10 µm.

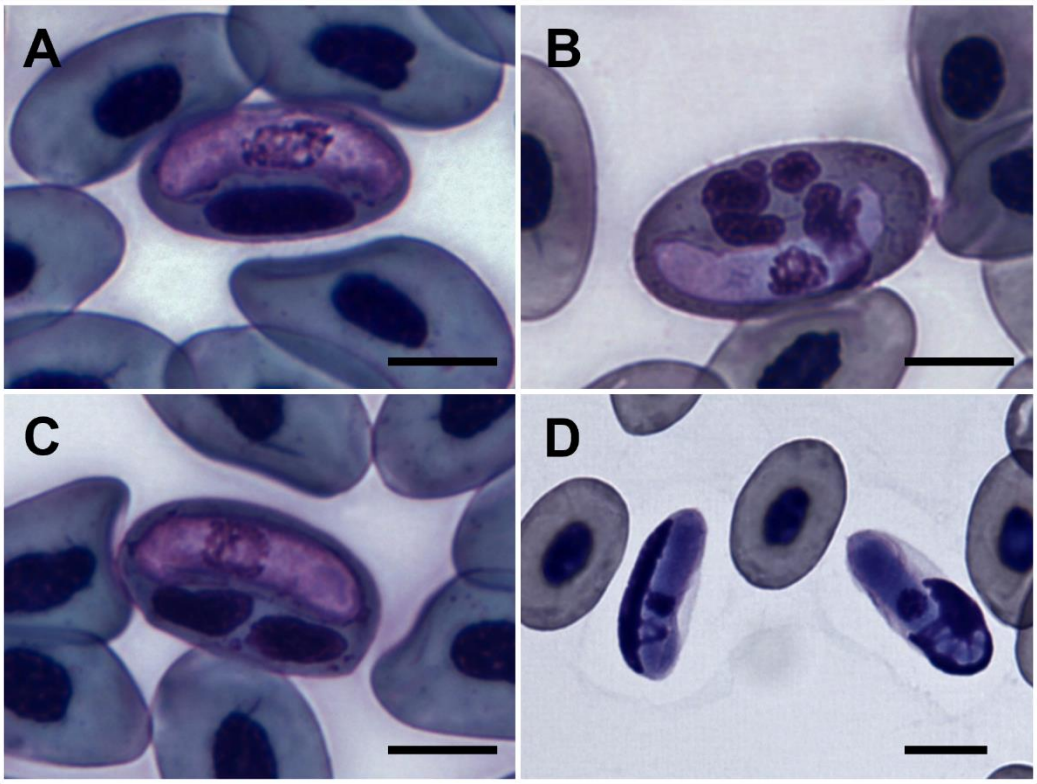

Figure 19. Photomicrographs of *Hepatozoon* spp. infecting green frogs *Rana clamitans* showing the variation in the effects on the host erythrocyte nuclei. **A.** The unfragmented nucleus is displaced by the gamont and slightly elongated. **B.** The nucleus is fragmented into many smaller pieces often connected by visible strands. **C.** The nucleus fragmentation appears incomplete and has only split into two lobes. **D.** Nuclei appear melted or liquified, losing their shape and seeming to fill available cell space. Scale Bar = 10 µm.

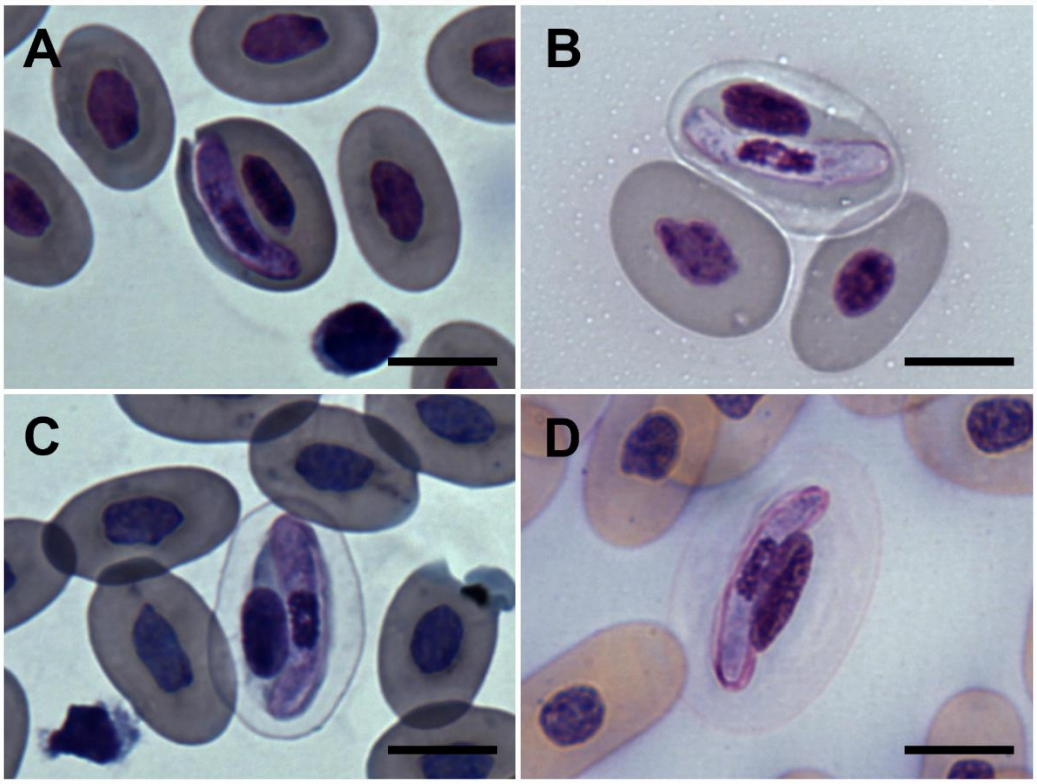

Figure 20. Photomicrographs showing variation and possible progression of cytoplasm clearing in snake erythrocytes infected with *Hepatozoon* cf. *sipedon*. **A.** No cytoplasm clearing. The apparent rip of the cell is most likely an artifact of slide preparation. **B.** Cytoplasm clearing noticeable but not extensive. **C.** Cytoplasm almost fully cleared, but the cytoplasm remains opaque around the erythrocyte nucleus and gamont. **D.** Cytoplasm fully cleared and the erythrocyte nucleus and gamont are forced very close together. A and C are from *Thamnophis proximus*, B is from *Nerodia rhombifer*, and D is from *Agkistrodon contortrix*, however examples of all degrees of cytoplasm clearing were observed in all three snake species. Scale Bar = 10 µm.

Table 10. PCR primers used for amplification and sequencing of the 18s rRNA, ITS-1, and CO3 genes from *Hepatozoon* spp. infecting frogs and snakes, their annealing temperatures, and fragment lengths.

Target Gene	Host	Primer Name	Purpose	Primer sequence	Anneal temperature	Fragment Length	Citation
18s rRNA	Frogs and Snakes	18s EF	Forward	5'-CCA GTA GTC ATA TGC TTG TC-3'	49°C	1660 bp	This study
	Frogs and Snakes	18s ER	Reverse	5'-GTT ACG ACT TCT CCT TCC TC-3'	51°C	1660 bp	This study
	Frogs and Snakes	18s IF	Sequencing	5'-CAA TTG GAG GGC AAG TCT GG-3'	60°C	1660 bp	This study
	Frogs and Snakes	18s IR	Sequencing	5'-GTG CCC TTC CGT CAA TTC C-3'	60°C	1660 bp	This study
ITS-1	Frogs and Snakes	ITS-1 F	Forward	5'-GTA GGT GAA CCT GCG GAA GG-3'	60°C		This study
	Frogs*	ITS-1 FR	Reverse	5'-CGA TGC AAA CCA AGG TAT CC-3'	54°C	195 bp*	This study
	Snakes*	ITS-1 SR	Reverse	5'-TCG ATG CAA ACC AAG GTA TCC-3'	60°C	254 bp*	This study
CO3	Frogs	Hep_CO3_2852F	Forward	5'-ATT GCA TGG TAC CGA GGT C-3'	56°C	653 bp	This study
	Frogs	Hep_SSUE_3706R	Reverse	5'-GCT CGT CAC GCC ACT GTA-3'	56°C		Léveillé et al. 2014
	Snakes	S-CO3F	Forward	5'-GCY CAT TTA CAA ACA TAT CC-3'	50°C	630 bp	This study
	Snakes	S-CO3R	Reverse	5'-TAA TTC WAC RAA ATG CCA G-3'	50°C		This study

*The ITS-1 region differs in length between *Hepatozoon* from frogs and snakes. Additionally, different reverse primers were used for amplifying ITS-1 from frogs and snakes.

Table 11. Measurements of *Hepatozoon* gamonts infecting red blood cells of frogs and snakes, arranged by host. Numbers in cells represent the average ± 1SD and the range.

Host species	Gamont Development		Gamont Length	Gamont Width	Gamont Nucleus Length	Gamont Nucleus Width
Rana catesbeiana	Mature	N= 18	24.2 ± 2.31	5.5 ± 1.15	5.5 ± 0.92	3.9 ± 1.13
			(21 - 29)	(3 - 8)	(4 - 8)	(3 - 7)
	Immature	N= 10	12.4 ± 0.84	4.4 ± 0.70	5.9 ± 0.57	3.8 ± 0.79
			(11 - 14)	(4 - 6)	(5 - 7)	(3 - 5)
Rana clamitans	Mature	N= 72	25.2 ± 2.68	5.1 ± 1.39	6.3 ± 1.03	4.0 ± 0.96
			(19 - 31)	(3 - 12)	(4 - 10)	(2 - 7)
	Immature	N= 2	12.5 ± 0.71	4.5 ± 0.71	5.5 ± 0.71	4.0 ± 0.00
			(12 - 13)	(4 - 5)	(5 - 6)	(4 - 4)
Rana sphenocephala	Mature	N= 22	22.8 ± 1.97	5.1 ± 1.13	5.8 ± 0.96	4.3 ± 0.94
			(20 - 27)	(2 - 7)	(4 - 8)	(3 - 6)
	Immature	N= 3	12.0 ± 1.00	5.0 ± 1.00	6.0 ± 0.00	4.0 ± 1.00
			(11 - 13)	(4 - 6)	(6 - 6)	(3 - 5)
Nerodia rhombifer	Mature	N= 20	20.3 ± 0.66	3.8 ± 0.44	6.4 ± 1.19	2.5 ± 0.51
			(19 - 21)	(3 - 4)	(4 - 8)	(2 - 3)
Thamnophis proximus	Mature	N= 20	18.8 ± 1.40	3.7 ± 0.57	5.7 ± 0.92	2.5 ± 0.51
			(16 - 20)	(3 - 5)	(4 - 7)	(2 - 3)

Table 12. Measurements of *Hepatozoon* gamonts infecting red blood cells (RBC) of frogs, arranged by the effect on the host RBC nucleus. Numbers in cells represent the average ± 1SD and the range.

Nucleus character	Gamont development		Gamont Length	Gamont Width	Gamont Nucleus Length	Gamont Nucleus Width
Fragmented	Mature	N= 30	25.2 ± 2.60	4.2 ± 0.55	6.9 ± 0.91	3.5 ± 0.63
			(19 - 30)	(3 - 5)	(6 - 10)	(2 - 5)
Not fragmented	Mature	N= 79	24.4 ± 2.66	5.5 ± 1.36	5.7 ± 0.88	4.3 ± 1.00
			(20 - 31)	(2 - 12)	(6 - 10)	(3 - 7)
	Immature	N= 15	12.3 ± 0.82	4.5 ± 0.74	5.9 ± 0.52	3.9 ± 0.74
			(11 - 14)	(4 - 6)	(5 - 7)	(3 - 5)

Table 13. Measurements of *Hepatozoon* from frogs and snakes arranged by genotype. Numbers in cells represent the average ± 1SD and the range.

	Gamont Development		Gamont Length	Gamont Width	Gamont Nucleus Length	Gamont Nucleus Width
Genotype A	Mature	N= 26	23.7 ± 1.64 (20 - 26)	5.4 ± 1.06 (3 - 8)	5.6 ± 0.85 (4 - 8)	3.9 ± 1.16 (3 - 7)
	Immature	N= 12	12.4 ± 0.79 (11 - 14)	4.4 ± 0.67 (4 - 6)	5.8 ± 0.58 (5 - 7)	3.8 ± 0.72 (3 - 5)
Genotype B	Mature	N= 22	26.5 ± 2.92 (20 - 31)	6.3 ± 1.70 (5 - 12)	5.6 ± 1.01 (4 - 8)	4.8 ± 0.81 (3 - 6)
Genotype D	Mature	N= 22	25.6 ± 2.15 (22 - 31)	4.4 ± 0.50 (4 - 5)	6.5 ± 0.96 (5 - 10)	3.8 ± 0.53 (3 - 5)
Unsequenced	Mature	N= 42	23.6 ± 2.61 (19 - 30)	4.8 ± 1.08 (2 - 7)	6.3 ± 1.03 (4 - 8)	3.9 ± 0.98 (2 - 6)
	Immature	N= 3	12.0 ± 1.00 (11 - 13)	5.0 ± 1.00 (4 - 6)	6.0 ± 0.00 (6 - 6)	4.0 ± 1.00 (3 - 5)
Snake Genotype	Mature	N= 40	19.6 ± 1.32 (16 - 21)	3.7 ± 0.51 (3 - 5)	6.1 ± 1.11 (4 - 8)	2.5 ± 0.51 (2 - 3)

Table 14. Effect on the host erythrocyte nucleus and genotype sequenced from samples of infected frogs. For CO3 sequences, genotypes are grouped by relationships to sequences in Léveillé et al. (2021). For ITS-1 and 18s rRNA, two clades were recovered. Clade 1 corresponds to samples identified as Genotype A at the CO3 locus. Clade 2 corresponds to samples identified as Genotype B and D at the CO3 locus. Samples with ~ deviated slightly (1-2 bp difference) from the dominant gene sequence.

Pure Unfragmented Infections									
Frog ID	Host Species	State Collected	Unfragmented	Fragmented	Two lobed	Melted	CO3	ITS-1	18s
H1	*R. catesbeiana*	Oklahoma	X				A	1	1
H2	*R. catesbeiana*	Oklahoma	X				A	1	1
H4	*R. catesbeiana*	Oklahoma	X				A	1	1
H10	*R. catesbeiana*	Oklahoma	X				A	1	-
H11	*R. catesbeiana*	Oklahoma	X				D	2	-
H3	*R. clamitans*	Oklahoma	X				D	2	2
H8	*R. clamitans*	Oklahoma	X				A	1	1
W9	*R. clamitans*	Wisconsin	X				A	1	1
H6	*R. sphenocephala*	Oklahoma	X				A	1	1
Pure Fragmented infections									
Frog ID	Host Species	State Collected	Unfragmented	Fragmented	Two lobed	Melted	CO3	ITS-1	18s
H14	*R. clamitans*	Arkansas		X			B	2	~2
NH5	*R. clamitans*	New Hampshire		X			A	1	1
NH6	*R. clamitans*	New Hampshire		X			B	-	-
W13	*R. clamitans*	Wisconsin		X			B	-	~2
Mixed Fragmented and Unfragmented Infections									
Frog ID	Host Species	State Collected	Unfragmented	Fragmented	Two lobed	Melted	CO3	ITS-1	18s
H9	*R. clamitans*	Oklahoma	X			X	D	2	2
H21	*R. clamitans*	Arkansas	X		X		B	2	~2
NH2*	*R. clamitans*	New Hampshire	X	X		X	A*	1*	~2*
NH4	*R. clamitans*	New Hampshire	X	X			B	2	2
W1	*R. clamitans*	Wisconsin	X	X	X		A&B	2	2

*Sample NH2 was a mixed infection and sequenced as Genotype A at CO3 but was clade 2 at 18s rRNA.

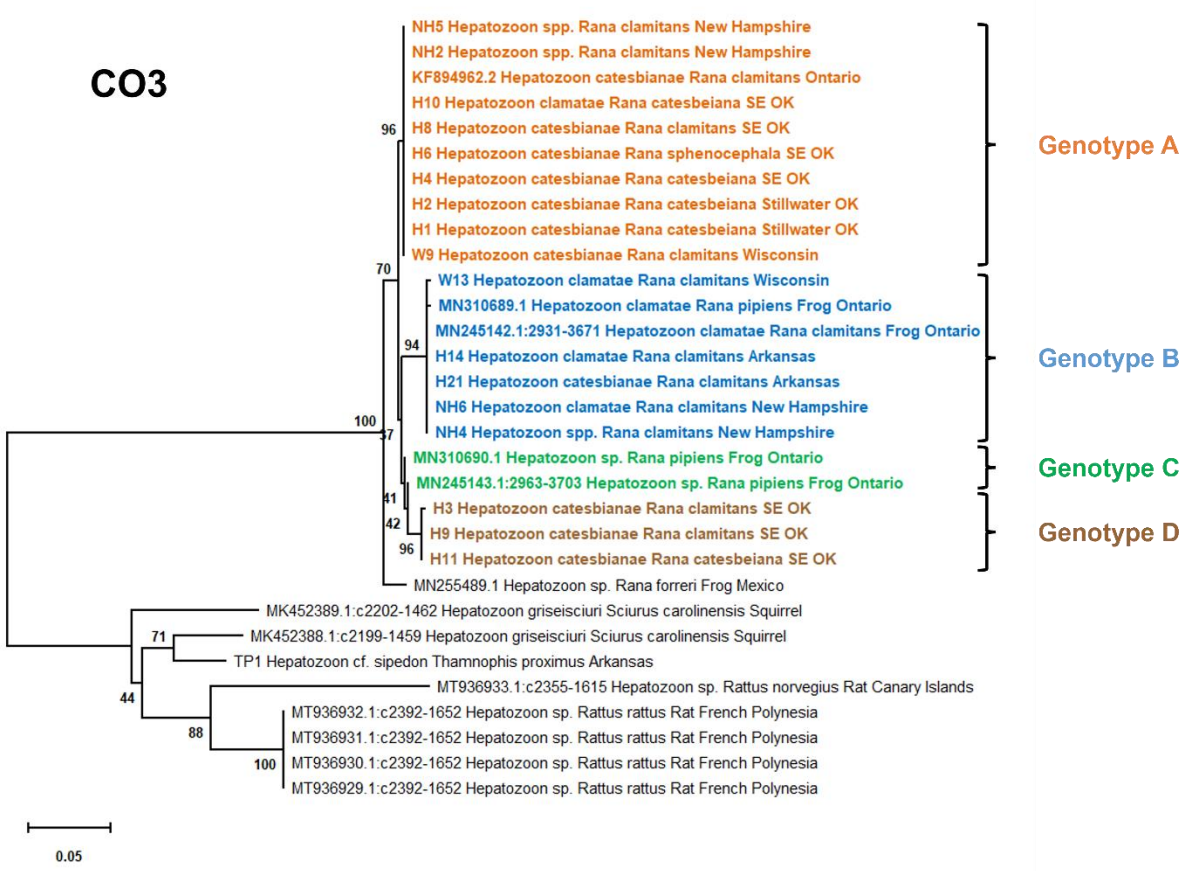

Figure 21: Maximum Likelihood phylogeny of the partial cytochrome oxidase subunit III nucleotide gene sequences (629 bp, -Ln = -2102.34) using the GTR+G model in MEGA X (Kumar et al., 2018). Values at nodes represent bootstrap support values, assessed with 1000 replications. Clades are colored according to their genetic similarity to genotypes identified by Léveillé et al. (2021), which are taxa with GenBank accession numbers.

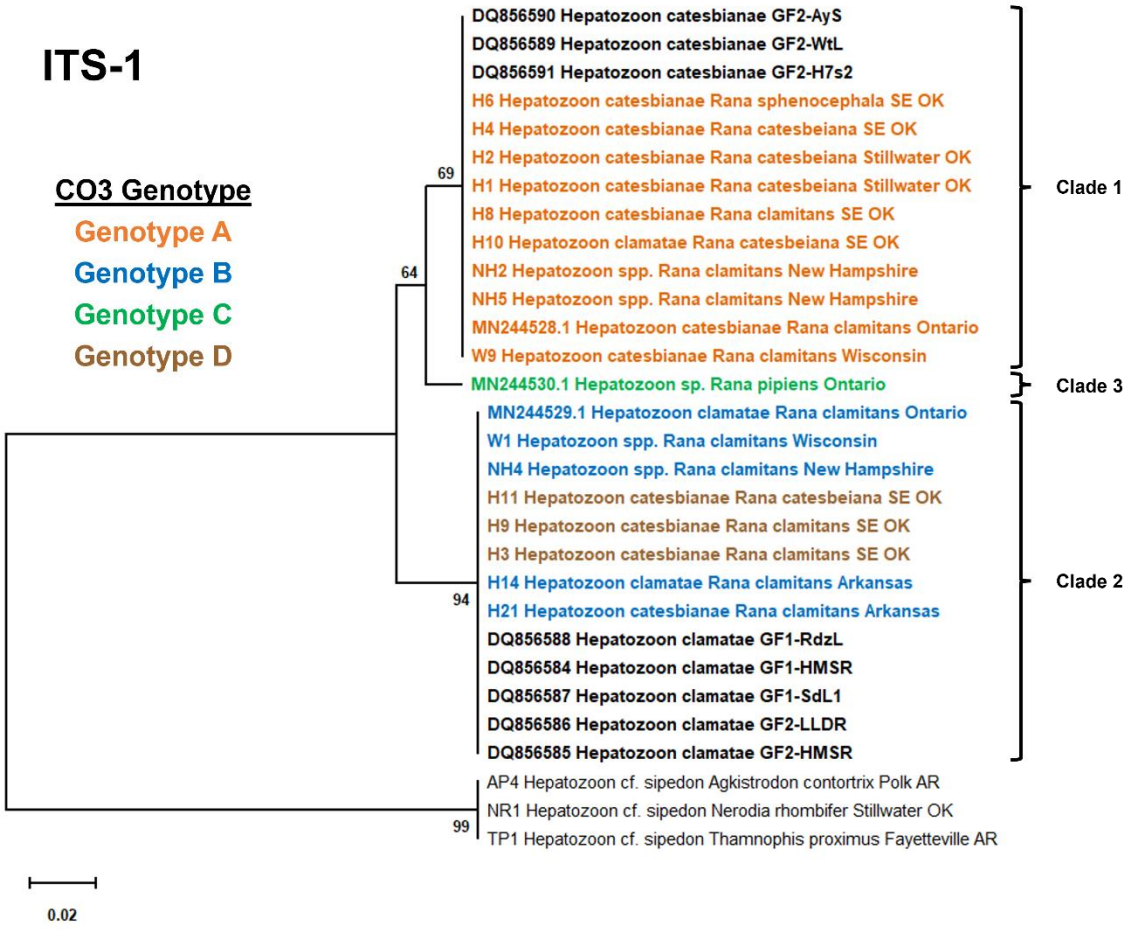

Figure 22: Maximum Likelihood phylogeny of the internal transcribed spacer region 1 (163 bp, -Ln = -270.06) using the T92 model in MEGA X (Kumar et al., 2018). Values at nodes represent bootstrap support values, assessed with 1000 replications. Genotypes of frogs are colored according to their identity at the CO3 locus, following Léveillé et al. (2021, Fig. 21).

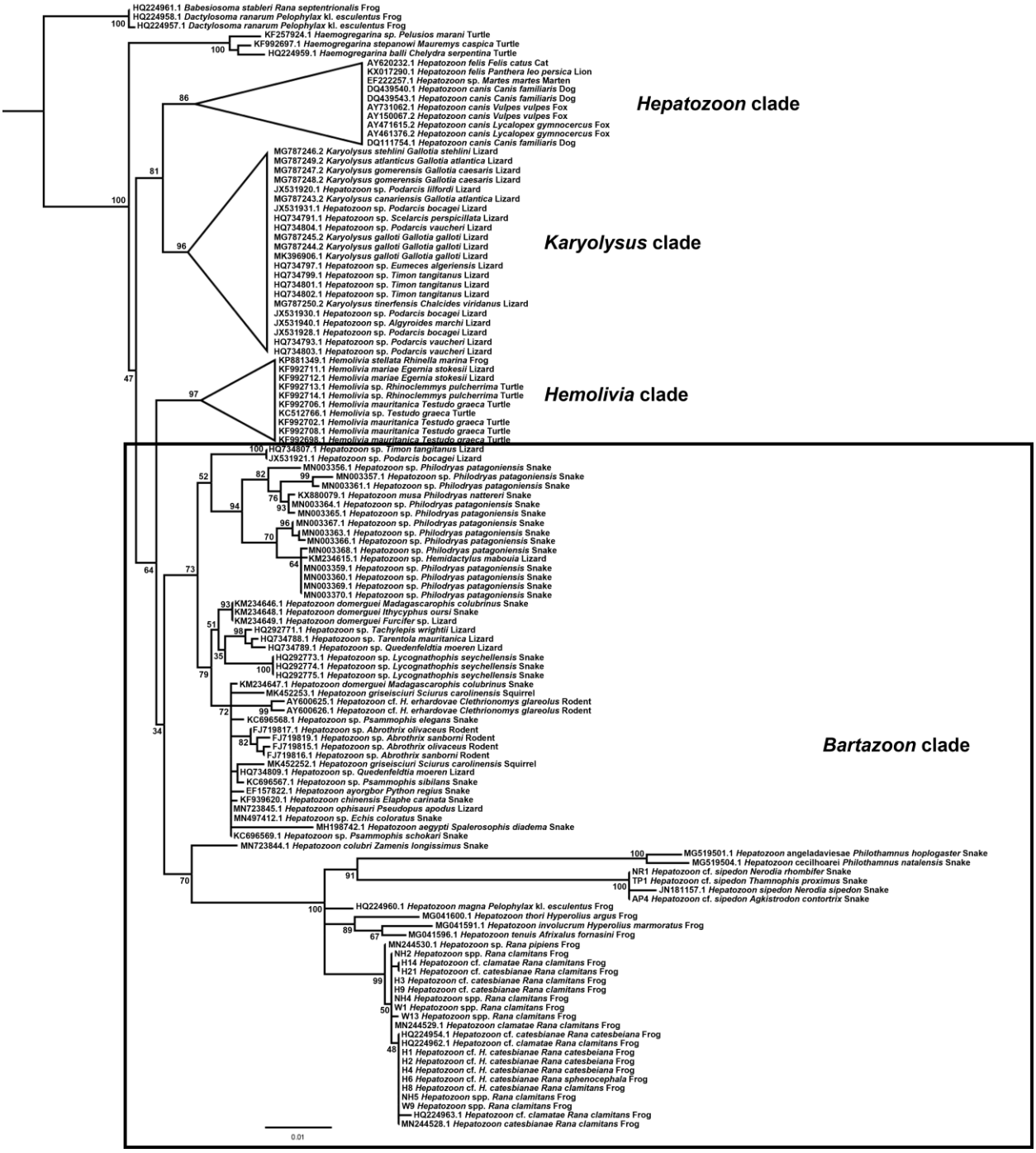

Figure 23: Maximum Likelihood phylogeny of the partial 18s rRNA gene (1090 bp, -Ln = -4814.63) using the HKY+G+I model in MEGA X (Kumar et al., 2018). Values at nodes represent bootstrap support values, assessed with 1000 replications. Clades are

labeled according to Karadijan et al. (2015). The inset of the Bartazoon clade is shown in Figure 24.

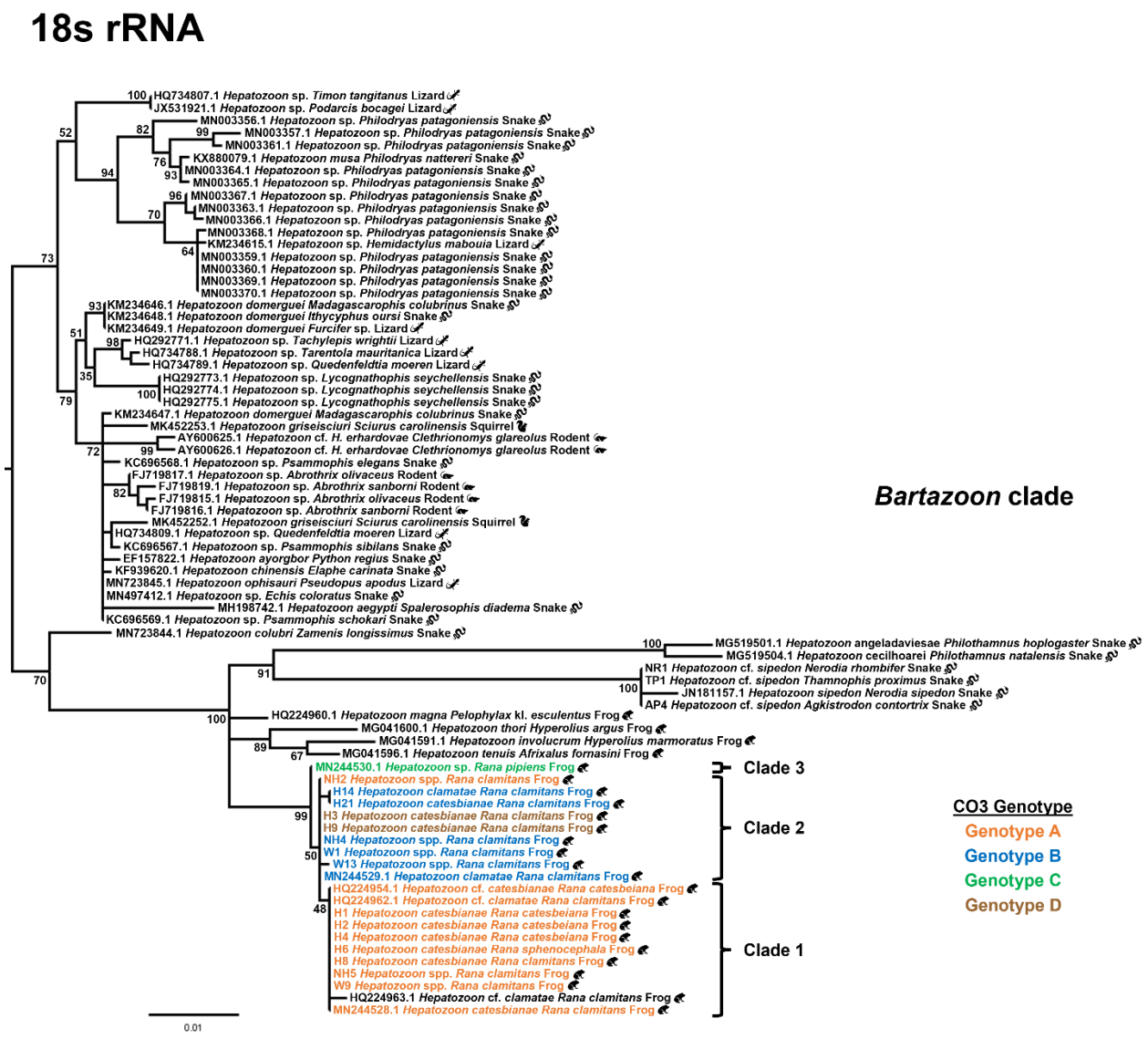

Figure 24: The Bartazoon clade from the 18s rRNA phylogeny (Fig. 23). The phylogeny was estimated with Maximum Likelihood framework on the partial 18s rRNA gene (1090 bp, -Ln = -4814.63) using the HKY+G+I model in MEGA X (Kumar et al., 2018). Values at nodes represent bootstrap support values, assessed with 1000 replications. Genotypes of frogs are colored according to their identity at the CO3 locus, following Léveillé et al. (2021, Fig. 21).

CHAPTER VI

CONCLUSIONS

Blood parasites represent an incredibly diverse subset of parasites that infect all major groups of vertebrates and are transmitted by numerous blood feeding invertebrates. However, quantifying blood parasite diversity is difficult due to the challenges presented by a lack of morphological characters and genetic markers suitable for species delineation. This dissertation investigated the challenges to quantify diversity of two genera of blood parasites that infect amphibians and reptiles, *Trypanosoma* and *Hepatozoon*.

Chapter II detailed new methods to link sequence data to trypanosome cell morphology by isolating single trypanosome cells for gene sequences, which proved to be a powerful tool to identify the forms in mixed trypanosome infections and elucidate pleomorphic species. Future studies on amphibian trypanosomes can use the techniques in Chapter II to sequence new trypanosomes cells and compare the 18s rRNA and gGAPDH gene sequences to the species described in Chapter IV.

.

Chapter III uses the sequence data linked to trypanosome morphology generated in Chapter II to investigate amphibian trypanosome morphological diversity in a phylogenetic context. Of the fifteen amphibian species examined, six were found to be infected with trypanosomes. These included four species of true frogs (*Rana blairi*, *Rana catesbeiana*, *Rana clamitans*, and *Rana sphenocephala*), and two species of treefrogs, (*Hyla avivoca* and *Hyla cinerea*). Twelve trypanosome morphotypes were recovered, six in true frogs and six in treefrogs. Most infected frogs were infected with multiple trypanosome morphotypes, with as many as five morphotypes occurring in an individual frog. Two pairs of morphotypes were suspected of being pleomorphic species based on coinfection frequency and morphological similarity, however all morphotypes were found to be genetically distinct. Previous claims that amphibian trypanosome morphology is not conserved are challenged by reviewing sequence data obtained from cultured trypanosomes. The removal of questionable sequences resulted in four clades of amphibian trypanosomes with general morphological similarities, suggesting that amphibian trypanosome morphology is phylogenetically conserved across sampling locations in Europe and North America.

Chapter IV reports the description of three new trypanosome species and one redescription of a trypanosome species previously misidentified in North American anurans based on the data generated in Chapters II and III. Future studies on amphibian trypanosomes can use the techniques in Chapter II to sequence new trypanosomes cells and compare the 18s rRNA and gGAPDH gene sequences to these species.

Chapter V investigates characters for species differentiation of three *Hepatozoon* species in North America, two that infect frogs, *Hepatozoon catesbianae* and *Hepatozoon*

clamatae, and one, *Hepatozoon sipedon*, that infects snakes. Of the three ranid species found infected with *Hepatozoon* spp., *Rana catesbeiana*, *R. clamitans*, and *R. sphenocephala*, only *R. clamitans* had infected erythrocytes with fragmented nuclei. Similar to previous studies, the character that differentiates *H. catesbianae* and *H. clamatae*, the fragmentation of the host erythrocyte nucleus, did not correlate with genotypes. Additionally, *Hepatozoon* cf. *sipedon* is reported and characterized from three snake species collected in Oklahoma and Arkansas. Infected erythrocytes in these snakes displayed variation in cytoplasm clearing. While frog *Hepatozoon* spp. infecting frogs were in a single clade on the 18s rRNA phylogeny, *Hepatozoon* spp. infecting snakes were found in multiple clades with other hosts including lizards, small mammals, and frogs, suggesting snakes may be capturing *Hepatozoon* spp. from their prey.

I argue that combining morphological measurements linked to sequence data is the way forward in describing the diversity of amphibian blood parasites, allowing for studies on life cycles, development, and host parasite interactions on known species. Additionally, the continued generation of sequences linked to morphology and host cell effects will test the usefulness of these characters in identifying blood parasites species. The current research provides hope that with careful considerations of possible pitfalls (mixed infections and pleomorphism) we can reliably identify these organisms and uncover the hidden diversity of amphibian blood parasites.

REFERENCES

Attias, M., L. H. Sato, R. C. Ferreira, C. S. A. Takata, M. Campaner, E. P. Camargo, M. M. G. Teixeira and W. de Souza. 2016. Developmental and Ultrastructural Characterization and Phylogenetic Analysis of *Trypanosoma herthameyeri* n. sp. of Brazilian Leptodactilydae Frogs. Journal of Eukaryotic Microbiology **63**: 610-622.

Ball, G. H., J. Chao and S. R. Telford Jr. 1967. The life history of *Hepatozoon rarefaciens* (Sambon and Seligmann, 1907) from *Drymarchon corais* (Colubridae), and its experimental transfer to *Constrictor constrictor* (Boidae). The Journal of Parasitology 897-909.

Ball, G. H., J. Chao and S. R. Telford Jr. 1969. *Hepatozoon fusifex* sp. n., a hemogregarine from *Boa constrictor* producing marked morphological changes in infected erythrocytes. The Journal of Parasitology 800-813.

Bardsley, J. and R. Harmsen. 1973. The trypanosomes of Anura. Advances in Parasitology **11**: 1-73.

Barta, J. R., Y. Boulard and S. S. Desser. 1989. Blood parasites of *Rana esculenta* from Corsica: Comparison of its parasites with those of eastern North American ranids in the context of host phylogeny. Transactions of the American Microscopical Society **108**: 6-20.

Barta, J. R. and S. S. Desser. 1984. Blood parasites of amphibians from Algonquin Park, Ontario. Journal of Wildlife Diseases **20**: 180-189.

Barta, J. R. and S. S. Desser. 1989. Development of *Babesiosoma stableri* (Dactylosomatidae; Adeleida; Apicomplexa) in its leech vector (*Batracobdella picta*) and the relationship of the dactylosomatids to the piroplasms of higher vertebrates. Journal of Protozoology **36**: 241-253.

Barta, J. R., J. D. Ogedengbe, D. S. Martin and T. G. Smith. 2012. Phylogenetic position of the adeleorinid coccidia (Myzozoa, Apicomplexa, Coccidia, Eucoccidiorida, Adeleorina) inferred using 18S rDNA sequences. J Eukaryot Microbiol **59**: 171-180.

Bernal, X. E. and C. M. Pinto. 2016. Sexual differences in prevalence of a new species of trypanosome infecting túngara frogs. International Journal for Parasitology: Parasites and Wildlife **5**: 40-47.

Booden, T., J. Chao and G. H. Ball. 1970. Transfer of *Hepatozoon* sp. from *Boa constrictor* to a lizard, *Anolis carolinensis*, by mosquito vectors. Journal of Parasitology.

Boulianne, B., R. C. Evans and T. G. Smith. 2007. Phylogenetic analysis of *Hepatozoon* species (Apicomplexa: Adeleorina) infecting frogs of Nova Scotia, Canada, determined by ITS-1 sequences. Journal of Parasitology **93**: 1435-1441.

Brown, T. A. 2020. Gene cloning and DNA analysis: an introduction. John Wiley & Sons, 432.

Bush, A. O., K. D. Lafferty, J. M. Lotz and A. W. Shostak. 1997. Parasitology meets ecology in its own terms: Margolis et al. revisited. Journal of Parasitology **83**: 575-583.

Cook, C. A., E. C. Netherlands, N. J. Smit and J. Van As. 2018. Two new species of *Hepatozoon* (Apicomplexa: Hepatozoidae) parasitising species of *Philothamnus* (Ophidia: Colubridae) from South Africa.

Darsie Jr, R. F. and R. A. Ward. 2005. Identification and geographic distribution of the mosquitoes of North America. North of Mexico. University Press of Florida, Gainesville, Florida, 383p.

Desser, S. S. 2001. The blood parasites of anurans from Costa Rica with reflections on the taxonomy of their trypanosomes. Journal of Parasitology **87**: 152-160.

Desser, S. S., H. Hong and D. S. Martin. 1995. The life history, ultrastructure, and experimental transmission of *Hepatozoon catesbianae* n. comb., an apicomplexan parasite of the bullfrog, *Rana catesbeiana* and the mosquito, *Culex territans* in Algonquin Park, Ontario. Journal of Parasitology **81**: 212-222.

Diamond, L. S. 1950. A new trypanosome, *Trypanosoma pipientis* n. sp. from the leopard frog, *Rana pipiens*. Journal of Parasitology **36**: 24.

Diamond, L. S. 1965. A study of the morphology, biology and taxonomy of the trypanosomes of Anura. Wildlife Disease **44**: 1-85.

Edgar, R. C. 2004. MUSCLE: multiple sequence alignment with high accuracy and high throughput. Nucleic Acids Research **32**: 1792-1797.

Espinosa-Álvarez, O., P. A. Ortiz, L. Lima, A. G. Costa-Martins, M. G. Serrano, S. Herder, G. A. Buck, E. P. Camargo, P. B. Hamilton and J. R. Stevens. 2018. *Trypanosoma rangeli* is phylogenetically closer to Old World trypanosomes than to *Trypanosoma cruzi*: independent adaptation to different niches of mammals, even humans, and triatomine vectors. International Journal for Parasitology **48**: 569-584.

Fantham, H. B., A. Porter and L. R. Richardson. 1942. Some Hematozoa Observed in Vertebrates in Eastern Canada. Parasitology **34**: 199-226.

Forzán, M. J., R. V. Vanderstichel, C. T. Ogbuah, J. R. Barta and T. G. Smith. 2012. Blood collection from the facial (maxillary)/musculo-cutaneous vein in true frogs (family Ranidae). Journal of Wildlife Diseases **48**: 176-180.

França, C. and M. Athias. 1906. Recherches sur les trypanosomes des amphibiens. I. Les trypanosomes de le *Rana esculenta*. Arquivos do Instituto Bacteriológico Câmara Pestana **1**: 127-165.

Freund, R. J., W. J. Wilson and D. L. Mohr. 2010. Statistical Methods. Academic Press, Cambridge, 796p.

Hamilton, P. B., W. C. Gibson and J. R. Stevens. 2007. Patterns of co-evolution between trypanosomes and their hosts deduced from ribosomal RNA and protein-coding gene phylogenies. Mol Phylogenet Evol **44**: 15-25.

Hamilton, P. B., K. E. Lefebvre and R. D. Bull. 2015. Single cell PCR amplification of diatoms using fresh and preserved samples. Frontiers in Microbiology **6**: 1084.

Hamilton, P. B., J. R. Stevens, M. W. Gaunt, J. Gidley and W. C. Gibson. 2004. Trypanosomes are monophyletic: evidence from genes for glyceraldehyde phosphate dehydrogenase and small subunit ribosomal RNA. International Journal for Parasitology **34**: 1393-1404.

Harkness, L. M., A. E. Drohan, C. M. Dickson and T. G. Smith. 2010. Experimental transmission of *Hepatozoon clamatae* (Apicomplexa: Adeleida) to the wood frog, *Rana sylvatica*, and to the mosquito *Culex pipiens*. Journal of Parasitology **96**: 434-436.

Harris, D. J., I. Damas-Moreira, J. P. Maia and A. Perera. 2014. First report of *Hepatozoon* (Apicomplexa: Adeleorina) in caecilians, with description of a new species. Journal of Parasitology **100**: 117-120.

Hasegawa, M., H. Kishino and T.-a. Yano. 1985. Dating of the human-ape splitting by a molecular clock of mitochondrial DNA. Journal of Molecular Evolution **22**: 160-174.

Jones, S. R. M. and P. T. Woo. 1986. *Trypanosoma chattoni* Mathis & Leger, 1911 in *Rana pipiens* of southern Ontario: morphometrics and a description of the division process. Systematic Parasitology **9**: 57-62.

Jones, S. R. M. and P. T. Woo. 1989. Use of kidney impressions for the detection of trypanosomes of anura. Journal of Wildlife Diseases **25**: 413-415.

Karadjian, G., J.-M. Chavatte and I. Landau. 2015. Systematic revision of the adeleid haemogregarines, with creation of *Bartazoon* ng, reassignment of *Hepatozoon argantis* Garnham, 1954 to *Hemolivia*, and molecular data on *Hemolivia stellata*. Parasite **22**.

Kauffman, K. L., A. Sparkman, A. M. Bronikowski and M. G. Palacios. 2017. Vertical transmission of *Hepatozoon* in the garter snake *Thamnophis elegans*. Journal of Wildlife Diseases **53**: 121-125.

Kim, B., T. G. Smith and S. S. Desser. 1998. The life history and host specificity of *Hepatozoon clamatae* (Apicomplexa: Adeleorina) and ITS-1 nucleotide sequence variation of *Hepatozoon* species of frogs and mosquitoes from Ontario. Journal of Parasitology **84**: 789-797.

Kudo, R. 1922. On the protozoa parasitic in frogs. Transactions of the American Microscopical Society **41**: 59-76.

Kumar, S., G. Stecher, M. Li, C. Knyaz and K. Tamura. 2018. MEGA X: Molecular Evolutionary Genetics Analysis across computing platforms. Molecular Biology and Evolution **35**: 1547-1549.

Landau, I., A. Chabaud, J. Michel and E. Brygoo. 1970. Evidence of a double mode of transmission of *Hepatozoon* of Malagasy reptiles. C R Acad Sci **270**: 2308-2310.

Landau, I., J. C. Michel, A. G. Chabaud and E. R. Brygoo. 1972. Cycle biologique d'Hepatozoon domerguei; discussion sur les caractères fondamentaux d'un cycle de Coccidie. Zeitschrift für Parasitenkunde **38**: 250-270.

Lankester, E. R. 1871. On Undulina, the type of a new group of Infusoria. Quarterly Journal of Microscopical Science **11**: 387-389.

Laveran, A. and F. Mesnil. 1901. Sur la structure du trypanosome des grenouilles et sur l'extension du genre *Trypanosoma* Gruby. Comptes Rendus des Seances de la Societe de Biologie **53**: 678-680.

Laveran, A. and F. Mesnil. 1907. Trypanosomes and Trypanosomiases. Trans. D. Nabarro. W. T. Keener & Co., Chicago, 540p.

Lehmann, D. L. 1959a. The description of *Haemogregarina boyli* n. sp. from the yellow-legged frog *Rana boyli boyli*. Journal of Parasitology **45**: 198-203.

Lehmann, D. L. 1959b. *Karyolysus sonomae* n. sp., a blood parasite from the California yellow-legged frog, *Rana boyli boyli*. Proceedings of the American Philosophical Society **103**: 545-547.

Lehmann, D. L. 1960. *Haemogregarina aurorae* n. sp. from *Rana a. aurora*. Proceedings of the American Philosophical Society **104**: 202-204.

Léveillé, A. N., E. G. Zeldenrust and J. R. Barta. 2021. Multilocus genotyping of sympatric *Hepatozoon* species infecting the blood of Ontario ranid frogs reinforces species differentiation and identifies an unnamed *Hepatozoon* species. The Journal of Parasitology **107**: 246-261.

Levine, N. D. 1988. The protozoan phylum Apicomplexa. Volume I. Volume II. CRC Press, Inc., Boca Raton, Florida,

Lowichik, A. and R. G. Yaeger. 1987. Ecological aspects of snake hemogregarine infections from two habitats in southeastern Louisiana. The Journal of parasitology 1109-1115.

Maia, J. P., S. Carranza and D. J. Harris. 2016. Comments on the systematic revision of adeleid haemogregarines: are more data needed? Journal of Parasitology **102**: 549-552.

Maia, J. P., A. Crottini and D. J. Harris. 2014. Microscopic and molecular characterization of *Hepatozoon domerguei* (Apicomplexa) and *Foleyella furcata* (Nematoda) in wild endemic reptiles from Madagascar. Parasite **21**.

Martin, D. S. and S. S. Desser. 1990. A light and electron microscopic study of *Trypanosoma fallisi* N. sp. in toads (*Bufo americanus*) from Algonquin Park, Ontario. Journal of Protozology **37**: 199-206.

Martin, D. S. and S. S. Desser. 1991. Development of *Trypanosoma fallisi* in the leech, *Desserobdella picta*, in toads (*Bufo americanus*), and in vitro. Parasitology Research **77**: 18-26.

Martin, D. S., S. S. Desser and H. Hong. 1992. Allozyme comparison of three *Trypanosoma* species (Kinetoplastida: Trypanosomatidae) of toads and frogs by starch-gel electrophoresis. Journal of Parasitology **78**: 317-322.

Martin, D. S., A. D. G. Wright, J. R. Barta and S. S. Desser. 2002. Phylogenetic position of the giant anuran trypanosomes *Trypanosoma chattoni*, *Trypanosoma fallisi*, *Trypanosoma mega*, *Trypanosoma neveulemairei*, and *Trypanosoma ranarum* inferred from 18S rRNA gene sequences. Journal of Parasitology **88**: 566-571.

Maslov, D. A., J. Lukeš, M. Jirku and L. Simpson. 1996. Phylogeny of trypanosomes as inferred from the small and large subunit rRNAs: implications for the evolution of parasitism in the trypanosomatid protozoa. Molecular and Biochemical Parasitology **75**: 197-205.

Mathis, C. and M. Leger. 1911. Trypanosomes des batrachiens du Tonkin. Annales de l'Institute Pasteur **25**: 671-681.

Mayer, A. F. I. C. 1843. Spicilegium observationum anatomicarum de organo electrico in Raiis anelectricis et de Haematozois. Bonnae.

McAllister, C. T., R. P. Shannon, T. J. Fayton and H. W. Robison. 2020. Hemoparasites (Apicomplexa: Hepatozoon; Kinetoplastida: Trypanosoma) of Green Frogs, Rana clamitans (Anura: Ranidae) from Arkansas. Journal of the Arkansas Academy of Science **74**: 37-40.

Mercier, B., C. Gaucher, O. Feugeas and C. Mazurier. 1990. Direct PCR from whole blood, without DNA extraction. Nucleic acids research **18**: 5908.

Miyata, A. and H. S. Yong. 1994. Trypanosome parasites in four species of ranid frogs from Peninsular Malaysia. Malaysian Journal of Science **15**: 31-33.

Nei, M. and S. Kumar. 2000. Molecular evolution and phylogenetics. Oxford University Press, USA,

Netherlands, E. C., C. A. Cook, L. H. Du Preez, M. P. Vanhove, L. Brendonck and N. J. Smit. 2018. Monophyly of the species of *Hepatozoon* (Adeleorina: Hepatozoidae) parasitizing (African) anurans, with the description of three new species from hyperoliid frogs in South Africa. Parasitology **145**: 1039-1050.

Netherlands, E. C., C. A. Cook, D. J. Kruger, L. H. du Preez and N. J. Smit. 2015. Biodiversity of frog haemoparasites from sub-tropical northern KwaZulu-Natal, South Africa. International Journal for Parasitology **4**: 135-141.

Nigrelli, R. F. 1945. Trypanosomes from North American Amphibians, with a Description of *Trypanosoma grylli* Nigrelli (1944) from *Acris gryllus* (Le Conte). Zoologica: Scientific Contributions of the New York Zoological Society **30**: 47.

Oda, S. N., J. Chao and G. H. Ball. 1971. Additional instances of transfer of reptile hemogregarines to foreign hosts. Journal of Parasitology **57**: 1377-1378.

Paperna, I. and R. Lainson. 2004. *Hepatozoon* cf. *terzii* (Sambon & Seligman, 1907) infection in the snake *Boa constrictor constrictor* from north Brazil: transmission to the mosquito *Culex quinquefasciatus* and the lizard *Tropidurus torquatus*. Parasite **11**: 175-181.

Roberts, L. S., J. Janovy Jr and S. Nadler. 2013. Foundations of Parasitology. McGraw-Hill Higher Education, 688p.

Rohlf, J. F. and R. R. Sokal. 1995. Statistical Tables, 3rd ed. Freeman, New York, 199.

Schneider, C. A., W. S. Rasband and K. W. Eliceiri. 2012. NIH Image to ImageJ: 25 years of image analysis. Nature Methods **9**: 671-675.

Sloboda, M., M. Kamler, J. Bulantová, J. Votýpka and D. Modrý. 2007. A new species of *Hepatozoon* (Apicomplexa: Adeleorina) from *Python regius* (Serpentes: Pythonidae) and its experimental transmission by a mosquito vector. Journal of Parasitology **93**: 1189-1198.

Smith, T. G. 1996. The genus *Hepatozoon* (Apicomplexa: Adeleina). Journal of Parasitology **82**: 565-585.

Smith, T. G., S. S. Desser and D. S. Martin. 1994. The development of *Hepatozoon sipedon* sp. nov. (Apicomplexa: Adeleina: Hepatozoidae) in its natural host, the Northern water snake (*Nerodia sipedon sipedon*), in the culicine vectors *Culex pipiens* and *C. territans*, and in an intermediate host, the Northern leopard frog (*Rana pipiens*). Parasitology Research **80**: 559-568.

Smith, T. G., B. Kim and S. S. Desser. 1999. Phylogenetic relationships among *Hepatozoon* species from snakes, frogs and mosquitoes of Ontario, Canada, determined by ITS-1 nucleotide sequences and life-cycle, morphological and developmental characteristics. International Journal for Parasitology **29**: 293-304.

Spodareva, V. V., A. Grybchuk-leremenko, A. Losev, J. Votýpka, J. Lukeš, V. Yurchenko and A. Y. Kostygov. 2018. Diversity and evolution of anuran trypanosomes: insights from the study of European species. Parasites Vectors **11**: 447.

Stebbins, J. H. 1904. Upon the occurrence of haemosporidia in the blood of *Rana catesbiana*, with an account of their probable life history. Transactions of the American Microscopical Society **25**: 55-62.

Stebbins, J. H. 1905. On the occurrence of a large sized parasite of the *Karyolysus* order, in the blood of *Rana clamata*. Zentralblatt für Bakteriologie, Parasitenkunde, Infektionskrankheiten und Hygiene I Abt: Medizinish-hygienische Bakteriologie, Virusforschung und Parasitologie Originale **38**: 315-318.

Stebbins, J. H. 1907. On the occurrence of trypanosomes in the blood of *Rana clamitans*. Transactions of the American Microscopical Society **27**: 25-30.

Stenberg, P. L. and W. J. Bowerman. 2008. Hemoparasites in Oregon spotted frogs (Rana pretiosa) from central Oregon, USA. J Wildl Dis **44**: 464-468.

Stevens, J., H. Noyes and W. Gibson. 1998. The evolution of trypanosomes infecting humans and primates. Memórias do Instituto Oswaldo Cruz **93**: 669-676.

Stothard, J. R. 2000. Trypanosome trees and homologies. Parasitology Today **16**: 173.

Tamura, K. 1992. Estimation of the number of nucleotide substitutions when there are strong transition-transversion and G+C content biases. Molecular Biology and Evolution **9**: 678-687.

Tamura, K. and M. Nei. 1993. Estimation of the number of nucleotide substitutions in the control region of mitochondrial DNA in humans and chimpanzees. Molecular Biology and Evolution **10**: 512-526.

Team, R. C. 2022. R: A language and environment for statistical computing. R Foundation for Statistical Computing. URL https://www.R-project.org/.

Telford Jr, S. R., J. Butler and R. S. Telford. 2005. *Hepatozoon polytopis* n. sp. parasitic in two genera and species of colubrid snakes in southern Florida. Journal of Parasitology **91**: 144-147.

Telford Jr, S. R., J. A. Ernst, A. Clark and J. Butler. 2004. *Hepatozoon sauritus*: A polytopic hemogregarine of three genera and four species of snakes in North Florida, with specific identity verified from genome analysis. Journal of Parasitology **90**: 352-358.

Telford Jr, S. R., P. E. Moler and J. Butler. 2008. *Hepatozoon* species of the timber rattlesnake in northern Florida: Description of a new species, evidence of salivary gland oocysts, and a natural cross-familial transmission of an *Hepatozoon* species. Journal of Parasitology **94**: 520-523.

Telford Jr, S. R., E. J. Wozniak and J. Butler. 2001. Haemogregarine specificity in two communities of Florida snakes, with descriptions of six new species of *Hepatozoon* (Apicomplexa: Hepatozoidae) and a possible species of *Haemogregarina* (Apicomplexa: Haemogregarinidae). Journal of Parasitology **87**: 890-905.

Telford, S. R. 2009. Hemoparasites of the Reptilia: Color Atlas and Text. CRC Press, Boca Raton, Florida, 394.

Tomé, B., J. P. Maia and D. J. Harris. 2012. *Hepatozoon* infection prevalence in four snake genera: influence of diet, prey parasitemia levels, or parasite type? Journal of Parasitology **98**: 913-917.

Tomé, B., J. P. Maia and D. J. Harris. 2013. Molecular assessment of apicomplexan parasites in the snake *Psammophis* from North Africa: do multiple parasite lineages reflect the final vertebrate host diet? The Journal of Parasitology **99**: 883-887.

Vickerman, K. 1965. Polymorphism and mitochondrial activity in sleeping sickness trypanosomes. Nature **208**: 762-766.

Vickerman, K. 2000. Order Kinetoplastea. *In* The Illustrated Guide to the Protozoa. J. J. Lee, G. F. Leedale and P. Bradbury. **2:** 1159-1185.

Werner, J. K., J. S. Davis and K. S. Slaght. 1988. Trypanosomes of *Bufo americanus* from northern Michigan. Journal of Wildlife Diseases **24**: 647-649.

Werner, J. K. and K. Walewski. 1976. Amphibian trypanosomes from the McCormick Forest, Michigan. Journal of Parasitology **62**: 20-25.

Woo, P. T. 1969. The haematocrit centrifuge for the detection of trypanosomes in blood. Canadian Journal of Zoology **47**: 921-923.

Wozniak, E. J. and S. R. Telford Jr. 1991. The fate of *Hepatozoon* species naturally infecting Florida black racers and watersnakes in potential mosquito and soft tick vectors, and histological evidence of pathogenicity in unnatural host species. International Journal for Parasitology **21**: 511-516.

Zechmeisterová, K., H. Javanbakht, J. Kvičerová and P. Široký. 2021. Against growing synonymy: Identification pitfalls of *Hepatozoon* and *Schellackia* demonstrated on North Iranian reptiles. European Journal of Protistology **79**: 125780.

APPENDICES

Supplementary Video 1. *Trypanosoma desseri* n. sp. swimming in blood plasma diluted in phosphate buffered saline. Note how the undulating membrane flutters quickly, however the actual movement of the whole cell is gentle. Sometimes spinning and tumbling, the main direction of cell movement is perpendicular to the anterior-posterior axis, towards the undulating membrane

Supplementary Video 2. *Trypanosoma curvus* n. sp. swimming in blood plasma diluted in phosphate buffered saline. Note how the curved form moves toward the curved anterior end as the undulating membrane flutters along the length of the cell. Additionally, *T.* cf. *chattoni* is pictured, which is a nonmotile trypanosome morphotype.

Supplementary Video 3. *Trypanosoma louisdiamondi* n. sp. swimming in blood plasma diluted in phosphate buffered saline. Note how the posterior end generally stays straight, and the anterior end rotates as the flagellum pulls it in a circle.

Supplementary Video 4. *Trypanosoma* cf. *ranarum* swimming in blood plasma diluted in phosphate buffered saline. Note how the free flagellum extends forward away from the cell and twists rapidly, pulling the rest of the cell anteriorly in a spiral.

VITA

Ryan Patrick Shannon

Candidate for the Degree of

Doctor of Philosophy

Dissertation: HIDDEN IN PLAIN SIGHT: MORPHOLOGICAL AND GENETIC DIVERSITY OF BLOOD PROTOZOA FROM NORTH AMERICAN AMPHIBIANS

Major Field: Integrative Biology

Biographical:

Education:

Completed the requirements for the Doctor of Philosophy in Integrative Biology at Oklahoma State University, Stillwater, Oklahoma in December, 2022.

Completed the requirements for the Master of Science in Zoology at Oklahoma State University, Stillwater, Oklahoma in 2016.

Completed the requirements for the Bachelor of Science in Microbiology at Oklahoma State University, Stillwater, Oklahoma in 2013.

Experience:
Teaching Assistant: 17 total semesters including:
General Parasitology 4104 – 8 semesters
Advanced Herpetology 4184 – 3 semesters
Introductory Biology 1114 – 3 semesters
Guest Lecturer:
General Parasitology, Mammalian Physiology, Advanced Herpetology

Professional Memberships:
American Society of Parasitologists
Annual Midwestern Conference of Parasitologists
Southwestern Association of Parasitologists
Rocky Mountain Conference of Parasitologists
Society of Integrative and Comparative Biology